# High speed flexible rotor active magnetic bearing control

---

A dissertation presented to

The School of Electrical, Electronic and Computer Engineering

North-West University

---

In partial fulfilment of the requirements for the degree

Magister Ingeneriae

in Computer and Electronic Engineering

by

Charl Henri Marais

Supervisor: Prof. G. van Schoor

Assistant supervisor: Mr. E.O. Ranft

June 2006

Potchefstroom Campus

[24]Therefore whoever hears these sayings of Mine, and does them, I will liken him to a wise man who built his house on a rock.

[25]And the rain came down, and the floods came, and the winds blew and beat on that house. And it did not fall, for it was founded on a rock.

**Matt 7:24-25**

# *DECLARATION*

I hereby declare that all the material incorporated in this thesis is my own original unaided work except where specific reference is made by name or in the form of a numbered reference. The work herein has not been submitted for a degree at another university.

Signed: 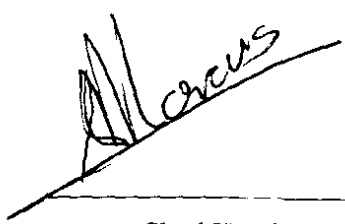

Charl Henri Marais

# *SUMMARY*

The School of Electrical, Electronic and Computer Engineering at the North-West University is in the process of establishing a knowledge base on Active Magnetic Bearings (AMBs). In support of this initiative this project is aimed at characterising an in-house developed double radial heteropolar AMB system.

Before characterising the AMB system the acoustic noise problem of the system had to be addressed and reduced to an acceptable level. To reduce the acoustic noise of the system a noise analysis was done to determine the source of the noise. The analysis revealed radiated noise from the electromagnets and power amplifiers (PA) and conducted noise on the signals to and from the controller. The conducted noise is reduced by using anti-aliasing (AAF) and anti-imaging filters (AIF) before and after the controller. The effect of the radiated noise is reduced by synchronising the sampling of the sensor signals with the switching of the PAs.

The characterisation of the AMB system starts with a Mass-Spring-Damper (MSD) simulation which is a linear representation of the AMB system. This simulation is used to understand the basic principles of a second order system and to compare its response to the nonlinear AMB simulation. The following step in characterising the AMB system is to determine the effect of filters on the nonlinear AMB simulation and to determine the simulation characteristics. These characteristics are compared to the MSD simulation and the actual AMB system. The characteristics compared between the MSD and AMB simulations are the static, second order and dynamic stiffness.

The actual AMB system was characterised before and after the AAF and AIF were implemented. This provided the opportunity to determine the effects of the filters on the actual system and not just from simulations. The characteristics measured on the actual AMB system include the static stiffness, dynamic stiffness, rotor dynamics and system sensitivity. The stiffness characteristics of the actual AMB system showed good correlation with the linear and nonlinear simulations. The measured results showed a decrease in static stiffness and an increase in system sensitivity because of the AAF, AIF and controller pole. It also showed that the effects of the filters can be reduced by moving the controller pole to a higher frequency.

The characterisation of the double radial heteropolar AMB system provides a fundamental understanding of the AMB performance aiding the AMB design process.

# *OPSOMMING*

Die Skool vir Elektriese, Elektroniese en Rekenaaringenieurswese by die Noordwes Universiteit is in die proses om kundigheid te vestig in Aktiewe Magnetiese Laers (AMLs). Ter ondersteuning van die inisiatief fokus die projek op die karakterisering van 'n in-huis, dubbelradiale, heteropolêre AML stelsel.

Voor die karakterisering van die AML stelsel kan plaasvind, moet die akoestiese geraasprobleem aangespreek en verminder word tot aanvaarbare vlakke. Om die akoestiese geraas te verminder moes 'n analise daarvan gedoen word, om die oorsprong te identifiseer. Die analise het stralingsgeraas vanaf die elekromagnete en die kragversterkers (KVs) as ook geleidingsgeraas geïnduseer in die seine na en van die beheerder geïdentifiseer. Die geleidingsgeraas word verminder deur van anti-aliaseringsfilters (AAF) and anti-beeld filters (ABF), voor en na die beheerder, gebruik te maak. Die effek van stralingsgeraas word verminder deur die sinchronisasie van die monstering van die sensor seine met die KV skakeling.

'n Massa–Demper-Veer (MDV) simulasie, wat 'n lineêre voorstelling is van die AML stelsel word eerstens gebruik om die AML stelsel te karakteriseer. Die simulasie word gebruik om die tweede orde gedrag van die MDV te vergelyk met die nie-lineêre AML simulasie. Die volgende stap in die karakterisering van die AML stelsel is om die effek van filters op die nie-lineêre AML simulasie te bepaal en om die karaktereienskappe van die werklike AML stelsel te simuleer. Hierdie karaktereienskappe word vergelyk met die MDV simulasie en ook met die werklike AML stelsel. Die karaktereienskappe wat bepaal word in die simulasies, is statiese styfheid, tweede orde styfheid en dinamiese styfheid

Die werklike AML stelsel is voor en na die implementering van die AAF en ABF gekarakteriseer, om die filter-effekte op die werklike AML stelsel te bepaal, en nie net deur simulasie nie. Die karaktereienskappe wat waargeneem word op die werklike AML stelsel is o.a. statiese styfheid, dinamiese styfheid, stelselsensitiwiteit en rotordinamika. Die karaktereienskappe van die werklike AML stelsel het merkwaardige korrelasie getoon met die lineêre- en nie-lineêre simulasies. Die gemete resultate het 'n vermindering in die statiese styfheid getoon en 'n verhoging in die stelselsensitiwiteit as gevolg van die AAF, ABF en beheerderpool. Daar word ook aangedui dat die filter-effek verminder kan word deur die beheerder pool te skuif na hoër frekwensies.

Die karakteriseering van die dubbelradiale heteropolêre AML stelsel lei tot 'n fundamentele begrip vir AML gedrag ter ondersteuning van die AML ontwerps proses.

# *ACKNOWLEDGEMENTS*

I would like to firstly thank M-Tech Industrial and THRIP for funding this research and granting me the opportunity to do my Masters' degree.

I would also want to gratefully acknowledge the assistance, guidance and contributions provided by the following people in the light of my project:

- Professor George van Schoor, my supervisor, for his input and guidance when I needed it and always having a positive word about everything.
- Eugén Ranft, my assistant supervisor and friend, for encouraging me to keep on going and guiding me in the right direction with big problems.
- My father Charl Marais for his support and inspirational words in morning sms's.
- My mother Anneke Marais for her support and phone calls at the right time.
- My two brothers PK and Oloff for always believing in everything I do.
- My grandfather, grandmothers and family for their love and loyalty.
- My friends, Tim Heckler, Zebedee, Sois and Deon

# *TABLE OF CONTENTS*

# *NOMENCLATURE*

## *LIST OF FIGURES*

# *LIST OF TABLES*



# *LIST OF ABBREVIATIONS*

| | |
|---|---|
| ADC | Analogue to digital converter |
| AMB | Active Magnetic Bearing |
| DAC | Digital to analogue converter |
| MSD | Mass-Spring-Damper |
| PA | Power Amplifier |
| PC | Personal Computer |
| rpm | Revolutions per minute |
| EMI | Electromagnetic emitions |
| AAF | Anti-Aliasing Filter |
| AIF | Anti-Imaging Filter |
| FFT | Fast Fourier Transform |
| PWM | Pulse Width Modulation |
| PD | Proportional and Differential controller |

# *LIST OF SYMBOLS*

| | |
|---|---|
| $b_{eq}$ | Equivalent damping |
| $C$ | Capacitance |
| $E$ | Electrical energy |
| $G_s(s)$ | System open loop transfer function |
| $H$ | Magnetic field intensity |
| $i_0$ | Bias current |
| $K_D$ | Differential gain of the PD controller |
| $k_{eq}$ | Equivalent position stiffness |
| $k_i$ | Force-current factor |
| $K_P$ | Proportional gain of the PD controller |
| $k_s$ | Force-displacement factor |
| $m$ | Suspended body mass / current slope |
| $N$ | Number of coil turns |
| $R$ | Electrical resistance |
| $s$ | Complex frequency |
| $T$ | Time interval |
| $X$ | Rotor position |
| $\omega$ | Rotational speed |
| $\omega_n$ | Natural frequency |
| $\zeta$ | Damping factor |
| $\theta$ | One half of the stator pole pitch |
| $A_g$ | air gap area |
| $g_0$ | air gap |
| $f_{ADC}$ | ADC sampling frequency |
| $f_{signal}$ | signal frequency |
| $X_{ref}$ | reference position |
| $F_d$ | disturbance force |
| $k_{ss}$ | static stiffness |
| $F_{max}$, $F_{min}$ | maximum and minimum forces |
| $x_{max}$, $x_{min}$ | maximum and minimum posion |
| $\sigma$ | decay rate of the ringing |
| $f_1$ | FFT frequency |
| $m_d$ | disturbance mass |
| $k_{sos}$ | second order stiffness |

| | |
|---|---|
| $P_{AAF}$ | Anti-Aliasing pole position |
| $P_P$ | Anti-Imaging pole position |
| $P_C$ | Controller pole position |
| $f_{cut\text{-}off}$ | cut-off frequency of the filters |
| $Mag$ | magnitude of the bode diagram |

# 1
# Chapter
# Introduction

*This chapter provides introductory information on active magnetic bearings in general. The problem statement is given, followed by the issues to be addressed and the methodology. A short overview of the document is also presented.*

## 1.1 Background

The School of Electrical, Electronic and Computer Engineering at the North-West University is in the process of establishing a knowledge base on Active Magnetic Bearings (AMBs). In support of this initiative this project is aimed at characterising an existing AMB system that was developed in-house.

### *1.1.1 Active Magnetic Bearings*

AMBs were primarily designed and built to overcome limitations posed by conventional bearings. The limitations include running in a vacuum, running at high speeds and operation in a radio active environment. Since these limitations set by conventional bearings can be overcome by AMBs the AMB became a valuable machine component in the modern day industrial environment.

The main drawback of the AMB system is its high installation cost and the fact that an AMB should be designed for each application. This makes the use of AMBs less attractive for commercial induction motors and standard turbines or generators. The industrial companies that use AMBs are original equipment manufacturers that implement AMBs in compressors, pumps, turbo expanders, steam turbines, gas turbines, motors and centrifuges. Companies that work together with OEMs in such developments are S2M, Revolve Magnetic Bearings Inc. and Waukesha Bearing Corporation.

### 1.1.2 AMB basic operating principles

The basic AMB system constitutes a sensor, controller, power amplifiers and electromagnets as configured in Figure 1-1. The position sensor monitors the rotor displacement and supplies the information to the controller which generates an appropriate control signal. This control signal is then amplified by the power amplifiers to drive the electromagnets. The electromagnets in turn exert forces on the rotor to correct the displacement and levitate the rotor.

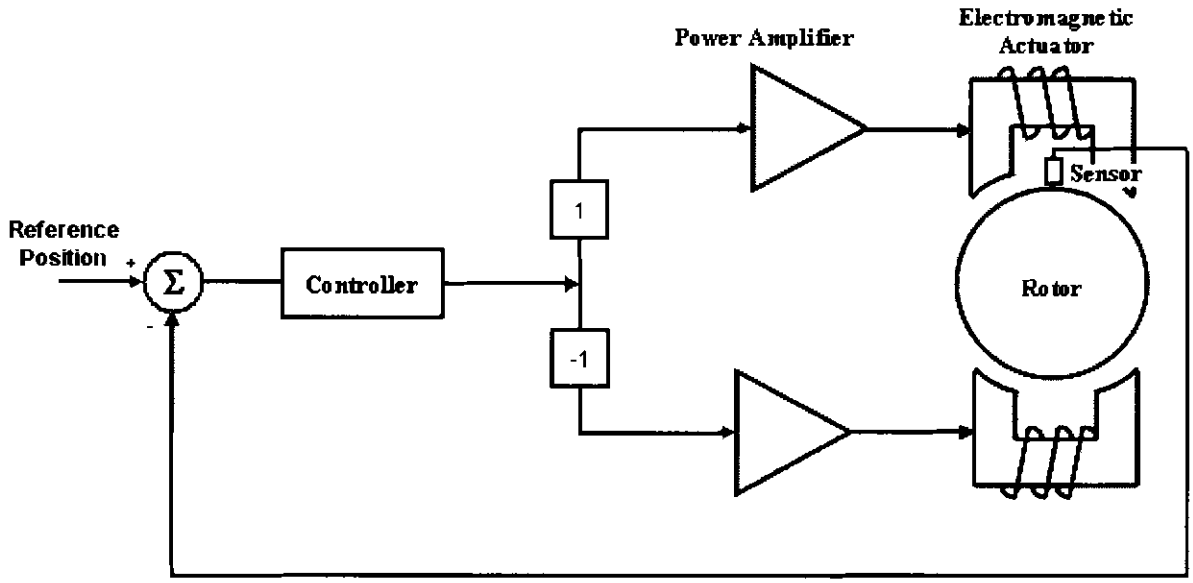


**Figure 1-1: AMB functional diagram**

### 1.1.3 Developed Heteropolar AMB

A double radial AMB system was developed in-house as part of the establishment of the basic research infrastructure. The developed system is shown in Figure 1-2. This system constitutes eight power amplifiers (PAs), two electromagnetic stators, five eddy current sensors, a controller and interchangeable flexible and rigid rotors.

The control of the AMB is realised by using dSpace® which is a real time development tool located inside a personal computer (PC). A ControlDesk® is used in dSpace® as an interface with the position of rotor, on and off switches of the PA and controller constants (Figure 5-11).

The in-house developed AMB showed some problems and characteristics that had to be explained and addressed. These problems include noise on the signals to and from the controller, eddy-current losses and low rotor speeds with rigid rotor. The characterisation of the AMB system was also identified as a fundamental requirement to enhance the understanding of AMB behaviour and its impact on AMB design.

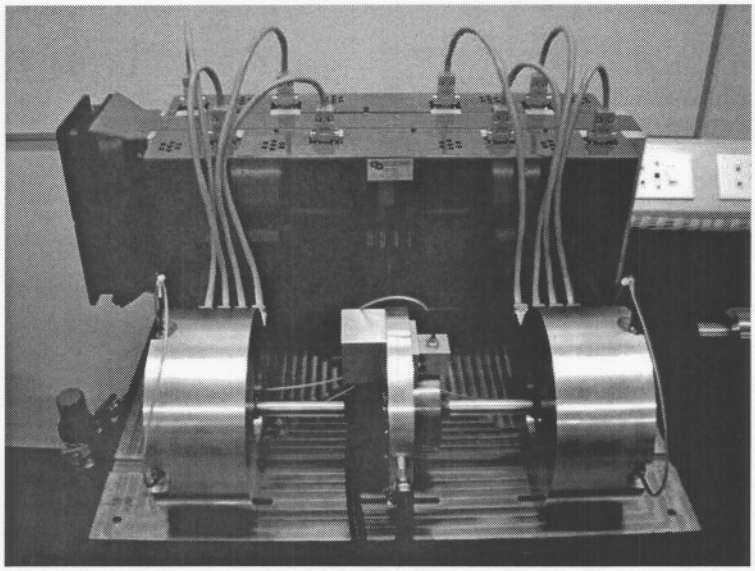

**Figure 1-2: Double radial flexible rotor AMB model**

The simulation of the AMB model also needs some refinement. These refinements include actual system dynamics and nonlinearities that are not modelled in the developed simulation.

## 1.2 Problem statement

The purpose of this study is to improve and characterise the in-house developed flexible rotor heteropolar active magnetic bearing system. Signal conditioning is investigated to reduce the acoustic noise of the AMB system and to increase the stability margin of the system. The system is also characterised in terms of stiffness to establish a fundamental understanding of AMB behaviour.

## 1.3 Issues to be addressed and methodology

### *1.3.1 Noise analysis*

The first objective of this project is to analyse the noise on the AMB system and to determine the source of the noise. The identified noise should then be reduced to an acceptable level.

Noise effects in the system will be analysed with an analogue spectrometer and the FFTs (Fast Fourier Transforms) of the signals to and from the controller. The identified noise will then be reduced to an acceptable level through appropriate filtering of the relevant signals.

### *1.3.2 AMB Mass Spring Damper (MSD) equivalence*

The MSD system is a linear representation of the AMB system and is used to analyse and understand the response of the nonlinear AMB system. The analysis of the MSD will be done analytically and through simulation focusing on the static, second order and dynamic stiffness of the system.

### *1.3.3 AMB characterisation*

In the characterisation of the AMB system it is important to determine and understand the nonlinearities and responses of the system to aid future AMB designs.

A flow diagram of the AMB and MSD comparison is shown in Figure 1-3. It is shown that the MSD and AMB simulations are compared to each other and to the actual AMB system. In each comparison the static, second order and dynamic stiffness of each system are compared to determine the effect of filters on the AMB system.

The actual AMB system is also characterised in terms of system sensitivity, rotor dynamics and step responses to obtain a more comprehensive understanding of the performance of the AMB system. The latter is analysed without and with filtering.

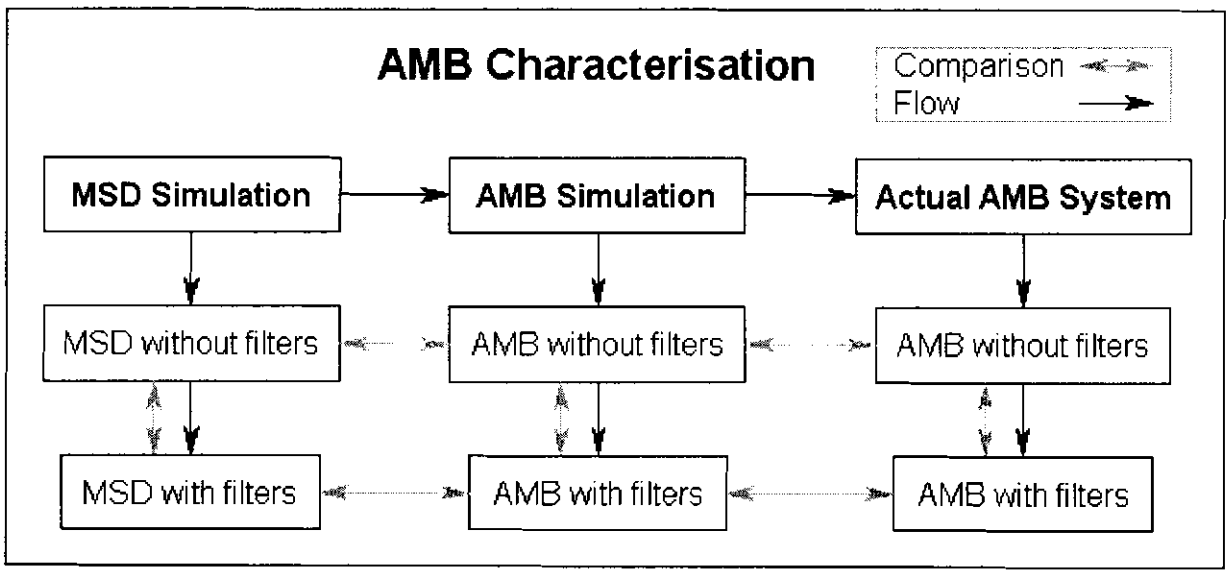


**Figure 1-3: AMB characterisation flow diagram**

## 1.4 Overview of the dissertation

Chapter 2 contains a literature study on AMB systems and the knowledge areas applicable to this study. The knowledge areas addressed include AMB noise, filters, stiffness, damping and sensitivity.

The noise analysis of the AMB system is done in chapter 3. The main focus of the noise analysis is to find the noise source and to reduce the noise. To do this the signals to and from the controller are analysed for noise and filters are implemented where necessary.

Chapter 4 characterises a MSD simulation that is equivalent to a linear AMB system. The simulation is characterised by simulating the static, second order and dynamic stiffness of the MSD system. The characterisation is done on the MSD system with and without filters to determine the effect of the filters on a linear system.

The simulated and actual AMB system are characterised in chapter 5 using the methods defined in chapter 2. The characterisation of the simulated system includes the static, second order and dynamic stiffness and can be compared to the MSD simulation in chapter 4. The actual AMB system is then characterised by measuring the static stiffness, dynamic stiffness, system sensitivity, rotor dynamics and step response. These measurements are compared to the simulated measurements of the MSD and AMB systems.

Chapter 6 contains the conclusion and recommendations of this study. This chapter concludes that the implementation of filters and synchronisation resulted in an improved of the signal to noise ratio and improved controller performance. The characterisation also showed that the specified stiffness in the designer specifications, can be realised in a practical AMB system.

The included CD in Appendix A contains: MS Word® format of this dissertation, Matlab® simulation of the MSD and AMB systems and dSpace® experiment files.

*Chapter 1 gave some background on the AMB system as an introduction to the problem statement. This is followed by the issues that need to be addressed and an overview on all the chapters. The main issues that were focused on were the noise analysis and system characterisation.*

# 2
# Chapter

# Literature Study

*This chapter contains a literature study on some knowledge areas of AMB technology. It starts with an introduction to AMBs, discussing the basic operating principles and some advantages and disadvantages. Some of the knowledge areas that are discussed are: noise, filters, stiffness, damping and sensitivity.*

## 2.1 Active Magnetic Bearings

An AMB (Active Magnetic Bearing) is a system that levitates rotors or axles in mid air with no mechanical friction by using electromagnets.

AMBs were designed and built to overcome certain restrictions of conventional bearings. These restrictions include running at high speeds, operation in a vacuum and specific stiffness and damping requirements. Since the AMB can overcome these restrictions contributed to the fact that the AMB grew extensively in applications [1].

### *2.1.1 Basic Operating Principles*

The basic operation of the AMB can be explained in terms of four basic building blocks: electromagnets, a control system, power amplifiers and position sensors. A block diagram of the AMB, using these building blocks is shown in Figure 2-1 [2].

The sensor in Figure 2-1 is used to measure the exact position of the rotor between the electromagnets. This data is then used in a PD controller to determine the control current from the power amplifier (PA) to the electromagnets as shown in Figure 2-1. The control current is the current needed to excite the electromagnets and keep the rotor in the centre of the magnets.

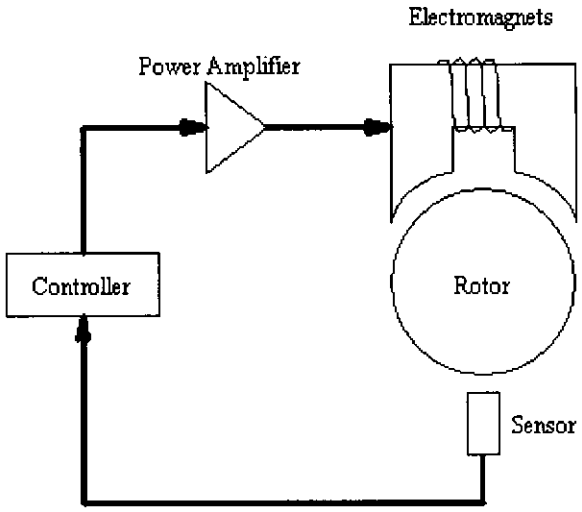


**Figure 2-1: Block diagram of a basic AMB [3]**

### *2.1.2 Advantages*

AMBs are mostly used in centrifugal compressors, electric power plants, petroleum refining, machine tools, satellites and military weapons. Using AMBs improves machine life because it controls damping of high-speed rotors that virtually eliminate critical speed vibrations of the rotor. AMBs also reduce the wear and fatigue of a bearing by not being dependent on lubrication and not having any friction on the mechanical parts. This means that the AMB will have fewer problems with the associated potential for leakages and low rotational torque losses [4].

Losses in an AMB system constitute the active power losses, parasitic losses and windage losses. The active power losses constitute the coil and amplifier losses and the parasitic losses constitute the eddy current and hysteresis losses. Comparing the AMB with a fluid film bearing the losses in the fluid film bearing include: pump power, cooling power, oil shear losses and friction losses [5]. It can thus be deducted that the fluid film bearing has more losses than the AMB system. It can also be said that the AMB shows remarkably low bearing losses compared to other bearings.

AMB control makes it possible to change the stiffness and damping of the system to meet the specifications. Since the stiffness can be changed the critical frequency of the rotor can be modified to occur at different frequencies. This means that the system can be controlled to avoid the critical frequency and reduce structural vibration to extend mechanical life [6]. Critical frequency or speed is defined as the shaft speed that coincides with the natural frequency which is excited by a rotor imbalance rotating at shaft speed. This means that the rotor does not vibrate as it appears to an external stationary observer but rather bows into the mode shapes as shown in Figure 2-2.

Adjustable stiffness and damping also make it possible to compensate for external disturbances on the system [7] [8].

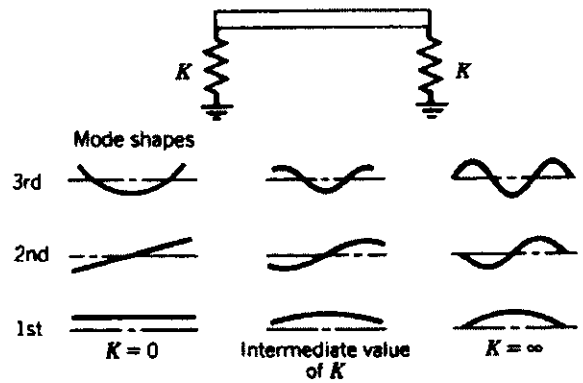


**Figure 2-2: Effect of stiffness *K* on lateral vibration modes of a rotor [6]**

### *2.1.3 Disadvantages*

AMB development and implementation cost is higher than that of conventional bearings because AMB components are more expensive. Conventional bearings are also easier to transport because they are not as bulky as AMBs.

An effective solution to one of these problems is to use the electromagnets for both sensing and actuation. This reduces the cost and weight of the system, making it more attractive to the industrial market.

## 2.2 Noise

The AMB model used in this project showed extensive acoustic noise that had to be reduced. To reduce the acoustic noise on the AMB a noise analysis had to be done. This noise analysis includes the in depth study of the noise from each of the components of the AMB shown in Figure 2-1.

One of these components is the switch-mode PA that was used to energise the electromagnets. Switch-mode PAs work at high voltages and has switching noise as shown in Figure 2-9. This makes the PA the biggest source of noise in the AMB system.

The second group of components that can have a big influence on the noise levels is the electromagnets. Electromagnets can radiate magnetic and electric fields that should be measured and managed.

The biggest problem with the noise in the AMB system is the noise radiators and the noise receivers. Noise producers are the PAs and the electromagnets as mentioned above and the receivers are the cables to and from the controller.

There are two types of noise that should be analysed in the AMB system namely radiated and conducted noise. The two noise types will be discussed in the sections to follow.

### *2.2.1 Radiated noise*

Radiation of noise requires both a noise source and a receiver where the noise is emitted into the system. Measurements showed that high energy components are radiated from the power amplifiers and electromagnets as shown in Figure 2-3. The power amplifiers are the main source of electrically radiated noise (E fields) and the electromagnets the main source of magnetically radiated noise (H fields) [9].

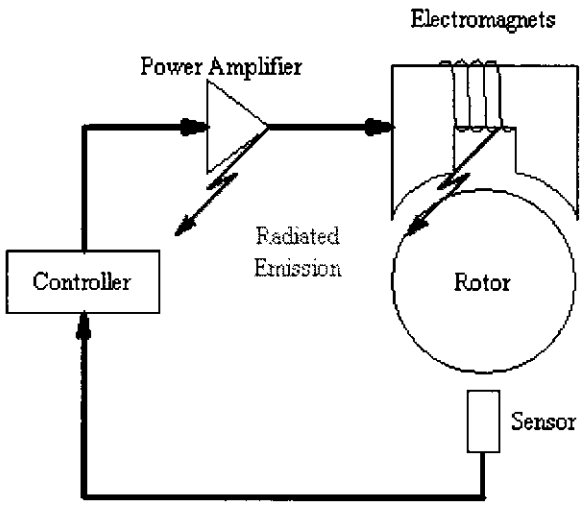


**Figure 2-3: Radiated noise in the AMB**

### *2.2.2 Conducted noise*

Noise that is carried on a signal (carrier signal) is called conducted noise. The main sources of conducted noise in the AMB are common mode noise, aliasing, imaging and radiated noise that becomes conducted noise as shown in section 2.2.1. The carrier signals of the conducted noise are shown in Figure 2-4.

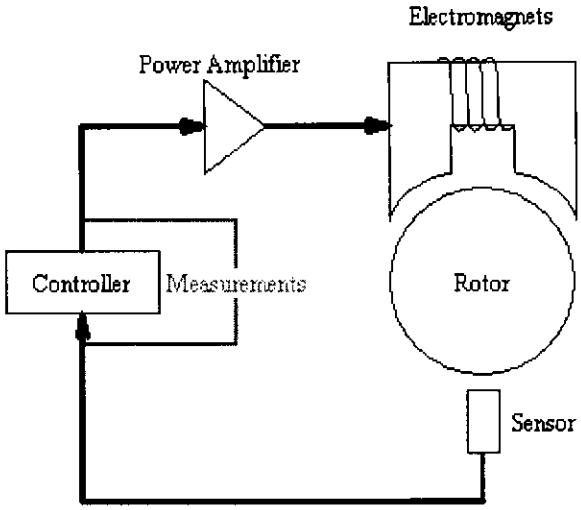


**Figure 2-4: Measurements for conducted noise**

- ***Aliasing***

Aliasing is the noise added by the Analogue to Digital Converter (ADC) as the signal is digitised for the controllers use.

If the ADC used in the dSPACE card samples in time intervals of $T$ (seconds) which is bigger than half the period of the sampled signal, another frequency component can be fitted in the samples as illustrated in Figure 2-5. The sampled frequency can be mistaken for a different frequency than the actual sampled signal because of the long sampling time. To obtain the same input and output frequency from the ADC the signal should be sampled at a frequency higher than the Nyquist frequency as expressed by (2-1) [10].

$$f_{ADC} \geq 2.f_{signal} \tag{2-1}$$

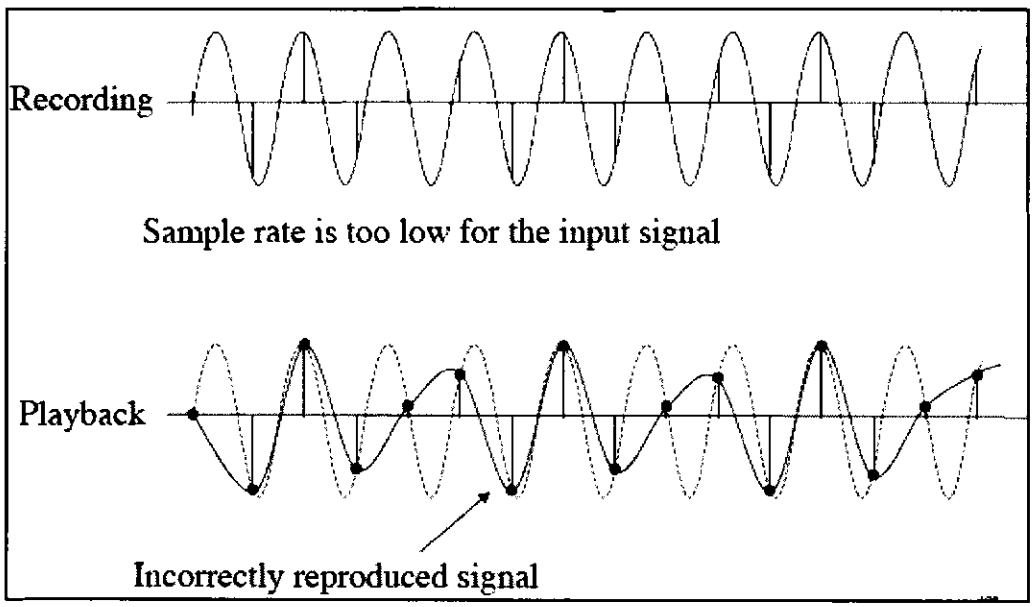


**Figure 2-5: Aliasing in the time domain [10]**

- ***Imaging***

DAC has a step output and not a smooth output as shown in Figure 2-6. A square wave or step signal has a wide frequency spectrum which means that the wave can produce noise from low to high frequencies. This noise is then added to the output signal of the DAC to give undesired spectral components above the Nyquist frequency [11].

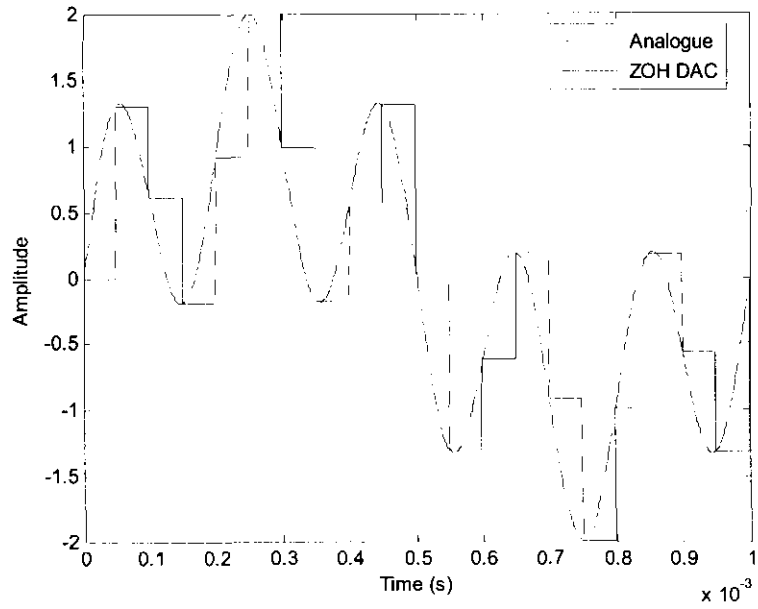


**Figure 2-6: Output impulses of the DAC [12]**

- ***Common mode noise***

Common mode noise is caused by internal EMI currents that flow out through output lines seeking a return path back to the noise source as shown in Figure 2-7. The best way of suppressing common mode noise is by using common mode filtering at the point closest to the noise source as indicated in Figure 2-8.

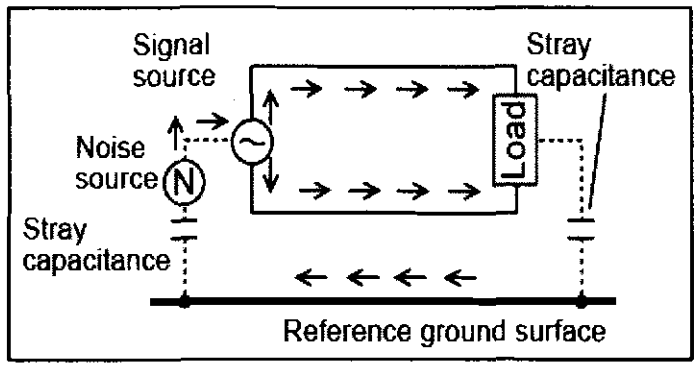


**Figure 2-7: Common mode noise source [13]**

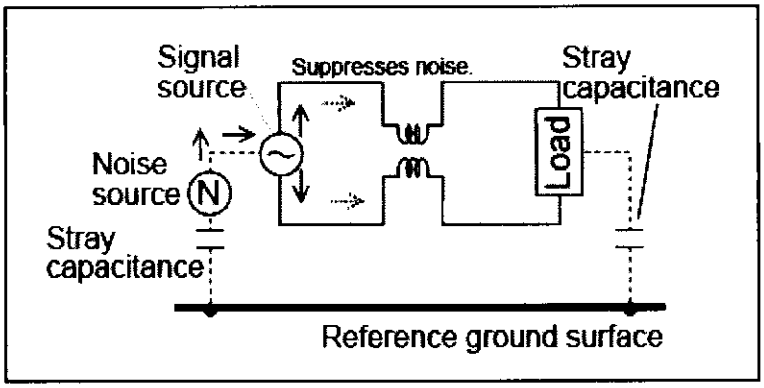


**Figure 2-8: Common mode noise filtering [13]**

### *2.2.3 Acoustic noise*

If the laminations in an electromagnet are not held tightly together they will start to vibrate when a high frequency disturbance is added to the coil current. This will cause acoustic noise since the force exerted by the coil current causes the lamination to contract and expand.

In an AMB system the current in the coils are produced by the PA. This means that the acoustic noise in the system is a result of the PA and the electromagnets combined. The switch-mode PA uses Pulse Width Modulation (PWM) with a fundamental frequency of 100 kHz to switch the output current of the PA as illustrated in Figure 2-9. The current then transfers the fundamental frequency to the electromagnets where the laminations start to vibrate to that frequency. This frequency is too high to hear but components of it will reflect to lower audible frequencies [14].

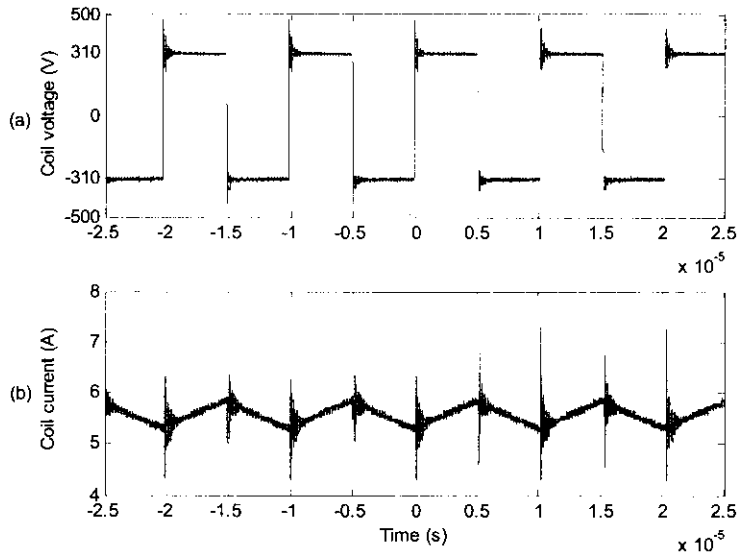


**Figure 2-9: Coil waveforms: (a) applied voltage, (b) coil current**

A second noise problem that affects the acoustic noise of the system is the natural frequency of the AMB. The natural frequency can be determined with (2-2), where $k_{eq}$ is the equivalent stiffness and $m$ the mass of the rotor.

$$\omega_n = \sqrt{\frac{k_{eq}}{m}} \qquad (2\text{-}2)$$

$$= \sqrt{\frac{4.99 \times 10^5}{3.89}}$$

$$= 183.96 \text{ rad/s } (29.3 \text{ Hz})$$

The FFT of the acoustic noise measured from the AMB system is shown in Figure 2-10. The sound was measured with a microphone and sound input of a PC that measures up to 20 kHz. This FFT shows that the natural frequency of the AMB system is one of the high energy components.

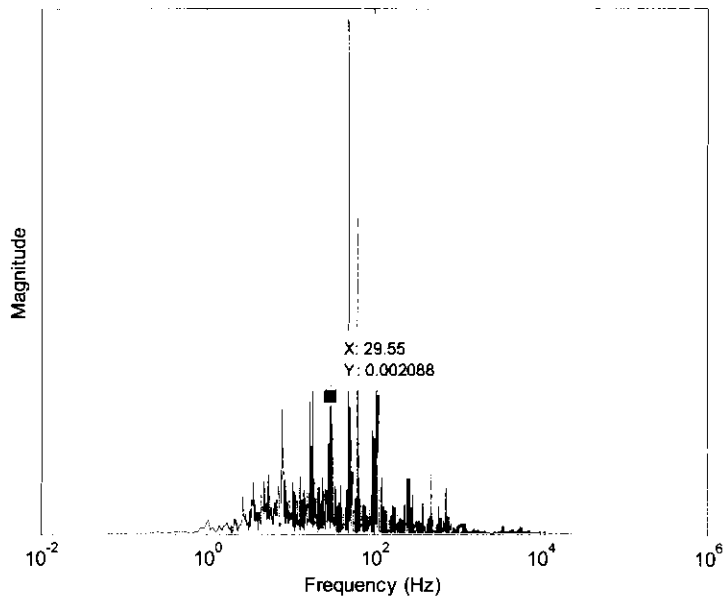


**Figure 2-10: FFT of the acoustic noise from the AMB**

## 2.3 Filters

Noise in the AMB is a big problem because of the radiation, common mode noise, aliasing and imaging as discussed above. To reduce this problem filters are needed to cut the unwanted frequencies out of the signals and keep the high energy components from filtering through.

The filters that are needed for this application are low pass filters with a small delay, phase shift and a unity gain in the pass band. The small delay and phase shift is needed because of the real time control of the AMB. Real time control gives immediate error correction as the error occurs and can not withstand a big phase shift or time delay in the pass band of the filter. The unity gain is needed to keep the signal inputs and outputs at the same constant level as before the filter.

### *2.3.1 Butterworth*

Butterworth filters are also called Maximally Flat approximations. The name does not refer to the type of filter but to its response. Figure 2-11 shows the low pass frequency response of the Butterworth filter from which it is prominent that there is no ripple between the pass and stop band and the pass band gain is maximally flat.

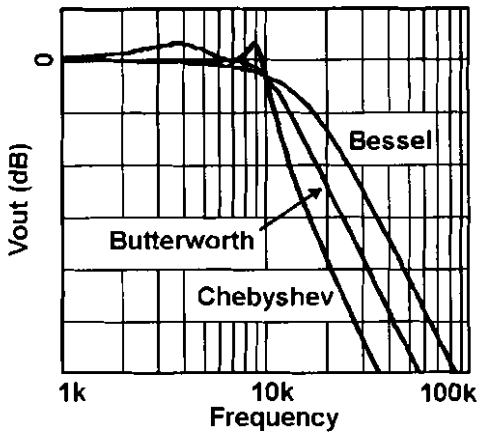


**Figure 2-11: Low pass filters frequency response [15]**

The Butterworth filter has a flat response in the pass band and a much steeper gradient descend from the pass band to the stop band than the Bessel filter. This makes the Butterworth filter a better application for systems where a steep reduction in energy above the pass band frequency is required and where the gains in the pass band play an important role in the output of the system.

The phase shift (Figure 2-12) of the Butterworth filter is also an average between the Bessel and Chebyshev filter. Thus to have no phase shift at the operating frequency of a Butterworth filter the cut-off frequency should be an order and a half higher than the operating frequency.

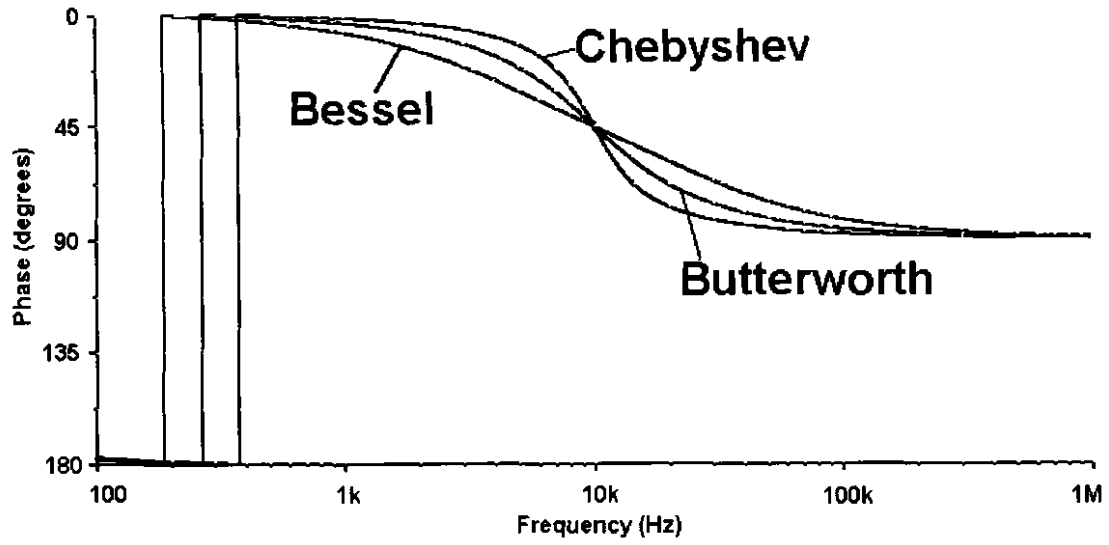


**Figure 2-12: Low pass filter phase diagram [15]**

Figure 2-13 shows the group delay of the three filters and that the Butterworth filter is a compromise between the Bessel and Chebyshev [15].

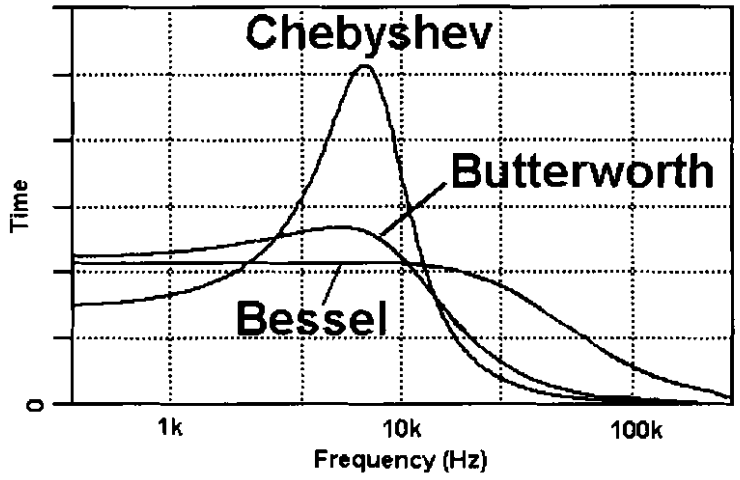


**Figure 2-13: Low pass filters group delay [15]**

From the information in Figure 2-11, Figure 2-12 and Figure 2-13 it is obvious that the Butterworth filter is an average between the Chebyshev and Bessel filters in all aspects. The biggest problem with the Butterworth filter is that it has the biggest group delay of all the filters at low frequencies.

### *2.3.2 Chebyshev*

As with the Butterworth filter, Chebyshev refers to the type of response rather than the filter design. Figure 2-11 shows the filter response where the increase in gain between the pass and stop band refers to the ripple of the filter. The Chebyshev filter can thus also be called an equal-ripple approximation.

The position and amount of ripple are determined by the order of the filter. Filters of even order generate ripple that appears above 0 dB and filters of odd order generate ripple below 0 dB.

In Figure 2-12 it is shown that the Chebyshev filter has the fastest rate of phase change of all the filters shown in the diagram. Chebyshev filters also have the highest group delay of all the filters between the pass and stop band (Figure 2-13). [16]

### *2.3.3 Bessel Filter*

The Bessel filter is mostly used for digital systems because of its capability to filter square waves. Most signals that are filtered are sine waves or close enough so that the effect of harmonics can be ignored. If a waveform with high harmonic content is filtered, such as a square wave, the harmonics can be delayed with respect to the fundamental frequency with a Butterworth or Chebyshev response. The Fourier series of a unit square wave is given by (2-3), where $\omega_0$ is equal to the frequency of the square wave.

$$x(t) = \frac{4}{\pi}\left[(\sin(\omega_0 t) + \frac{\sin(3\omega_0 t)}{3} + \frac{\sin(5\omega_0 t)}{5}\right] \quad \textbf{(2-3)}$$

This means that a square wave is the sum of an infinite series of odd harmonics or sine waves. If a square wave is to be transmitted without distortion all of these harmonics would have to be transmitted. This means that the square wave can be high pass filtered without distortion if the -3 dB point of the filter is significantly lower than the fundamental frequency. If the square wave is low pass filtered, however, the situation changes dramatically. Harmonics will be eliminated, producing distortion in the square wave. But the designer can still decide how many harmonics should be passed. Figure 2-14 gives the output with five harmonics.

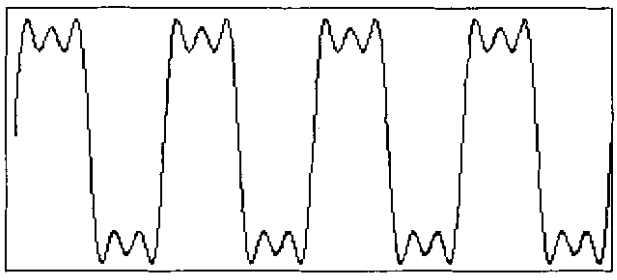

**Figure 2-14: Signal output of a five harmonics design**

Depending on the timing of the leading and trailing edge requirements of the waveform this may be acceptable to the designer. The elimination of harmonics will result in rounding of the edges, and therefore delay in the leading and trailing edges of the digital signal. Of more importance is the fact that the harmonics that are passed will not be delayed.

From Figure 2-11 it can be seen that the Bessel estimation has a smooth pass band and stop band response similar to that of the Butterworth. For the same filter order, the stop band attenuation of the Bessel approximation is much lower that that of the Butterworth approximation.

From Figure 2-13 the designer can see that there is no ripple in the pass band of a Bessel filter, and that it does not have as much rejection in the stop band as a Butterworth filter.

Figure 2-12 shows the phase response of the three filter types and that the Bessel response is the slowest [17].

### *2.3.4 RC filter*

An RC filter is the most commonly used filter in electronic circuits. It consists of a resistor and a capacitor as demonstrated in Figure 2-15 and Figure 2-16. This filter can be used as a low pass filter as illustrated in Figure 2-15 and as a high pass filter in Figure 2-16.

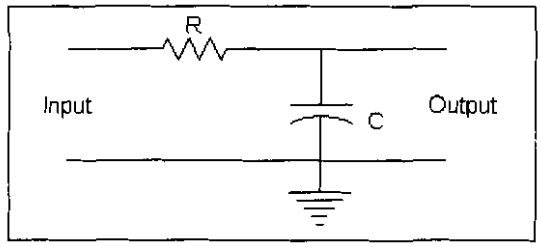


**Figure 2-15: First order low pass filter**

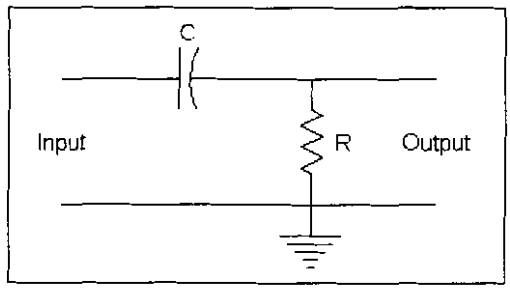


**Figure 2-16: First order high pass filter**

The -3 dB cut-off frequency of the RC filter is determined with (2-4) and (2-5) [18].

$$\omega = \frac{1}{RC} \tag{2-4}$$

$$f = \frac{1}{2\pi RC} \tag{2-5}$$

### 2.3.5 *Filter summary*

The filters used in the AMB should have a phase shift and time delay of almost zero because of the real time control. If the time delay and phase shift of the filter are too high the controller will not be able to control the AMB. The amount of filters can also contribute to the total time delay and phase shift of the system. This is because the time delay and phase shift of each of the filters are added to obtain the system time delay and phase shift.

Figure 2-12 and Figure 2-13 show that the Butterworth, Chebyshev and Bessel filters have a phase shift and a time delay in the pass band. If these filters should be used the time delay and phase shift would add up and make the controller unstable. In an RC filter the total time delay and phase shift will not make the system unstable because the RC filter has a much smaller phase shift and time delay in the pass band.

Thus because of the real time control of the AMB the system is limited to the use of RC filter.

## 2.4 AMB stiffness

The AMB system is equivalent to the mass-spring-damper (MSD) system as illustrated in Figure 2-17(a), with $k_{eq}$ equivalent stiffness and $b_{eq}$ equivalent damping. The sensors, controller, PA and electromagnet in Figure 2-17(b) determine the equivalent stiffness and damping of the AMB system.

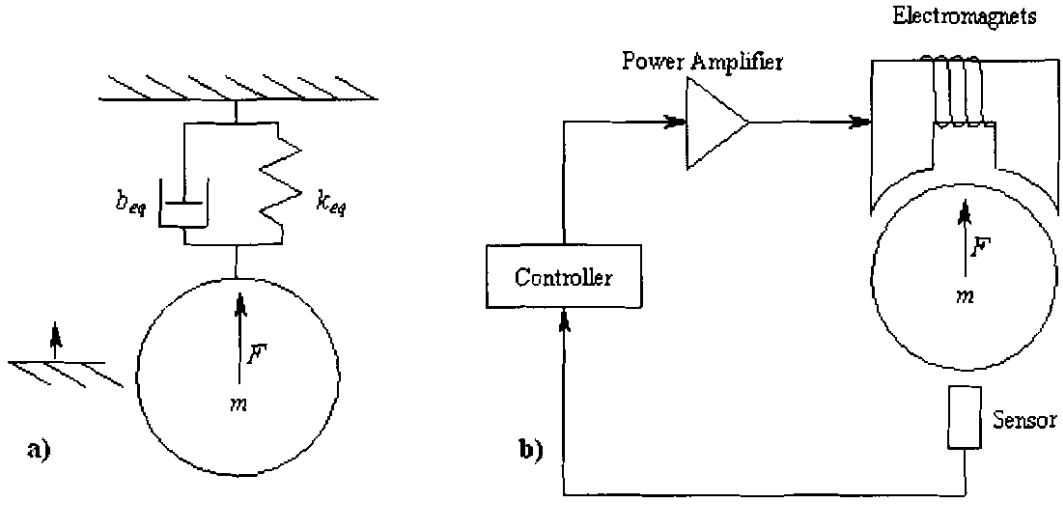


**Figure 2-17: AMB and MSD equivalence a) MSD and b) AMB equivalence**

The two figures shown in Figure 2-17 can be reduced to a control block diagram as illustrated in Figure 2-18. This block diagram is used to determine the transfer function of the linear system by using Mason's rule [19].

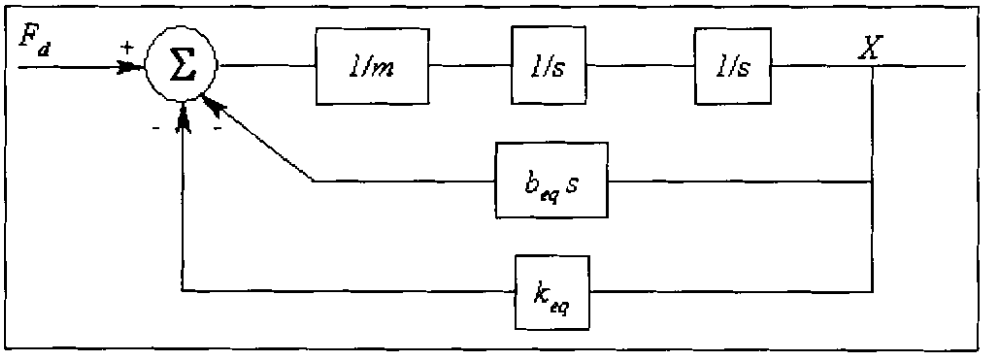


**Figure 2-18: MSD and AMB block diagram**

From the block diagram in Figure 2-18 the forward path connecting the input to the output is:

$$P_1 = \frac{1}{m}\cdot\frac{1}{s}\cdot\frac{1}{s} = \frac{1}{ms^2} \tag{2-6}$$

Two loops are identified:

$$L_1 = -\frac{b_{eq}}{ms},\quad L_2 = -\frac{k_{eq}}{ms^2} \tag{2-7}$$

Loops $L_1$ and $L_2$ touches, therefore the determinant is

$$\begin{aligned}\Delta &= 1-(L_1+L_2) \\ &= 1-(-\frac{k_{eq}}{ms^2}-\frac{b_{eq}}{ms})\end{aligned} \tag{2-8}$$

The cofactor of each forward path is evaluated by removing the loops that touch that specific path from the determinant. Therefore the cofactor is:

$$\Delta_1 = 1 \tag{2-9}$$

By substituting (2-6), (2-7), (2-8) and (2-9) into (2-10) the transfer function is obtained.

$$T(s) = \frac{X}{F} = \frac{P_1\cdot\Delta_1}{\Delta} \tag{2-10}$$

$$= \frac{1}{ms^2}\cdot\left(\frac{1}{1-[-\frac{k_{eq}}{ms^2}-\frac{b_{eq}}{ms}]}\right)$$

$$= \frac{1}{ms^2+b_{eq}s+k_{eq}} \tag{2-11}$$

(2-11) is the transfer function of the linear MSD system.

AMBs are highly nonlinear in the force-current and force-displacement relationship unlike the linear MSD model. Figure 2-19 shows the nonlinear model of the AMB system.

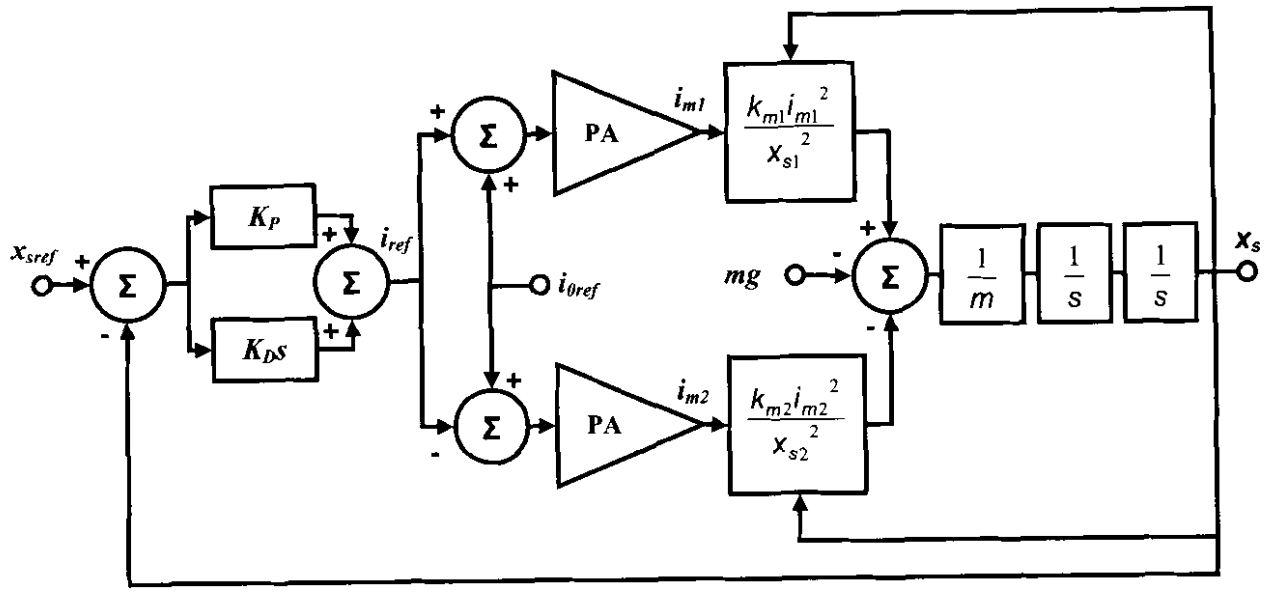


**Figure 2-19: AMB nonlinear system block diagram [3]**

To linearise the nonlinear system in Figure 2-19 the system is linearised around the operating point. This is done by multiplying the controller force with the force-current factors $k_i$ and the position of the rotor with the position stiffness $k_s$ as shown in Figure 2-20.

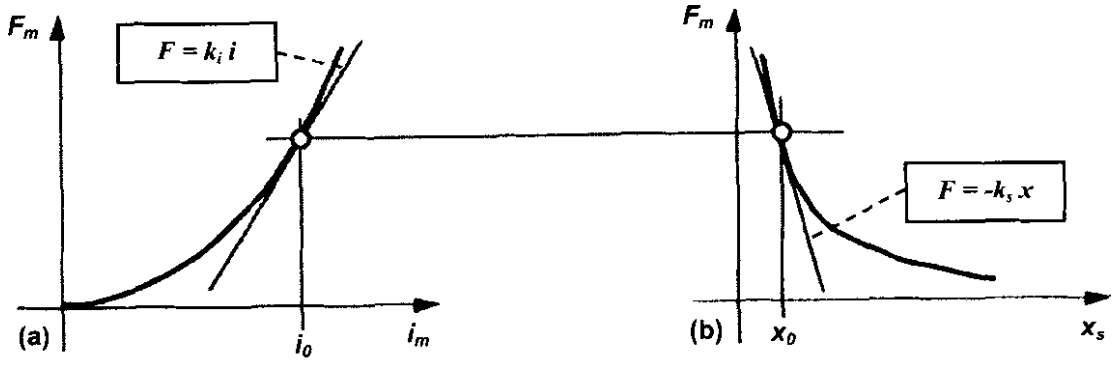


**Figure 2-20: Magnetic force as a function of (a) current and (b) air gap [6]**

The single magnetic actuator current gain is defined as

$$k_i = \left.\frac{\partial F}{\partial x}\right|_{i_m = i_0, x_s = g_0}$$

$$= 2\frac{\mu_0 N^2 i_0 A_g}{g_0^2}\cos(\theta) \qquad (2\text{-}12)$$

$$= 33.3 \text{ N/A}$$

and the position stiffness of the electromagnets are defined as

$$k_s = \left.\frac{\partial F}{\partial x}\right|_{i_m=i_0, x_s=g_0}$$

$$= 2\frac{\mu_0 N^2 i_0^2 A_g}{g_0^3}\cos(\theta) \qquad \textbf{(2-13)}$$

$$= 1.67\times10^5 \text{ N/m}$$

The constants used to determine the positions stiffness of the magnets and the power amplifier gain are:

| | |
|---|---|
| $A_g$ | air gap area |
| $N$ | number of coil turns |
| $g_0$ | air gap |
| $i_0$ | bias current |

Figure 2-21 illustrates the block diagram of the linerised AMB model. In this model the disturbance force of Figure 2-18 is substituted with *mg*.

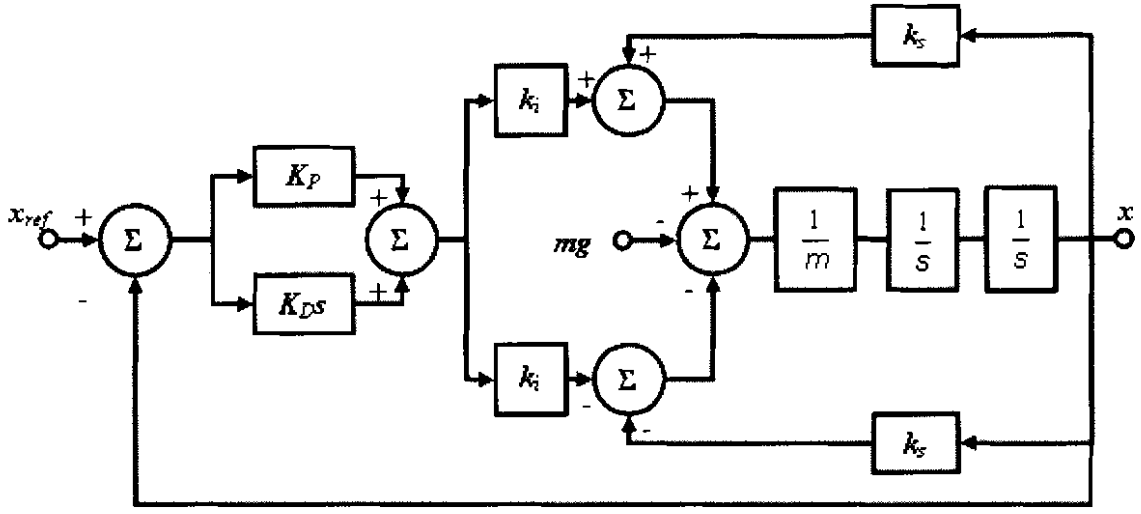


**Figure 2-21: AMB linearised system block diagram [3]**

The transfer function obtained from linerised AMB system Figure 2-21 and Mason's rule are

$$T(s) = \frac{x_{ref}}{mg} = \frac{X}{F_d}$$

$$= \frac{1}{ms^2 + 2K_D k_i s + (2K_P k_i - 2k_s)} \qquad \textbf{(2-14)}$$

where $K_P$ and $K_D$ are the proportional and differentiator gain of the PD controller used to control the AMB.

If the equivalent stiffness and damping of the linerised AMB and MSD systems are compared in (2-11) and (2-14), it is seen that the AMB controller constants and linearization constant are equal to the equivalent stiffness and damping of the MSD system as shown in (2-15) and (2-16) [3].

$$k_{eq} = 2K_P k_i - 2k_s \tag{2-15}$$

$$b_{eq} = 2K_D k_i \tag{2-16}$$

By substituting the equivalent stiffness and damping of the AMB into the MSD simulation the simulations should have the same response.

Stiffness can be measured as the ratio of a supported load to the displacement of the load. This is based on the understanding that it is a mechanical system. In classical ball bearings, the stiffness of the bearing depends on the elasticity of the oil and the deformation of the mechanical parts. In the AMB the stiffness of the system is dependent on the controller, power amplifiers and the electromagnets. To characterise the stiffness of an AMB the stiffness should be measured in two ways statically and dynamically [6].

### *2.4.1 Static stiffness*

Static stiffness is defined as the ability of a system to resist position changes.

Static stiffness of a system is measured by applying a force to the rotor and measuring the deviation of the rotor due to the force. This deviation ($x$) of the rotor and the force ($F_d$) is substituted into (2-17) to attain the static stiffness ($k_{ss}$) of the AMB [20].

$$k_{ss} = \frac{\Delta F_d}{\Delta x} = \frac{\Delta mg}{\Delta x} \tag{2-17}$$

The deviation of the rotor used to determine the static stiffness can only be used if the AMB controller does not include an integrator. An integrator in the controller can be added to minimise the error in the rotor position. The error is the difference between the position reference and the actual position of the mass. This means that if an integrator is added to the system the deviation because of a force will become zero and make the stiffness of the system arbitrarily high to the point were the system cannot oppose the applied force [21].

The static stiffness of an AMB system is equal to the equivalent stiffness of the system, which is also equal to the equivalent stiffness of the MSD system in Figure 2-17(a) for second order systems.

### 2.4.2 *Dynamic stiffness*

Dynamic stiffness is defined as the stiffness as a function of frequency. By obtaining the dynamic stiffness it can be shown that the system will be reliable at any frequency in the system bandwidth.

Dynamic stiffness is determined by applying a disturbance force ($F$) to the rotor of the AMB system at a specific frequency and measuring the deviation ($\Delta x$) of the rotor. (2-18) can then be used to calculate the dynamic stiffness where $F_{max}$ and $F_{min}$ are the maximum and minimum values of the disturbance force and $x_{max}$ and $x_{min}$ the maximum and minimum values of the rotor deviation.

$$k_{dyn}(f) = \frac{F_{\max} - F_{\min}}{x_{\max} - x_{\min}} \tag{2-18}$$

(2-17) and (2-18) show that the dynamic and static stiffness are equal to the force divided by the change in position, where as (2-11) and (2-14) shows that the transfer functions of the AMB and MSD are equal to the change in position divided by the force. Dynamic stiffness is thus but the inverse of the transfer function as shown in Figure 2-22.

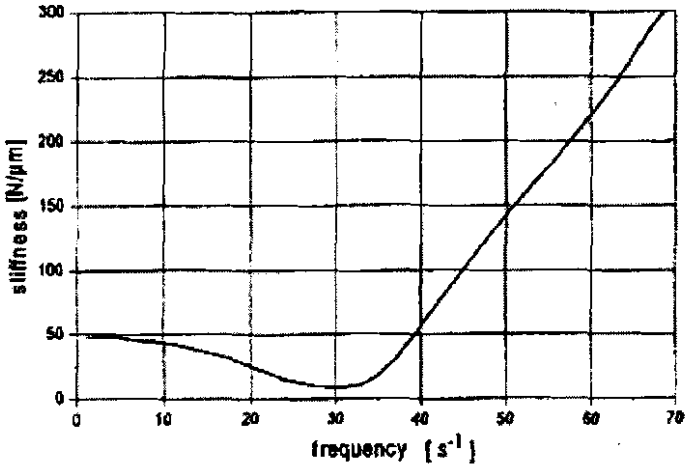


**Figure 2-22: Dynamic stiffness vs. frequency plot for an AMB system [10]**

Since the dynamic stiffness is equal to the inverse of the frequency response it can be said that dynamic stiffness is dependent on the bandwidth of the system. This means that if one of the function blocks in Figure 2-1 should reduce or increase the bandwidth of the system the dynamic stiffness will also change.

One of the limiting factors of the AMB bandwidth is the PAs and electromagnets. Since the PAs have a direct influence on the performance of the electromagnets the two components can be combined to form the magnetic actuator. The magnetic actuators have a cut-off frequency determined by the cut-off frequency of the PAs. This cut-off frequency of the PAs should be measured to determine the effect of the magnetic actuator on the bandwidth of the AMB system if no filters are used. If a filter is used on the PAs

the cut-off frequency and bandwidth of the system will be reduced to the cut-off frequency of the filter making the filter the limiting factor of the magnetic actuator [21].

A second bandwidth limiter is the AMB controller or the filters associated with the controller. If no filters are used before the controller the bandwidth of the controller is bound to be lower than that of the PA. This means that the controller will have the biggest influence on the bandwidth of the AMB if no filters are used. If filters are used the cut-off frequency of the filter will determine the bandwidth of the controller and reduce or leave the system bandwidth to be the same.

A typical frequency dependency of the dynamic stiffness is shown in Figure 2-22. At low frequencies dynamic stiffness will be equal to the static stiffness and with increasing frequency drop to a minimum because of the equivalent stiffness and damping of the system. If the stiffness is increased and the damping decreased the minimum will become lower and more prominent. After the minimum the stiffness will start to increase because of the inertia of the rotor [20].

The functional blocks in Figure 2-1 determine to bandwidth of the AMB system as explained above. If the bandwidth of the system should decrease the minimum of the dynamic stiffness as shown in Figure 2-22 will also decrease to a new minimum. This decrease can be contributed to the decrease in equivalent damping. Equivalent damping is equal to the differentiator and current gain as determined in (2-16), this means that if one of these constants should change the damping of the system will also change. The only component in the AMB that can have an effect on the constants is the PA. If the system starts to run into bandwidth problems the PAs starts to reduce the current gain and there by reducing the damping of the system. This effect then reduces the minimum of the dynamic stiffness as shown in Figure 2-22.

To conclude, the main focus of the dynamic stiffness is to predict the stiffness of the system at a specific frequency and to determine the absolute minimum of the stiffness. This information can then be used to design the filters, controller, electromagnets and power amplifiers to meet the specified stiffness at the operating speed.

## 2.5 AMB damping

The damping $b_{eq}$ of a system determines the decay rate $\sigma$ of the ringing after a disturbance force as shown in Figure 2-23. The frequency of the ringing is determined by the stiffness $k_{eq}$.

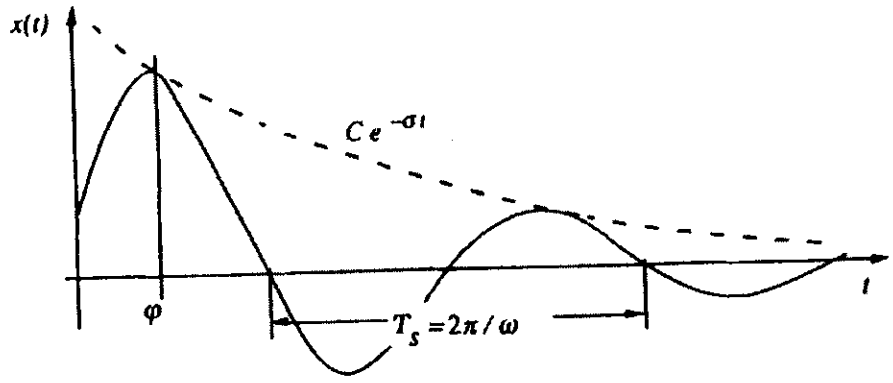


**Figure 2-23: Transient response with frequency $\omega$ and decay rate $\sigma$ [19]**

Damping can reduce noise and keep the system stable. The system becomes unstable for a damping value arbitrarily close to zero and amplifies noise with a high damping constant. A high damping factor is obtained by increasing the differentiator constant ($K_D$) in the controller. A high $K_D$ value will amplify the input of the differentiator path and therefore amplify noise if there is noise on the input signals.

The best damping constant for the AMB system should be between these two extremes and can be determined with (2-19). (2-19) shows that damping is dependent on the equivalent stiffness of the system making the stiffness the most important variable [6].

$$b_{eq} = 2\zeta\sqrt{m.k_{eq}} \tag{2-19}$$

If a study should be done on the characteristics of the stiffness the damping will also be included into the study because it is stiffness dependent. For this reason the focus of the study will mainly be on the stiffness and characteristics of stiffness.

## 2.6 System sensitivity

System sensitivity is the ratio of the change in the system transfer function to the change of a process function (or parameter) for a small incremental change. The sensitivity is readily obtained by using (2-20)

$$S_G^T = \frac{1}{1+G} = \frac{T}{G} \tag{2-20}$$

with $T$ the system transfer function and $G$ the forward path as shown in Figure 2-24 [19].

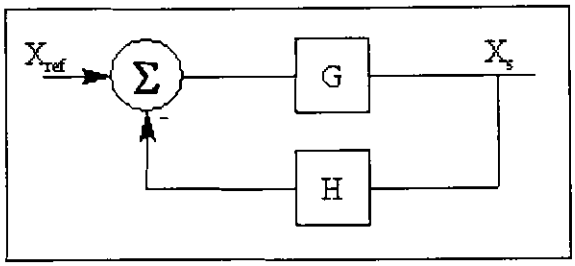


**Figure 2-24: A closed-loop control system**

The system transfer function is given by

$$T = \frac{X_s}{X_{ref}} = \frac{G}{1+G} \tag{2-21}$$

and the forward path by

$$G = \frac{X_s}{E}. \tag{2-22}$$

If (2-21) and (2-22) are substituted into (2-20) the sensitivity of the feedback system is given by (2-23)`

$$S_G^T = \frac{X_s}{X_{ref}} \frac{E}{X_s}$$

$$= \frac{E}{X_{ref}} \tag{2-23}$$

(2-24) is used to obtain the system sensitivity at specific frequencies in dB [3].

$$G_s(s) = 20 \cdot \log \frac{E}{X_{ref}} \tag{2-24}$$

The standards for the sensitivity of a system are discussed in the ISO CD14839-3 [22]. This international standard applies to industrial machines operating at nominal power greater than 15 kW, and is not limited by size or operational speed. These standards are shown in Table 2-1 and will also be used to determine the standard of the in-house developed AMB system.

**Table 2-1 Criteria of zone limits [22]**

| Zone | Peak of sensitivity |
|---|---|
| A/B | 8 dB |
| B/C | 12 dB |
| C/D | 14 dB |

**Zone A:** The sensitivity function of newly commissioned machines would normally fall within this zone.

**Zone B:** Machines with the sensitivity functions within this zone are normally considered acceptable for unrestricted long-term operation.

**Zone C:** Machines with the sensitivity functions within this zone are normally considered unsatisfactory for long-term continuous operation.

**Zone D:** The sensitivity function of machines within this zone is normally considered to be sufficiently severe to cause damage to the machine [22].

*The knowledge areas applicable to this study were discussed in this chapter. The type of filter that should be used for the different kinds of noise can be based on the literature specified. Stiffness, damping and sensitivity are also explained in this chapter. The next chapter discusses the noise analysis.*

# 3
# Chapter

# Noise analysis

*This chapter focuses on noise problems in the AMB system. The noise sources are identified, its impact assessed and solutions are devised where necessary.*

## 3.1 AMB noise

Analysis of the double radial heteropolar AMB has revealed certain noise problems. The most observable noise problem of the AMB is acoustic noise. The noise analysis also revealed that acoustic noise was not the only source of noise in the AMB. There are two other noise sources that should be measured and reduced: radiated noise and conducted noise.

## 3.2 Radiated noise

There are two types of radiated noise, magnetic and electric radiation that should be measured. Both can be measured by using an analogue spectrometer. The effect of the radiated noise can also be determined by comparing the FFT (Fast Fourier Transform) of the measured radiated noise on the sensor signals and coil currents.

A calibrated antenna is needed to measure the electric and magnetic radiated noise when the analogue spectrometer is used. The two types of radiated noise can be distinguished because they are perpendicular. By holding the antenna at different angles, the two can be measured independently. These antennas are very costly and for demonstrational purposes a coil is used to measure the noise. The coil is connected to the scope probe and FFTs of the measured signals are drawn as illustrated in Figure 3-1 and Figure 3-2.

If this method of measuring the radiated noise is used and the antenna is not calibrated the magnitude will not be of the right order but the energy peaks will be at the same frequency. The electric radiated noise is illustrated in Figure 3-1 and the magnetic radiated noise in Figure 3-2. This was measured by

turning the antenna at the PA and electromagnets till the highest energy components are measured. It is also observed that the two measurements have a ninety degree antenna position change between the two measurements which shows that it is electric and magnetic radiation noise that is received.

Figure 3-1 and Figure 3-2 shows energy components at 50 Hz and around 100 Hz that can have a big effect on the control of the system. The high energy components at high frequencies are a problem but can be filtered with a low pass filters if they should become conducted noise.

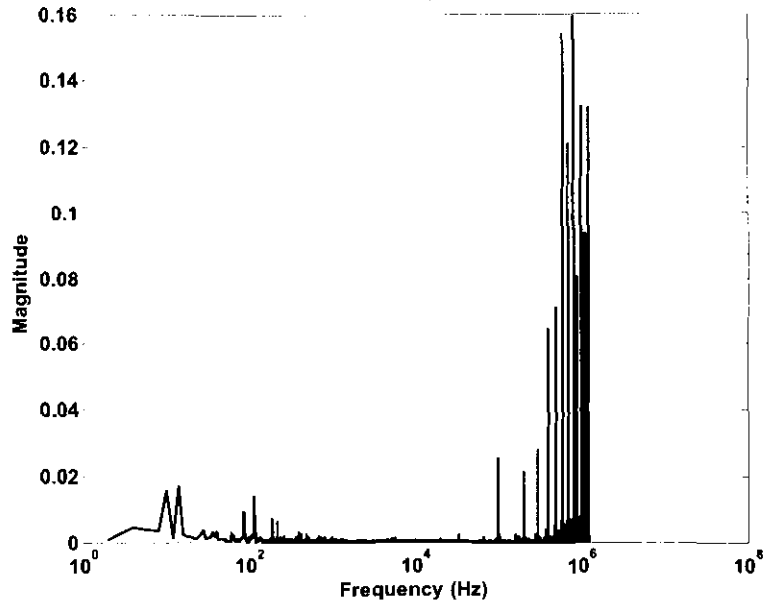


**Figure 3-1: Electric radiated noise from the PAs**

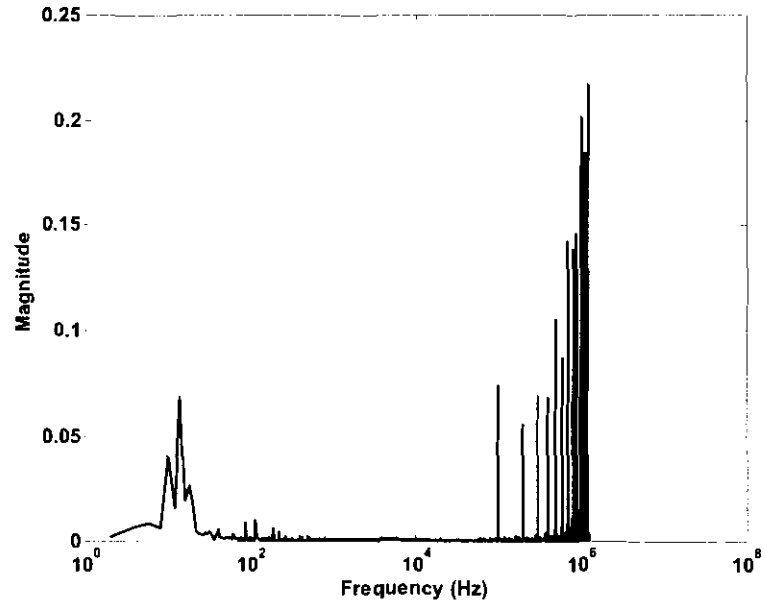


**Figure 3-2: Magnetic radiated noise from the electromagnets**

To determine if radiated noise is a problem in the system, the FFTs of the sensor signals are measured (Figure 3-3). The FFT is then compared to the radiated noise spectra to see if the same high energy

components occur in both sets of spectra. If the high energy components correlate, radiated noise can be assumed.

A comparison between Figure 3-1, Figure 3-2 and Figure 3-3 showed that the same frequency components occur in al three sets of data. The energy components are smaller in some of the FFTs but they are there.

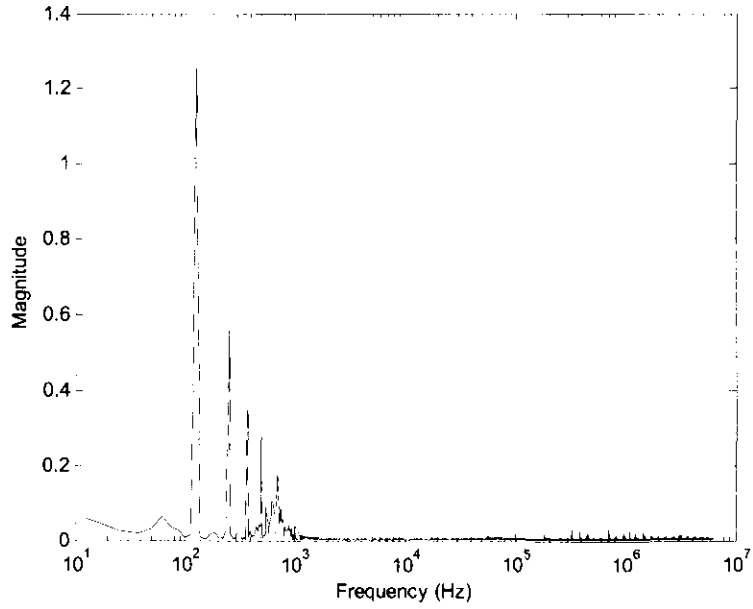


**Figure 3-3: FFT of the sensor signals**

To minimise the effect of the radiated noise, the signals can be measured in noise free areas of the position signal (sec 3.4) or filters can be implemented in the system. Shielding can also be used, but this is very expensive to implement.

## 3.3 Conducted noise

There are two types of conducted noise that should be analysed: the one is where the radiated noise becomes conducted noise as discussed in section 3.2 and the other is because of aliasing and imaging.

### 3.3.1 *Aliasing*

The aliasing noise is determined by measuring the position signal after the controller as illustrated in Figure 2-4. This measured signal is then used in an FFT to determine the high energy components in the frequency spectrum as illustrated in Figure 3-4.

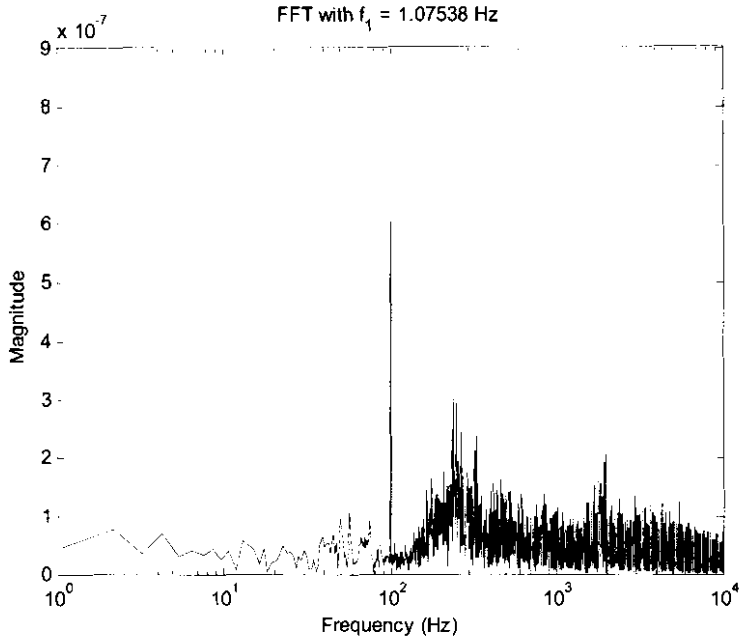


**Figure 3-4: Frequency spectrum of the sensor signal in dSPACE**

If Figure 3-4 is compared to the FFT of the position signal before the ADC in Figure 3-3 it is seen that a high energy component is added around 115 Hz. This high energy component can be attributed to the aliasing since Figure 3-4 and Figure 3-3 are the same signals but with an ADC between them.

### 3.3.2 *Imaging*

Imaging occurs after the controller as shown in Figure 2-6 which means that the imaging noise will have a direct influence on the power amplifier (sec 2.2.2). Any deviation from the precise control current will decrease or increase the current through the coils which implies that the rotor will not be in the middle of the magnets.

Figure 3-5 shows high energy components at 1 MHz and 10 MHz. These components are at high frequencies and can be filtered with an AIF (low pass filter).

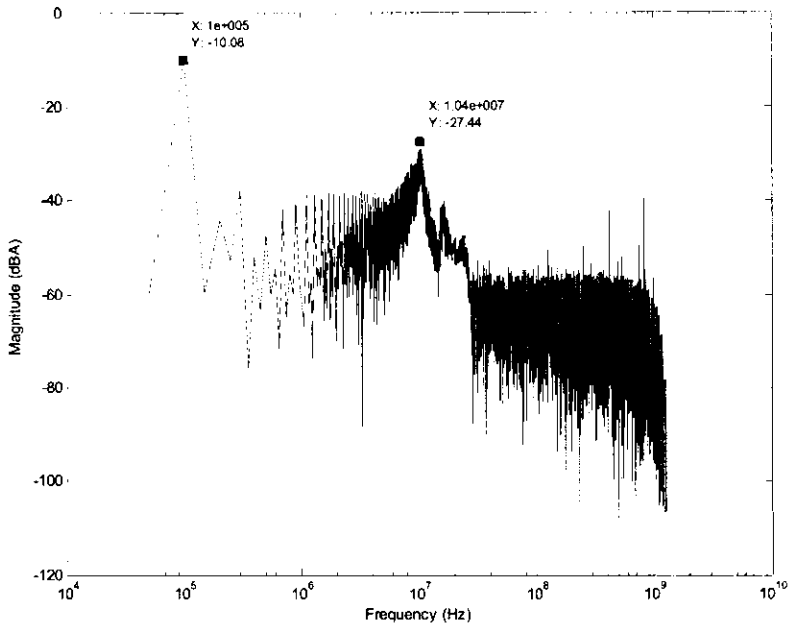


**Figure 3-5: FFT of the reference current**

## 3.4 Synchronisation

From Figure 3-6 it is evident that the 100 μm horizontal step response has a noise factor that seems to be periodic. This periodic noise can be attributed to aliasing and the radiated noise from the switching PA. From Figure 2-9, the coil current and voltage of the magnetic actuator, it is seen that the switching noise of the power amplifiers are periodic.

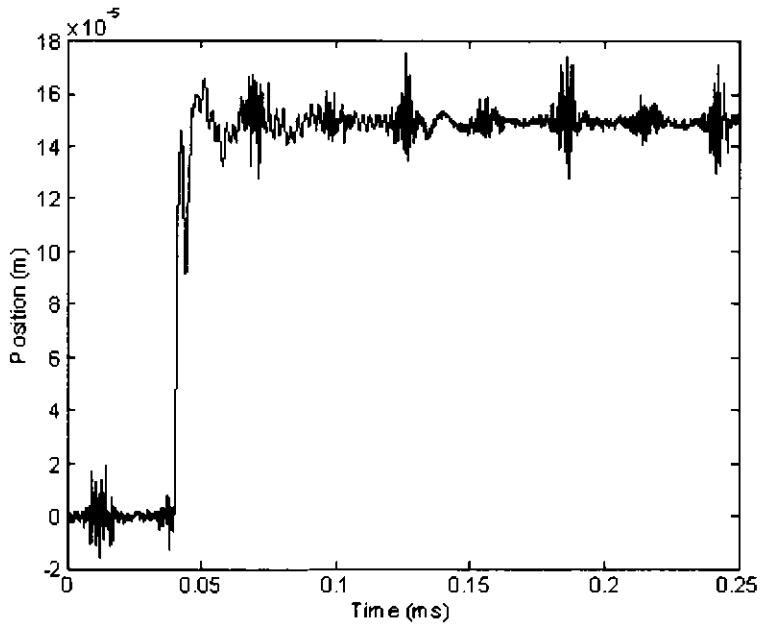


**Figure 3-6: Horizontal step response using asynchronous sampling**

To simulate this periodic occurrence of the noise a dc signal with 10 MHz noise at 10 μs intervals (Figure 3-7) is sampled at 20 kHz. The sampling of the signal is synchronised with the noise to not sample when the noise occurs as can be seen in Figure 3-8.

Because of inaccuracies in timing, it is almost impossible to accomplish this when using an asynchronous sampling scheme. The effect of asynchronous sampling is simulated by sampling the signal at 20.1 kHz, as illustrated in Figure 3-9. The figure clearly shows how the high-frequency noise now appears as a periodic low-frequency aliased signal.

Synchronous sampling can alleviate the aliasing effect of high-frequency temporal deterministic noise. This concept was also employed in the sampling scheme of the double radial AMB model in order to reduce the impact of the high-frequency noise caused by the switching of the power amplifiers as shown in Figure 2-9.

The simulation therefore confirms that the aliasing of the system is a problem and that the synchronisation can reduce the aliasing noise.

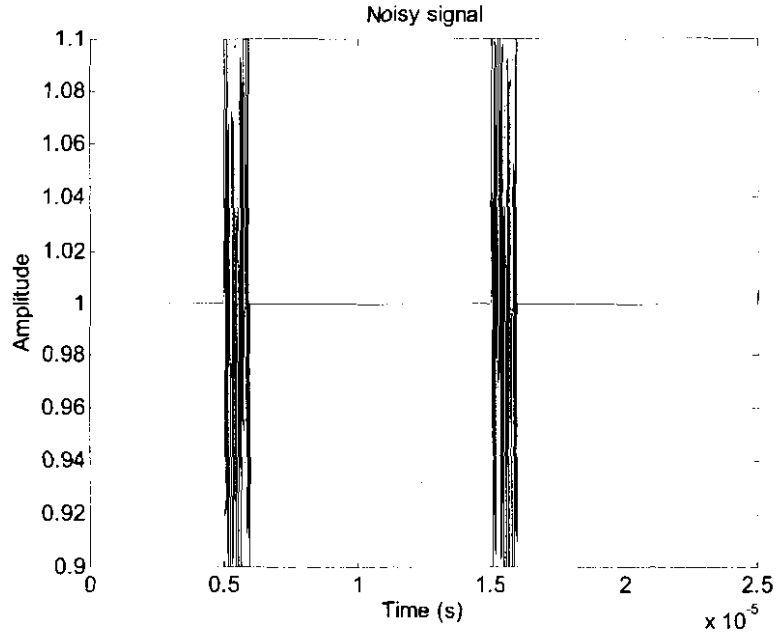


**Figure 3-7: Noisy signal**

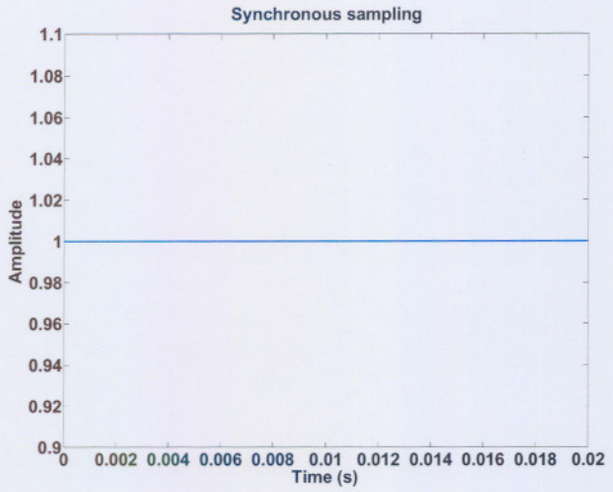


Figure 3-8: Synchronous sampling

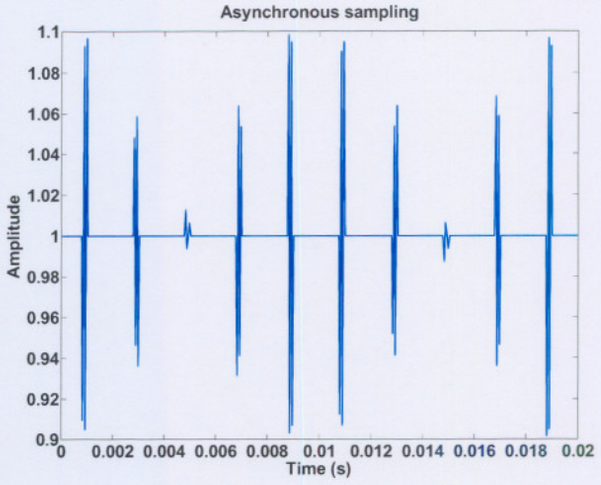


Figure 3-9: Asynchronous sampling

### 3.4.1 *Implementation on double radial AMB model*

The power amplifiers are synchronised using the rising edge of a PWM output of the dSPACE controller. As seen in Figure 3-10, there is a time delay between the sync signal and the actual switching of the power amplifiers, followed by some ringing of the coil current as illustrated in Figure 2-9. The ADC of all the position sensors are then synchronised with the falling edge of the synchronisation signal. By controlling the duty cycle of the PWM signal in the control software, the time delay between the synchronisation signal and the ADC conversion is set. A PWM duty cycle of 40% was determined to be adequate as shown in Figure 3-10.

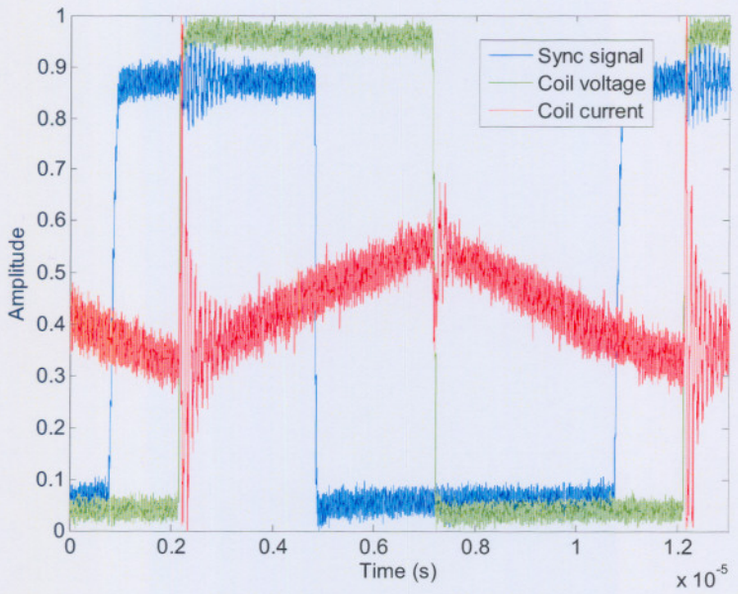


Figure 3-10: Measurements on AMB model

The effect of the synchronous operation on the characteristics of the double radial AMB model is quite profound. The audible noise produced is noticeably reduced and the position signal contains very little noise, as seen in the 100 μm horizontal step response of Figure 3-11.

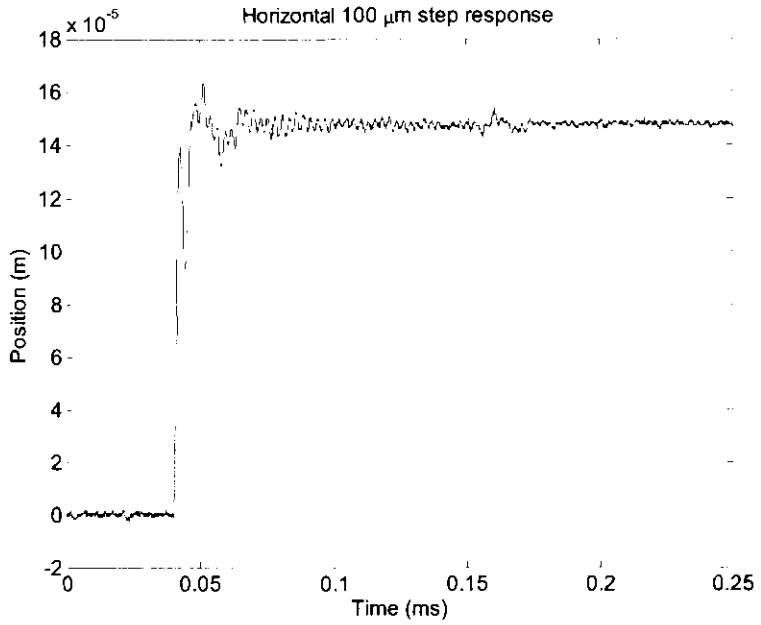


**Figure 3-11: Horizontal step response using synchronous sampling**

## 3.5 Anti-Aliasing Filter (AAF)

An anti-aliasing filter is a low pass filter used before the ADC to prevent aliasing in the sampled signal. As mentioned earlier, aliasing is prevented by removing frequency components higher than half the sampling frequency from the signal. When a 16-bit ADC is used, these frequency components must be attributed by 96 dB. Unfortunately these requirements result in a high order filter which will introduce a large phase shift that is undesired. The phase shift and time delay of the filter is important because it can have a big influence on the real time control of the AMB.

To find the best filter for the application the filters in section 2.3 were compared and it was found that the RC filters has the lowest time delay and phase shift of all the filters. The only drawback of the RC filter is the low attenuation of the filter between the pass and stop band.

Since the RC filter has the lowest time delay and phase shift of all the filters it was decided to use this filter as the anti-aliasing filter.

### *3.5.1 Anti-aliasing filter simulation*

To simulate a filter the cut-off frequency and type of filter should be known. For this application it was decided to use RC filters. The cut-off frequency of the filter is dependent on the bandwidth of the system and the sampling time of the ADC. If the cut-off frequency of the filter is too low the bandwidth of the system will decrease to the cut-off frequency of the filter. Therefore, the cut-off frequency should be as low as possible without having an effect on the system bandwidth.

The maximum working frequency of the system is 30 000 rpm or 500 Hz. Consequently the filter should not have a phase shift or time delay at that frequency. To have no phase shift or time delay at the working frequency the cut-off frequency of the filter was determined to be 2.77 kHz.

The simulated sensor signal with the noise is shown in Figure 3-12 and the signal after the filter in Figure 3-13. From the two figures it is seen that the noise is drastically reduced and that the measured sensor signal is closer to the theoretical position of the rotor.

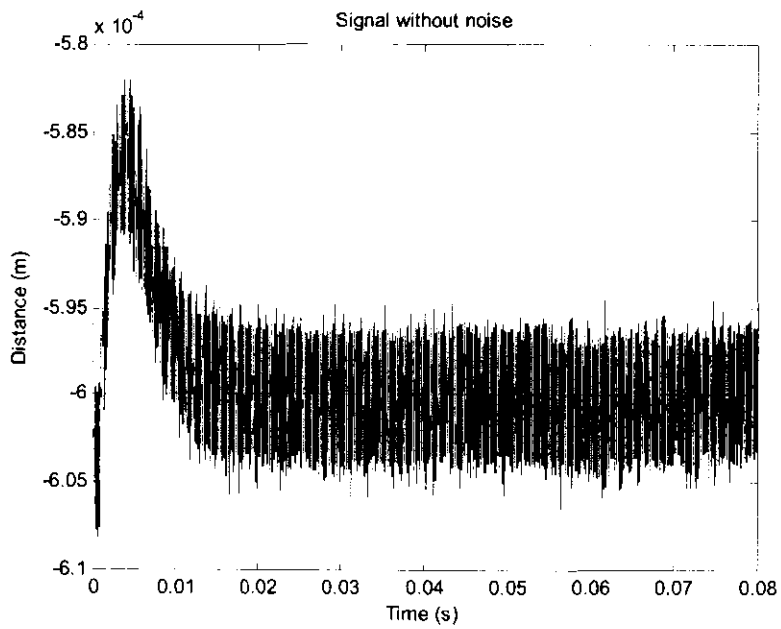


**Figure 3-12: Position signal before the RC filter**

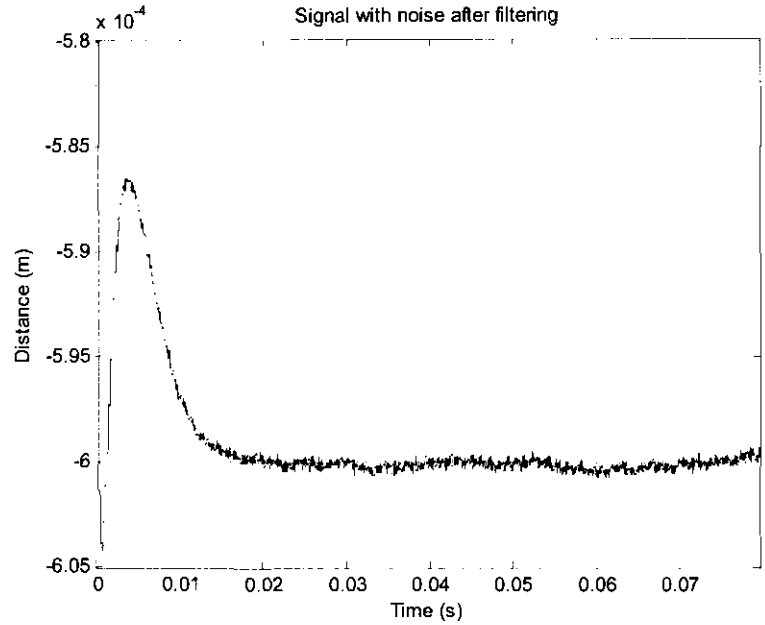


**Figure 3-13: Position signal after the RC filter**

### *3.5.2 RC filter design*

By using the cut-off frequency obtained in the simulation and a resistor value of 10 kΩ the capacitor value is determined.

$$C = \frac{1}{2\pi Rf} \tag{3-1}$$

$$= \frac{1}{2\pi(10\times10^{3})(2.77\times10^{3})}$$

$$= 5 \text{ nF}$$

A 4.7 nF capacitor is therefore used for an RC filter with a cut-off frequency of 2.77 kHz. The sensor signal before the RC filter is shown in Figure 3-14 and after the filter in Figure 3-15. From the two figures it is clear that the filter has a big influence on the signal to noise ratio of the sensor signal; the signal after filtering showing a 33 % improvement.

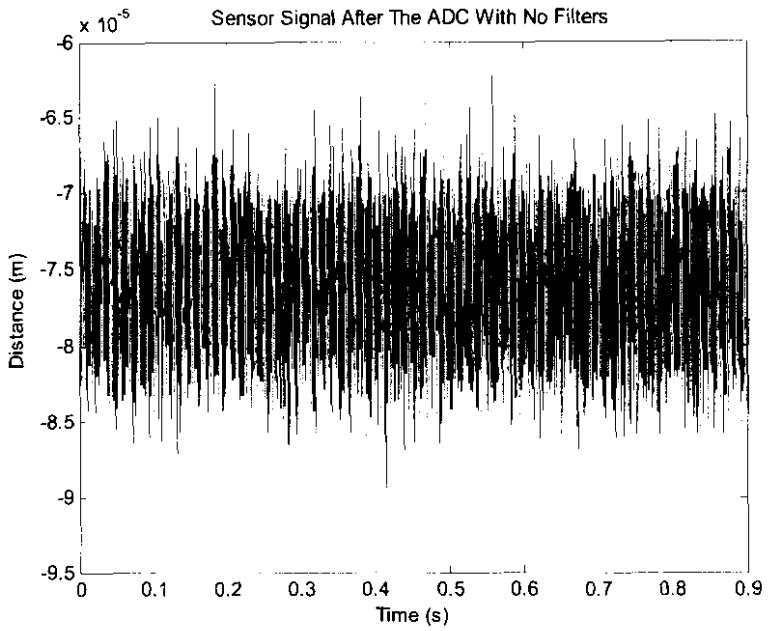


**Figure 3-14: Sensor signal after the ADC with no filters**

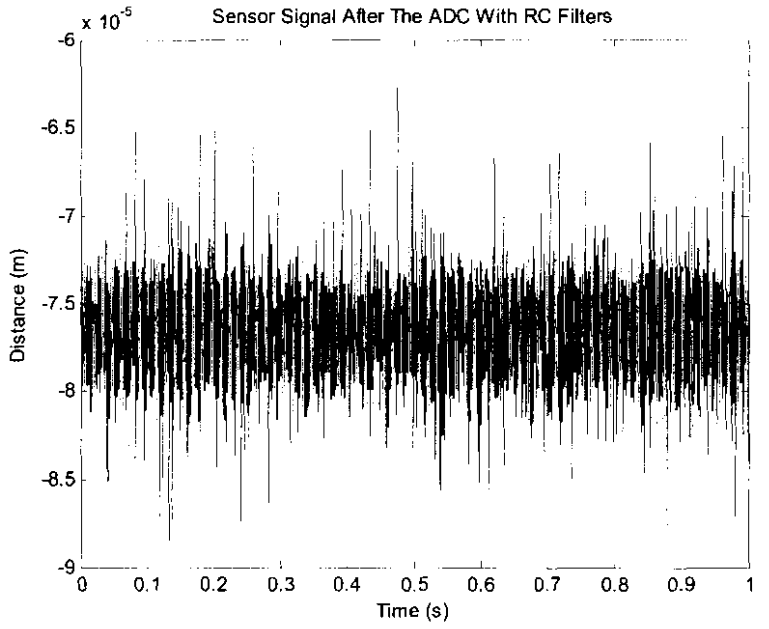


**Figure 3-15: Sensor signal after the ADC with a RC filter**

## 3.6 Anti-Imaging Filter (AIF)

The imaging frequency is higher than the Nyquist frequency as mentioned in section 2.2.2. An RC filter would then be the best option for this application because of its low attenuation at low frequencies.

The anti-imaging filter should be placed after the DAC and before the power amplifier in the AMB system. To do this the filter was placed before the error amplifier of the PA as illustrated in Figure 3-16.

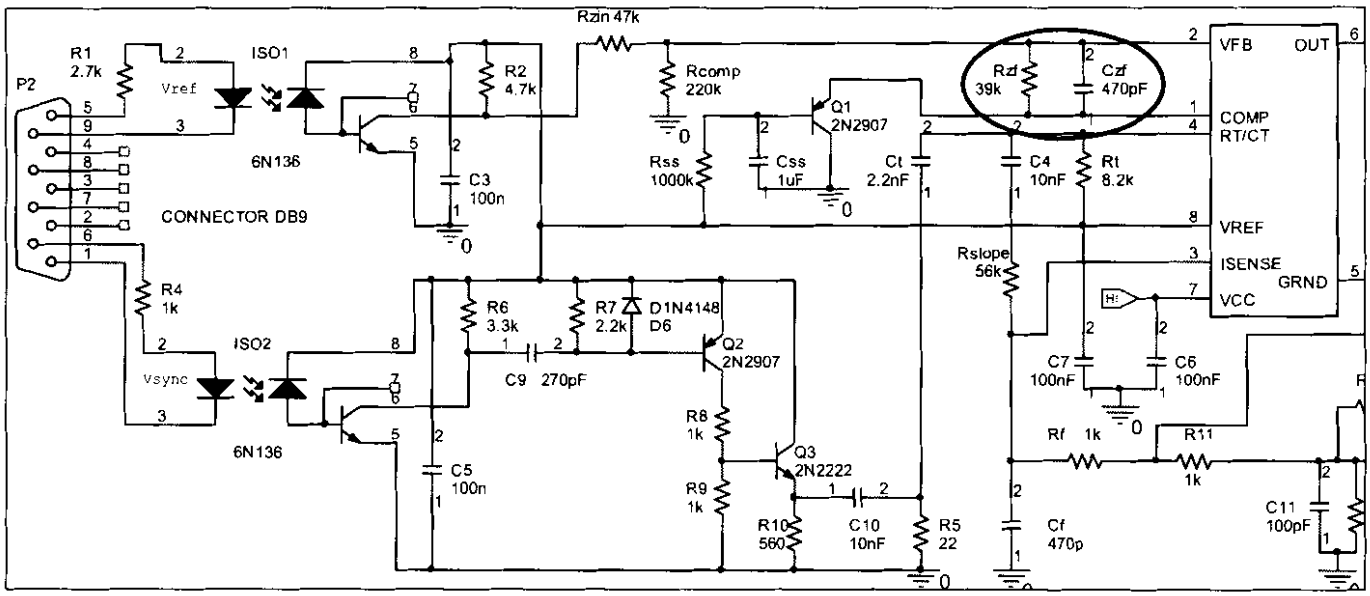


**Figure 3-16: RC filter before the error amplifier [3]**

### *3.6.1 RC Filter Design*

Keeping the bandwidth of the bearing at 500 Hz and ensuring a low phase shift and time delay at that frequency the cut-off frequency of the filter was determined to be 2.77 kHz. The cut-off frequency and the resistor value of 39 kΩ are used to determine the capacitor from (3-2).

$$C = \frac{1}{2\pi Rf} \tag{3-2}$$

$$= \frac{1}{2\pi(39\times10^{3})(2.77\times10^{3})}$$

$$= 1.47 \text{ nF}$$

The RC filter used as an anti-imaging filter uses the resistor in the circuit as shown in Figure 3-16 and a 1 nF capacitor in parallel with the 470 pF capacitor.

Figure 3-17 shows the simulated reference current before filtering and Figure 3-18 the reference current after filtering. The reference current controls the PA to deliver the desired current to the electromagnets. A big improvement is shown between Figure 3-17 and Figure 3-18 because of the filter. The output of the filter has a smoother transition and a slower settling time than the unfiltered reference current.

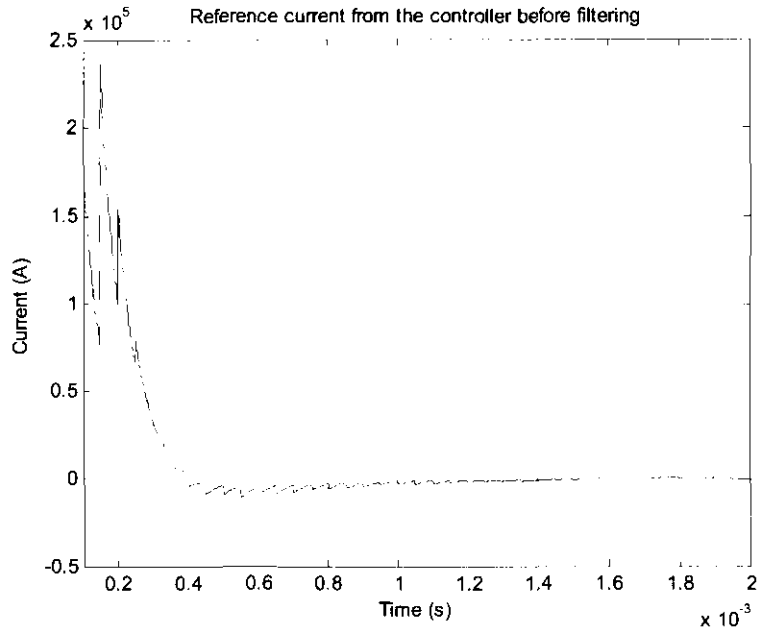


**Figure 3-17: Reference current from the controller before filtering**

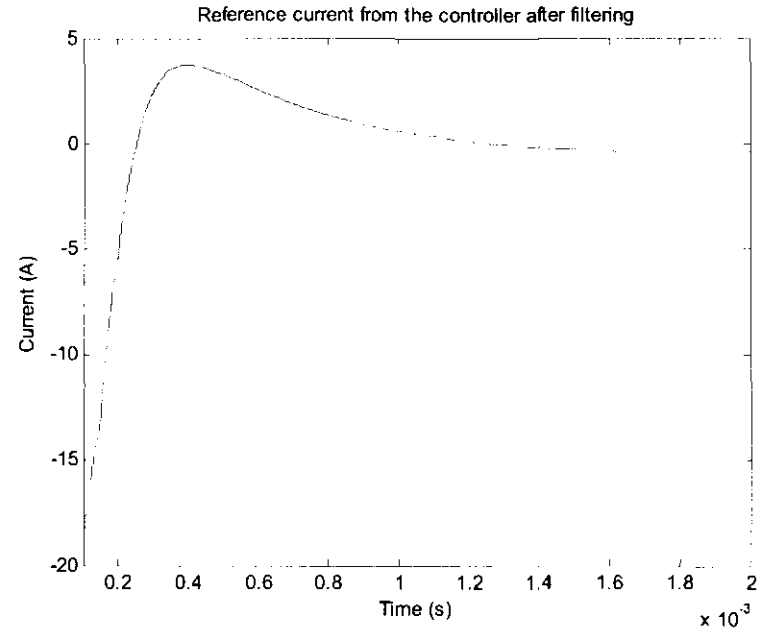


**Figure 3-18: Reference current from the controller after filtering**

## 3.7 Common Mode Filter

Common mode noise is caused by internal EMI currents that flow out through output lines seeking a return path back to the noise source. The best way of reducing the common mode noise is to filter the noise as close as possible to the noise source. Common mode loops can be formed in the cables to and from the PC which means that the noise should be filtered before the ADC and after the DAC as illustrated in Figure 3-19.

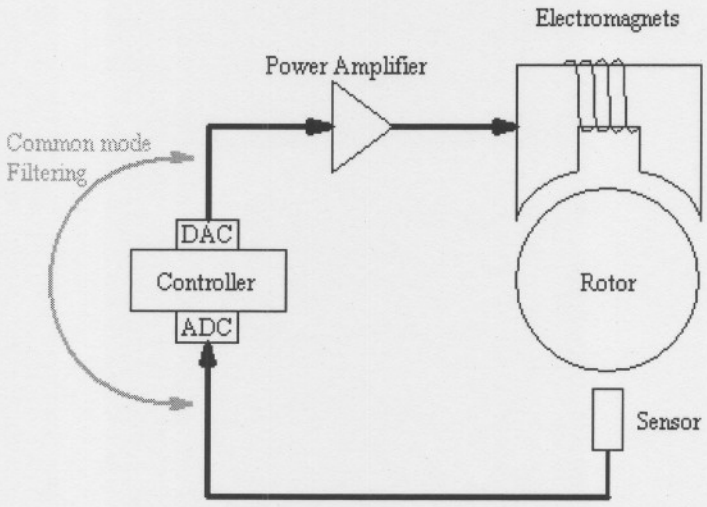


**Figure 3-19: Common mode filtering**

Ribbon cable ferrite beads are used as common mode filters. These beads are placed around each ribbon cable as shown in Figure 3-20. The filter attributes to the reduction of acoustic noise and noise on the position signals.

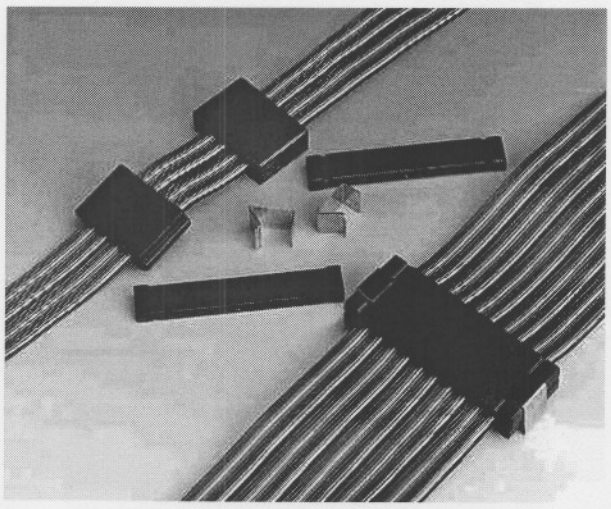

**Figure 3-20: Common mode filters on the ribbon cable**

## 3.8 Filter simulation results

The MATLAB® simulation of the AMB system shows good correlation to the analytical predictions as well as to the experimental results. Further refinement of the simulation model is however needed to improve testing and characterisation of the filters.

The first step in refining the system simulation is to include noise with the same spectral characteristics as the actual noise, in the position signal. High energy components should be added to the random noise at 100 kHz and at 10 MHz to replicate the sensor noise as indicated in Figure 3-3. This imitation of the position signal is then used to test the filters and find the best cut-off frequencies.

The anti-aliasing, anti-imaging and controller filters are applied to the signals in Figure 3-12 and Figure 3-17 to give the output signals shown in Figure 3-13 and Figure 3-18. The signal to noise ratio of the sensor signal after the filters is more than two times the original signal to noise.

Filters in the AMB system is a trade off between the signal to noise ratio and the stiffness and damping. The overshoot in the position signal (Figure 3-21) before settling can be attributed to the time delay and phase shift of the filters. If the filters and noise are removed from the position signals and current reference, the position signal will have no overshoot or ripple as shown in Figure 3-21 with the light line. This proves that the filters have an effect on the stiffness and damping of the system.

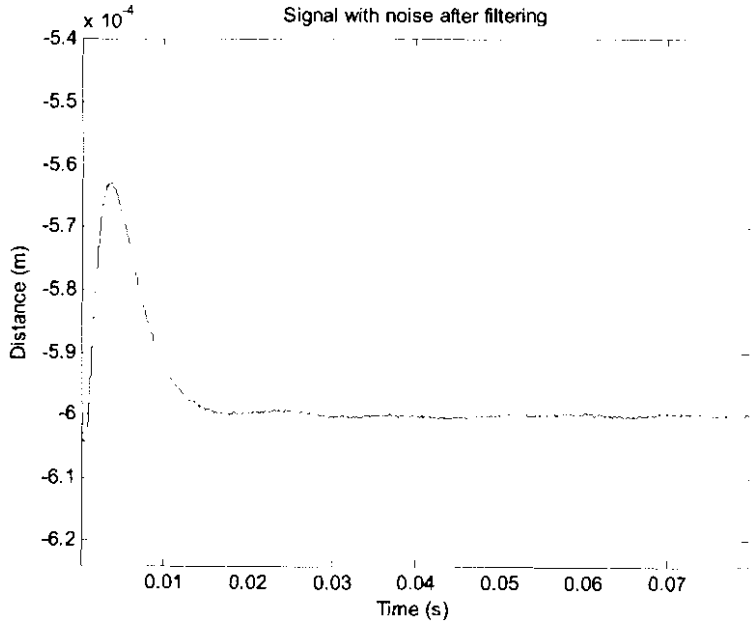


**Figure 3-21: Sensor signal with noise after filtering**

### 3.8.1 *Filter effects*

This study of filter effects are done to determine which filter has the biggest influence on the stability of the AMB system. The controller is used to test the stability. $K_D$ is kept constant and *Kp* is increased to the point were the system becomes unstable. The filter effects are then test by starting with the same cut-off frequency and then increasing *Kp* to the point were the system becomes unstable. The cut-off frequencies of the filters are then increased one by one to determine the minimum cut-off frequencies of the filters were the system is still stable for a high *Kp*. The filter with the highest cut-off frequency before the system becomes stable has the biggest influence on the stability of the system.

The following Kp values were used to determine the response of the system for specific cut-off frequencies.

*Kp* = 12500 (Blue)
= 20000 (Red)
= 40000 (Green)

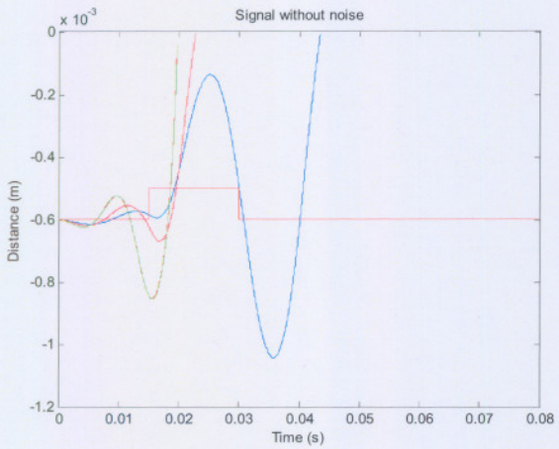


**Figure 3-22 : AMB response with anti-imaging and controller filter cut-off at 80 Hz**

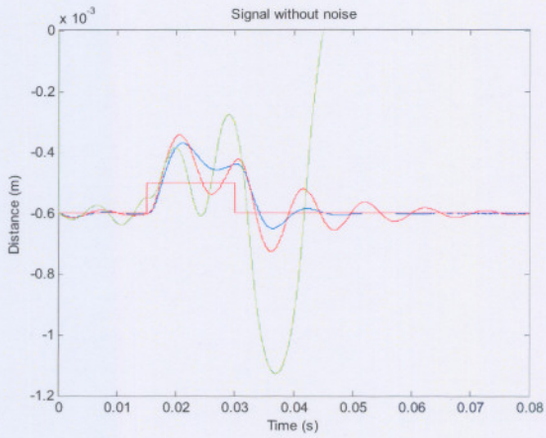


**Figure 3-23: AMB response with anti-imaging and controller filter cut-off at 500 Hz and 160 Hz**

When comparing Figure 3-22, Figure 3-23, Figure 3-24 and Figure 3-25 it is seen that the system starts to become unstable when the cut-off frequencies of the filters are too low. From Figure 3-23 to Figure 3-25 it can be seen that the anti-imaging filter has the biggest influence on the bandwidth of the system and for this reason the anti-imaging filter has the higher cut-off frequency of the two filters.

The effect of the anti-aliasing filter (AAF) is tested in Figure 3-26 and Figure 3-27. The first test (Figure 3-26) is done on the order of the filter with a constant *Kp* value of 12500 and the second test on the cut-off frequencies of the filter as illustrated in Figure 3-27. From these figures it can be seen that a second

order low pass filter with a cut-off frequency of 2.77 kHz would leave the system stable. This cut-off frequency is the same as the AIF and for this reason it can be said that the AAF and AIF has the most influence on the stability of the system.

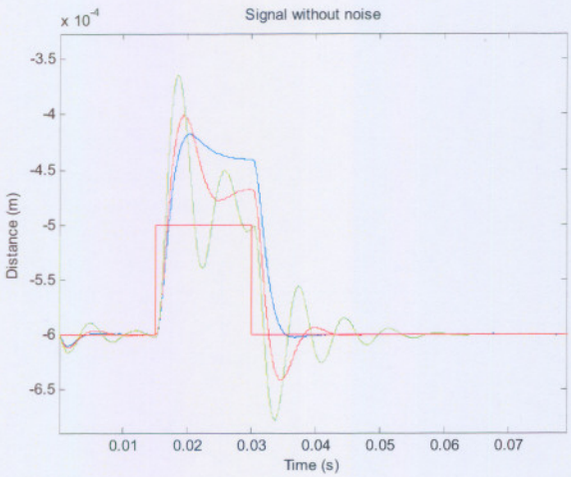


**Figure 3-24: AMB response with anti-imaging and controller filter cut-off at 500 Hz**

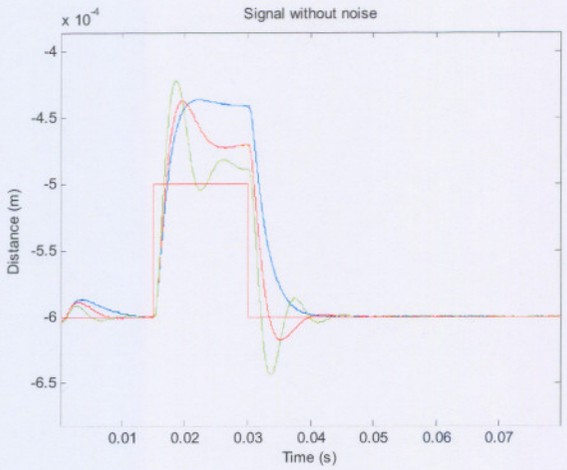


**Figure 3-25: AMB response with anti-imaging and controller filter cut-off at 2.77 kHz and 500 Hz**

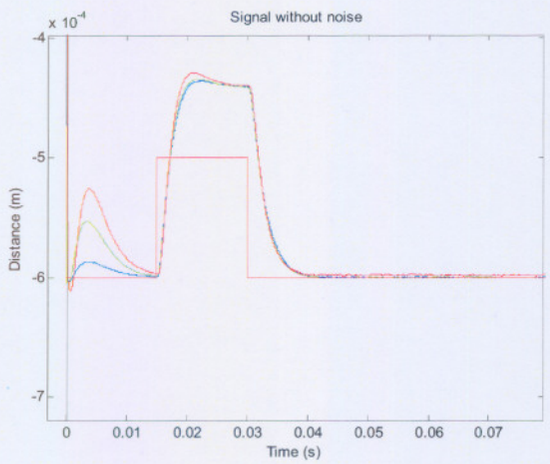


**Figure 3-26: AAF 5 kHz – second- (blue), fourth- (green), eight- (red) and sixteenth order (black)**

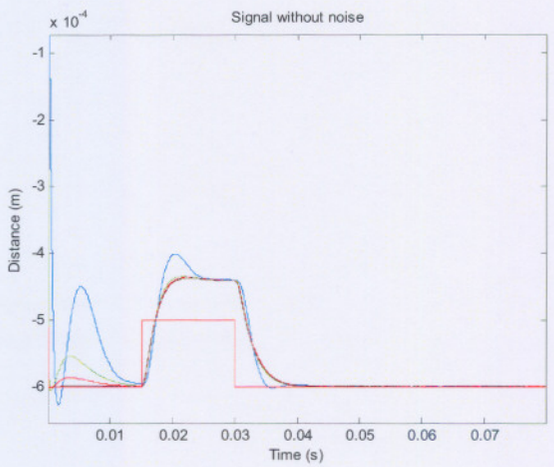


**Figure 3-27: AAF second order with a cut-off frequency of 500 Hz(blue), 2.77 kHz (green), 5 kHz (red) and 10 kHz (black)**

This proves that the AAF and AIF have the biggest influence on the stability of the AMB system and that there cut-off frequencies should be evaluation thoroughly before implementation.

*The first half of chapter 3 discussed and analysed the noise problems on the AMB system. The second half devises solutions to the noise problem. The AMB comparison with the MSD is discussed in chapter 4.*

# 4
# Chapter

# AMB equivalence to Mass-Spring-Damper

*The AMB and its equivalence to the Mass-Spring-Damper (MSD) system are discussed in this chapter. Both analytic and numeric methods are used to determine the static, dynamic and the second order stiffness of the MSD system. The effect of filters present in an actual system forms part of the analysis in this chapter.*

## 4.1 Analysis process

The analysis process of the AMB system starts with a linerised model of the AMB. This linerised model is equivalent to the MSD system as illustrated in Figure 2-17. The characterisation of the MSD system starts with the MSD without filters and then with filters as illustrated in Figure 4-1. The MSD system is analysed analytically with a bode-diagram and also numerically in MATLAB®. The results obtained from the MSD analyses are compared. These results are also referred to in chapter 5 for comparison to the actual system results.

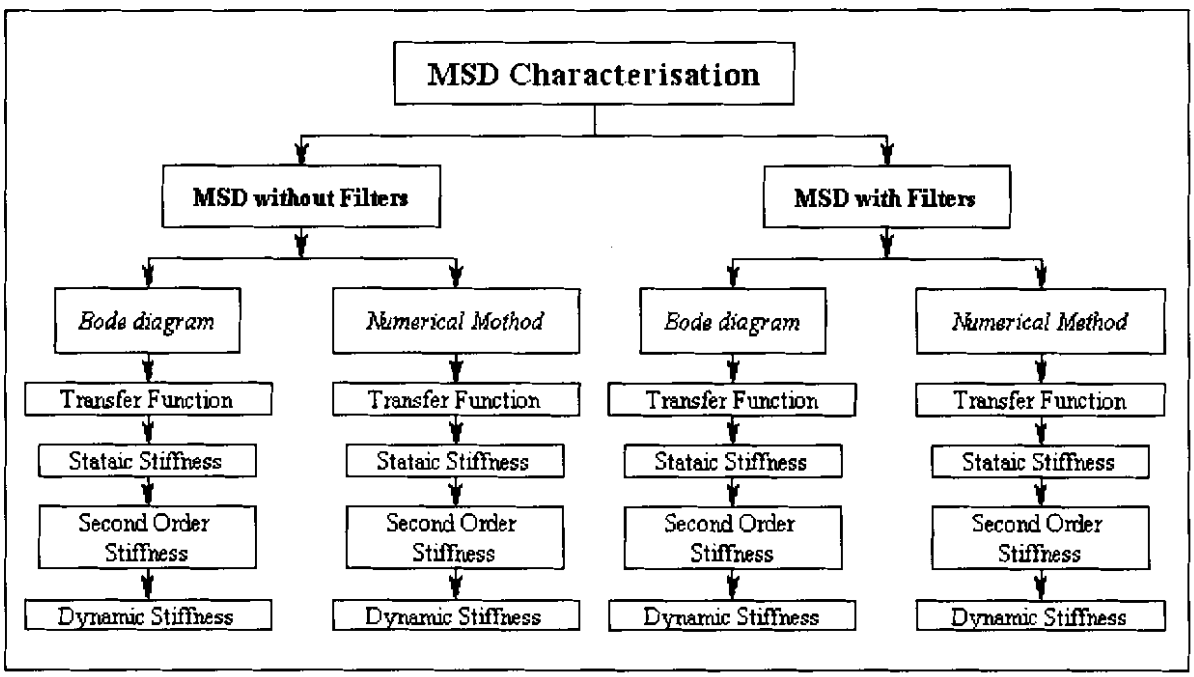


**Figure 4-1: MSD analysis process**

## 4.2 MSD characterisation

The simulation used in this chapter is a linerised AMB model as shown in Figure 4-2. Figure 4-2 is not the same as the model in Figure 2-18 since the damping force is fed back from the position and not from the output of the first integrator. This change in the block diagram does not change the transfer function of the two systems which leaves Figure 4-2 with (2-11) as the transfer function.

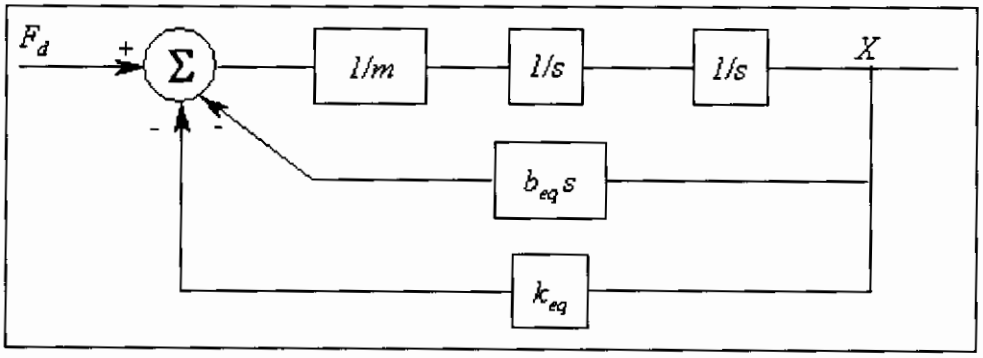


**Figure 4-2: MSD block diagram with no filters**

### *4.2.1 Static stiffness*

Static stiffness of the MSD is determined by using a disturbance force or by using the dynamic stiffness plot as explained in section 2.4.2.

#### Disturbance force

The disturbance force method of obtaining the static stiffness of the MSD is demonstrated in Figure 5-12 where an external force is applied to the mass and the deflection is measured. The static stiffness of the MSD is obtained by substituting the disturbance force $m_d g$ and deflection $x$ into (4-1). A small disturbance mass ($m_d$) added to the ball in Figure 2-17 is used as the disturbance force and the deviation from the equilibrium as the deflection ($x = x_1 - x_2$). A deflection from the equilibrium is shown in Figure 4-3. Therefore the stiffness determined from the disturbance force is

$$k_{ss} = \frac{m_d \cdot g}{x_1 - x_2} \qquad \textbf{(4-1)}$$

$$= 4.99 \times 10^5 \text{ N/m}$$

which is equal to the theoretical stiffness given in section 4.2.1(a).

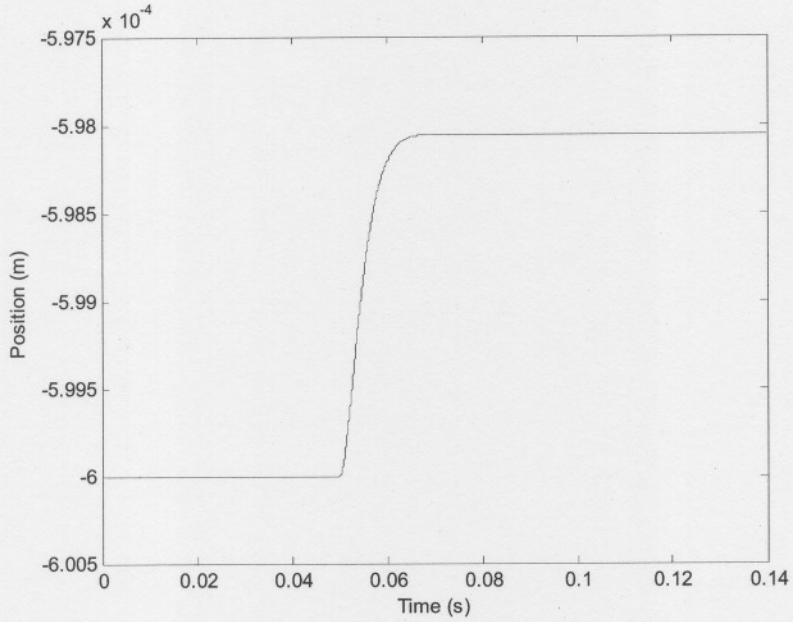


**Figure 4-3: Disturbance response of the MSD simulation**

The static stiffness for different deviations is shown in Figure 4-4. This constant stiffness shows that the stiffness of the MSD is not dependent on the magnitude of the deviations or forces applied to the mass.

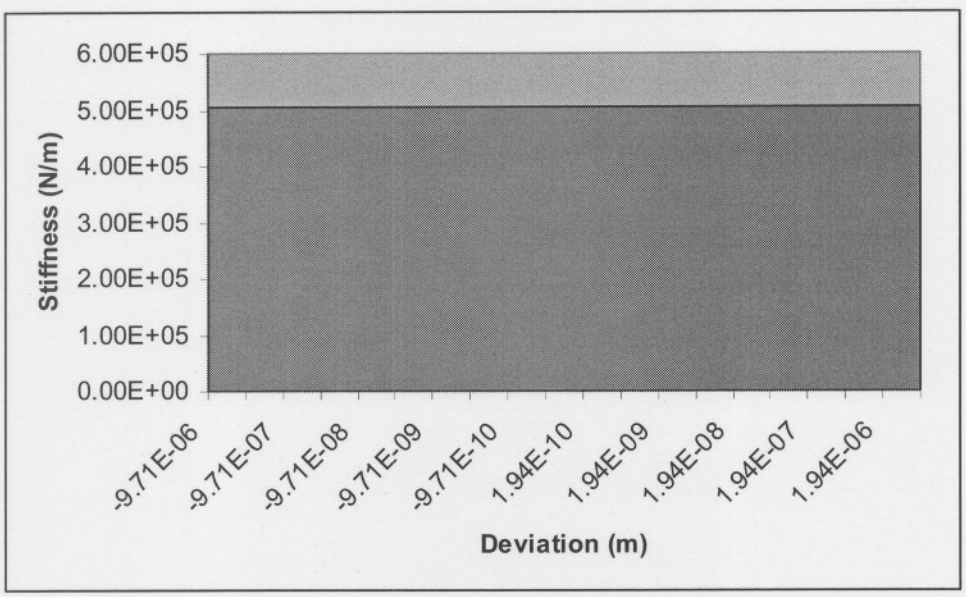


**Figure 4-4: Stiffness vs. deviation plot of the MSD**

### Bode diagram

Dynamic stiffness is determined from the transfer function as explained in section 2.4.2. By inverting the magnitude plot of the transfer function the dynamic stiffness is obtained. Static stiffness is equal to dynamic stiffness at low frequencies which means that the inverce magnitude plot can be used to determine the static stiffness as shown in (4-2).

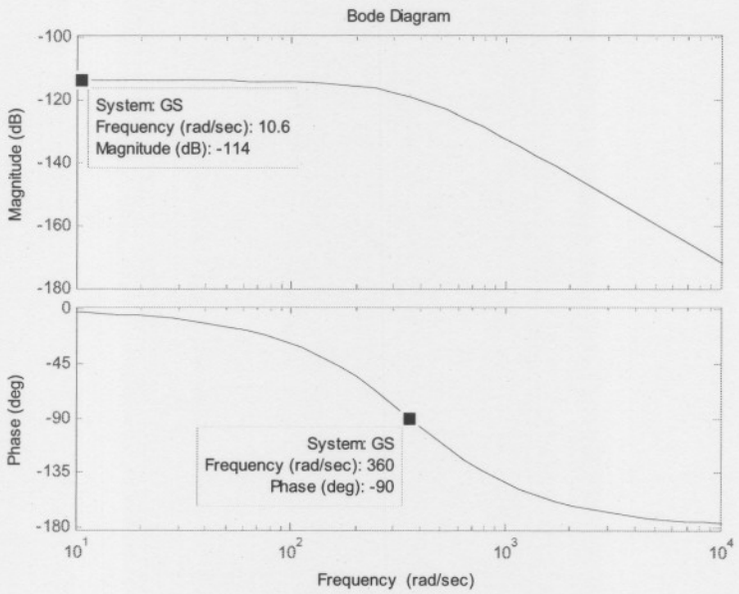


**Figure 4-5: Bode diagram from the MSD transfer function**

$$Mag = 20\log(\frac{X}{F})$$

Thus

$$k_{ss} = \frac{F}{x} = 10^{-\frac{Mag}{20}} \qquad (4\text{-}2)$$

$$= 5.0119 \times 10^5 \text{ N/m}$$

Where $Mag$ and $k_{ss}$ are the magnitude in dB and static stiffness of the system respectively. The measured static stiffness of the MSD has a 0.2 % deviation from the theoretical stiffness of $4.99 \times 10^5$ N/m.

### *4.2.2 Second order stiffness*

Second order stiffness is defined as the stiffness at the first natural frequency of the system. The first natural frequency of the MSD is obtained from the phase diagram at -90° (Figure 4-5) or from the root locus at a gain of one (Figure 4-8).

The root locus of MSD is obtained by reducing the block diagram of Figure 4-6 to Figure 4-7. After the block diagram reduction the root locus of GH is determined and not of the transfer function (4-5) [19].

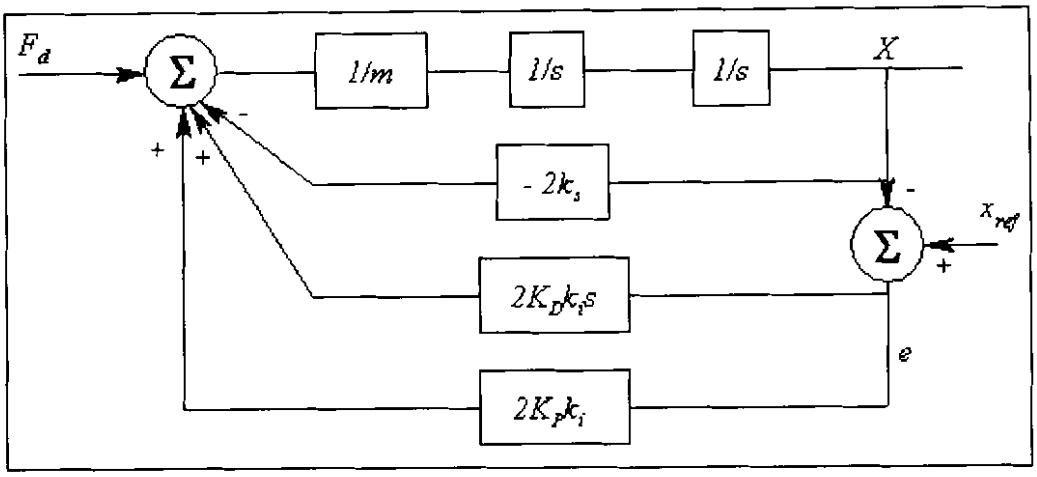


**Figure 4-6: Linear AMB block diagram with no filters**

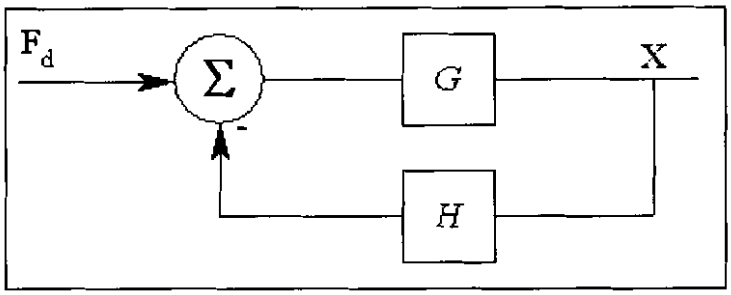


**Figure 4-7: Block diagram for the root locus**

From the block diagram in Figure 4-2 $G$, $H$ and $GH$ are equal to:

$$G = \frac{1}{ms^2} \tag{4-3}$$

$$H = 2K_Dk_is + 2K_pk_i - 2k_s \tag{4-4}$$

and

$$GH = \frac{2K_Dk_is + 2K_pk_i - 2k_s}{ms^2} \tag{4-5}$$

(4-5) is used to determine the root locus of the MSD. By determining the factors of the equation the number of poles and zeros can be determined as one zero and two poles. The two poles are both at the origin as shown in Figure 4-8. From the root locus and (4-5), it can be seen that the equivalent stiffness and damping has a direct influence on the position of the zero but not on the poles.

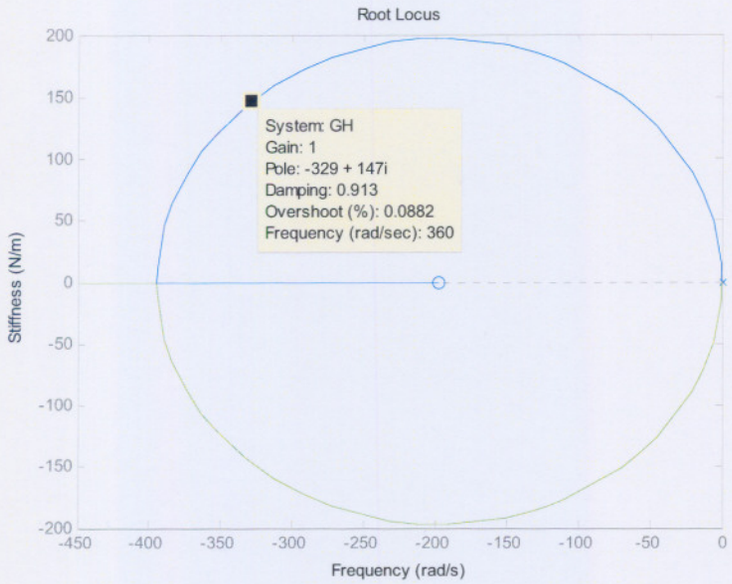


**Figure 4-8: Root locus of the MSD system**

The natural frequency of 360 rad/s was attained from the phase diagram (Figure 4-5) and the root locus (Figure 4-8) of the MSD. This natural frequency and (4-6) is used to determine the second order stiffness of the MSD.

$$\omega_n = \sqrt{\frac{k_{sos}}{m}}$$

$\therefore$

$$k_{sos} = \omega_n^2 m \qquad (4\text{-}6)$$
$$= 5.003 \times 10^5 \text{ N/m}$$

Second order stiffness and static stiffness will be the same if no poles are added to the system as shown in (4-2) and (4-6).

### *4.2.3 Dynamic stiffness*

Dynamic stiffness of the MSD can be derived from the bode diagram as shown in the first part of section 4.2.3 or from a disturbance force as shown in the second part of section 4.2.3.

#### Transfer function

Stiffness is equal to the disturbance force ($F_d$) divided by the deflection ($x$) and the transfer function of the system is equal to the deflection ($x$) divided by the disturbance force ($F_d$) as shown in (2-11). The dynamic stiffness of the MSD is equal to the magnitude plot of the inverse transfer function as illustrated in Figure 4-9.

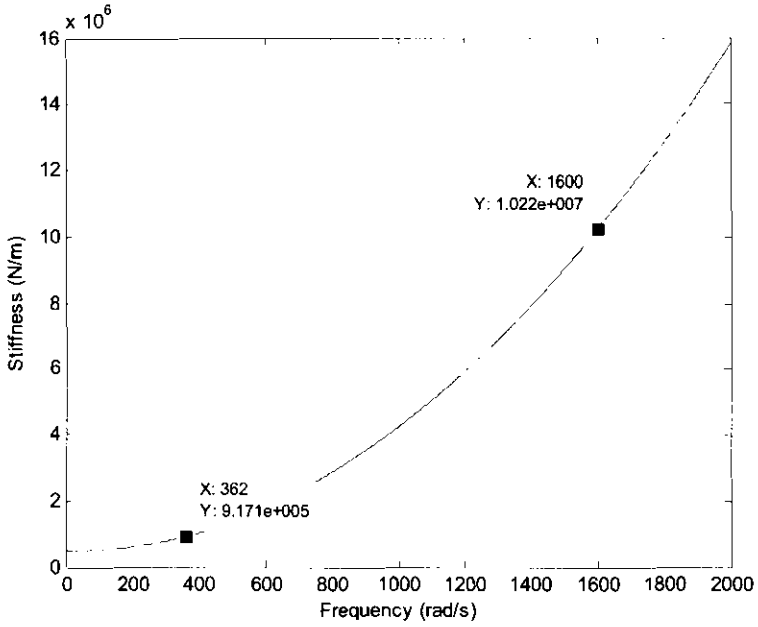


**Figure 4-9: Dynamic stiffness: $K_P$ = 12500 and $K_D$ = 38**

The transfer function of the MSD is dependent on the stiffness and damping of the system which makes the dynamic stiffness also dependent on the stiffness and damping. This means that if the equivalent stiffness and damping of the system should change, the shape of the graph in Figure 4-9 will also change. For instance, if $K_P$ would increase by 40 000 the static stiffness of the system will also increase and the minimum value will become more prominent at higher frequencies as shown in Figure 4-10. The opposite is also true: if $K_P$ decreases the minimum value will become less visible and move to a lower frequency. The damping in Figure 4-9 and Figure 4-10 has been kept the same to compare the effect of the stiffness on the dynamic stiffness in isolation.

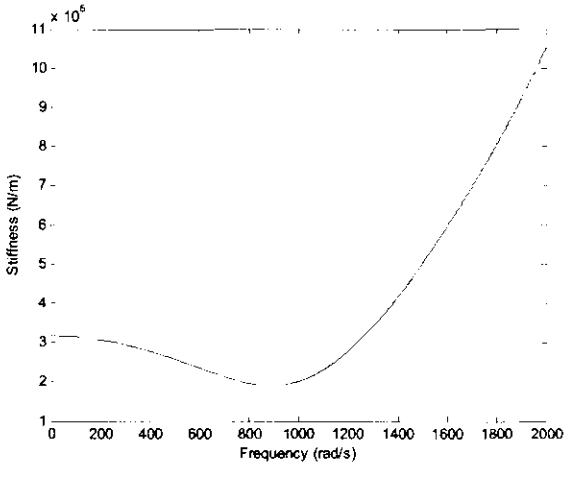


**Figure 4-10: Dynamic stiffness: $K_P$ = 52500 and $K_D$ = 38**

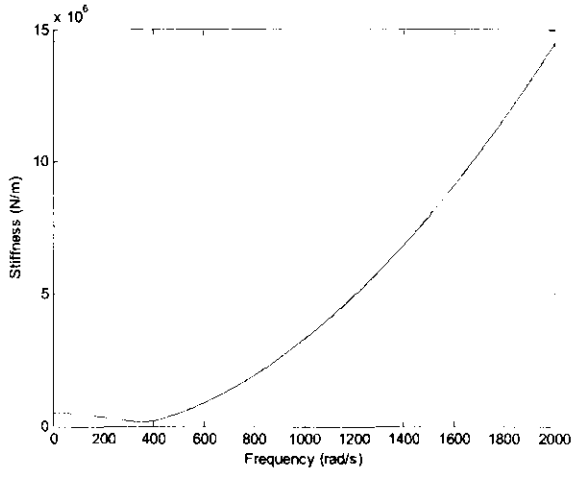


**Figure 4-11: Dynamic stiffness: $K_P$ = 12500 and $K_D$ = 8**

To demonstrate the effect of the equivalent damping on the dynamic stiffness of the system the $K_D$ value is decreased to 8 instead of 38 as illustrated in Figure 4-9 and Figure 4-11. The effect of the lower equivalent damping on the system is that the gradient of the rising edge is steeper and the minimum is more evident at the same frequency as for the higher damping. This can also be inverted for a higher damping where the minimum becomes less evident.

## Disturbance force

Dynamic stiffness of the MSD can be determined by applying a disturbance force at a specific frequency. The deviation from the equilibrium is measured for an applied force and this is then used in (2-18) to determine the stiffness of the system at a specific frequency. Using this technique the dynamic stiffness of the MSD with no filters or a controller pole is shown in Figure 4-12.

To verify the simulated results of the dynamic stiffness the two dynamic stiffness figures can be compared as shown in Figure 4-12. This comparison showed that the two methods give the same result.

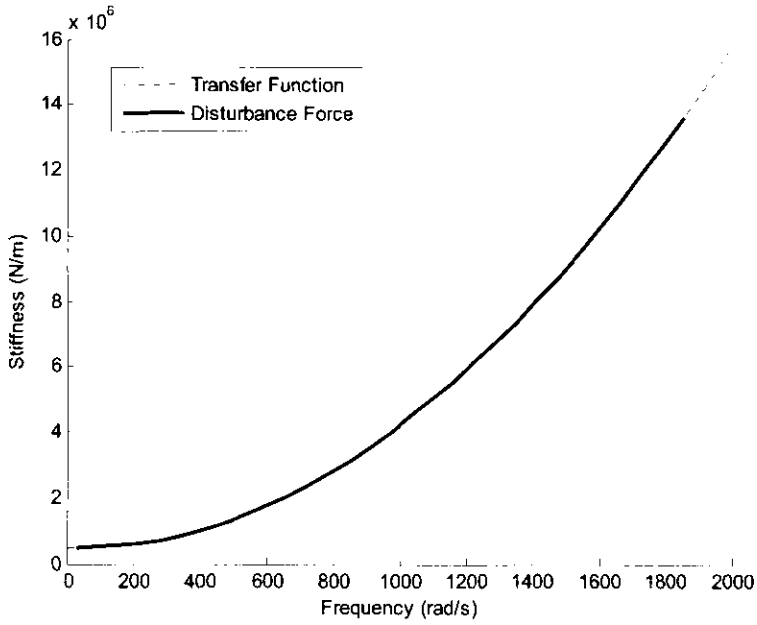


**Figure 4-12: Dynamic stiffness: $K_P$ = 12500 and $K_D$ = 38**

## 4.3 MSD with poles

The block diagram in Figure 4-2 is a representation of the AMB system without filters and controller pole. However the purpose of the MSD model is to create an uncomplicated characterisation of the AMB system, which means that the filters and poles should be included into the block diagram as shown in Figure 4-13. $P_{AAF}$ and $P_P$ represents the first order poles of the anti-aliasing and anti-imaging filters respectively used on the position signal and current reference. $P_C$ is the controller pole added by the differentiator in the PD controller.

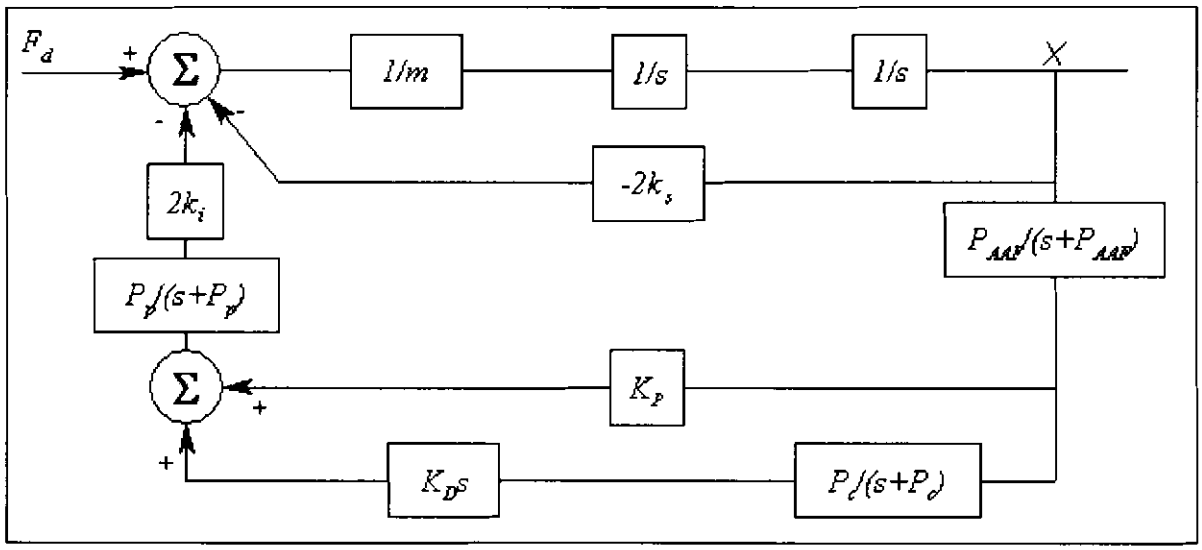


**Figure 4-13: MSD block diagram with filters and the controller pole**

The transfer function of the MSD system with filter is obtained by using Mason's rule [19]. From the block diagram in Figure 4-13 the forward path connecting the input to the output is:

$$P_1 = \frac{1}{ms^2} \tag{4-7}$$

The three loops in the flow diagram are:

$$L_1 = -\frac{2K_D k_i s}{ms^2}\left(\frac{P_{AAF}}{s+P_{AAF}}\right)\left(\frac{P_C}{s+P_C}\right)\left(\frac{P_p}{s+P_p}\right)$$

$$L_2 = -\frac{2K_p k_i}{ms^2}\left(\frac{P_P}{s+P_P}\right)\left(\frac{P_{AAF}}{s+P_{AAF}}\right) \tag{4-8}$$

$$L_3 = \frac{2k_s}{ms^2}$$

The transfer function of the flow diagram can now be obtained by substituting (4-7) and (4-8) into (2-10)

$$T(s) = \frac{1}{ms^2 - [2k_s - \left(\frac{P_p}{s+P_p}\right)\left(\frac{P_C}{s+P_C}\right)(2K_D k_i s)\left(\frac{P_{AAF}}{s+P_{AAF}}\right) - \left(\frac{P_p}{s+P_p}\right)(2K_p k_i)\left(\frac{P_{AAF}}{s+P_{AAF}}\right)]} \tag{4-9}$$

(4-9) shows that the filters and the controller pole add zeros and poles to the transfer function in (2-11) of the MSD, resulting in a more complex root locus as shown in Figure 4-16. The pole values are determined from the cut-off frequencies of the filters as discussed in chapter 3.

Table 4-1 shows the pole values determined from (4-10) that are used in the MSD simulation.

$$P = 2\pi f_{cut-off} \tag{4-10}$$

**Table 4-1: Pole frequencies**

| Filter | Filter cut-off frequency | |
|---|---|---|
| | kHz | rad/s |
| | | |
| Anti-aliasing filter | 2.77 | 1.70E+04 |
| Anti-imaging filter | 2.77 | 1.74E+04 |
| Controller pole | 0.159 | 1E+03 |

### *4.3.1 Static stiffness*

#### Bode diagram

The static stiffness of the MSD with the filters and the controller pole is determined by substituting the magnitude obtained from Figure 4-14 into (4-2) as shown below.

$$k_{ss} = \frac{1}{10^{\frac{-114}{20}}} \tag{4-11}$$

$$= 5.0119 \times 10^5 \text{ N/m}$$

The gains of the filters and the controller pole must be equal to 1 to prevent them from having an influence on the static stiffness of the system. (4-11) shows that the gains of the simulated filters and controller pole are almost equal to 1 because the static stiffness of the MSD has a 0.21 % error from the theoretical value of the static stiffness.

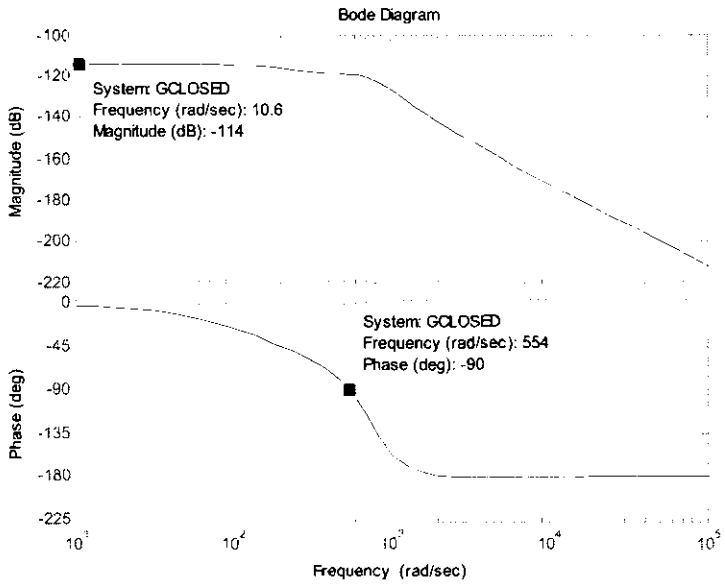


**Figure 4-14: Bode diagram with the filters and the controller pole added**

## Disturbance force

The static stiffness by a disturbance force (Figure 4-15) is determined as

$$k_{ss} = \frac{m_d \cdot g}{x_1 - x_2}$$

$$= 4.99 \times 10^5 \text{ N/m} \qquad \textbf{(4-12)}$$

which is equal to the theoretical stiffness of the system. The error between the bode diagram and disturbance force static stiffness is 0.2 %.

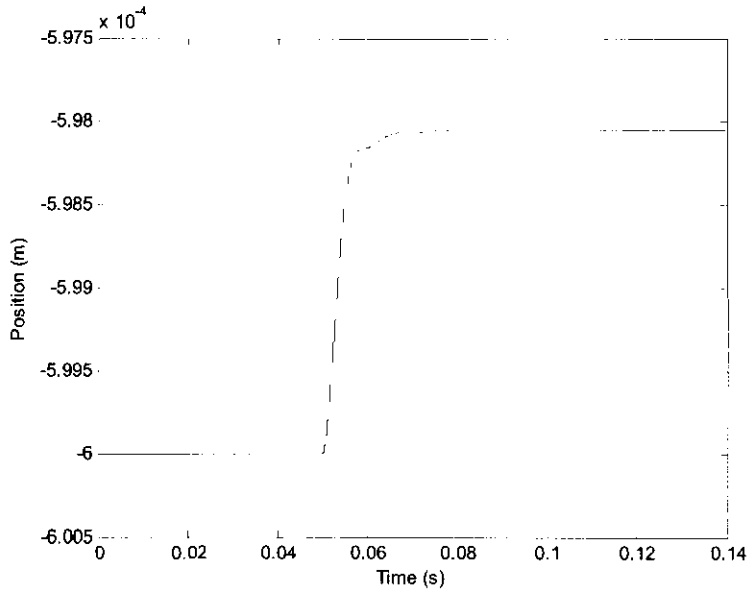


**Figure 4-15: Disturbance response with the filters and the controller pole added**

The static stiffness of the MSD with filters and the controller pole is constant over a range of deviations as with the system without the poles (Figure 4-4). Since the stiffness of the system with and without poles is the same it can be assumed that the static stiffness of the system is not dependent on the amount of poles or the force and deviation used to determine the static stiffness.

### 4.3.2 *Second order stiffness*

Second order stiffness is determined from the phase diagram and the root locus as explained in section 4.2.2. The phase diagram of the MSD with filters is shown in Figure 4-14 and the root locus is determined by reducing the block diagram in Figure 4-13 to Figure 4-7. The forward ($G$) and backward ($H$) paths are

$$G = \frac{1}{ms^2} \tag{4-13}$$

$$H = \left(\frac{P_p}{s+P_p}\right)\left(\frac{P_C}{s+P_C}\right)(2K_D k_i s)\left(\frac{P_{AAF}}{s+P_{AAF}}\right) + \left(\frac{P_p}{s+P_p}\right)(2K_p k_i)\left(\frac{P_{AAF}}{s+P_{AAF}}\right) - 2k_s \tag{4-14}$$

and

$$GH = \frac{\left(\frac{P_p}{s+P_p}\right)\left(\frac{P_C}{s+P_C}\right)(2K_D k_i s)\left(\frac{P_{AAF}}{s+P_{AAF}}\right) + \left(\frac{P_p}{s+P_p}\right)(2K_p k_i)\left(\frac{P_{AAF}}{s+P_{AAF}}\right) - 2k_s}{ms^2} \tag{4-15}$$

where the increase in poles and zeros are apparent. The root locus obtained from (4-15) is shown in Figure 4-16, this plot is not a second order system and can not be used to determine the natural frequency of the system.

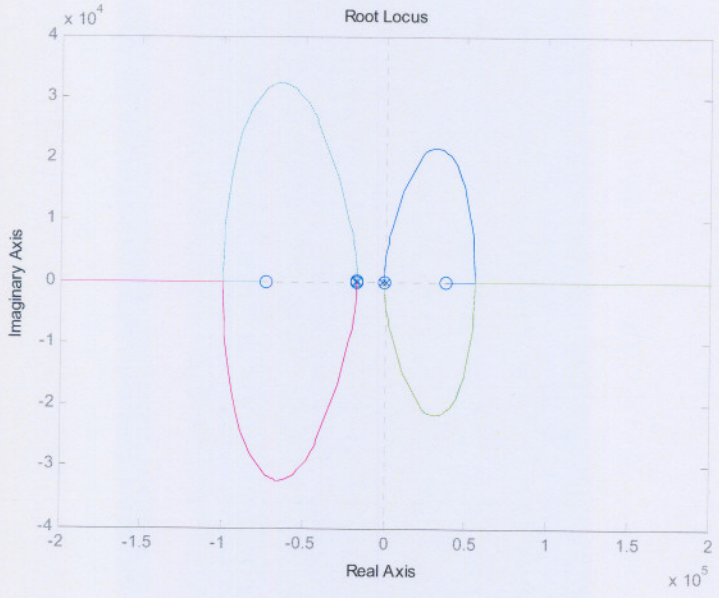


**Figure 4-16: Root locus with filters and the controller pole added**

A first natural frequency of 554 rad/s is obtained from the phase diagram which is used to determine the second order stiffness. The second order stiffness of the MSD can be determined by substituting the first natural frequency and the mass of the ball into (4-16).

$$k_{sos} = \omega_n^2 m \qquad \text{(4-16)}$$

$$= 1.18 \times 10^6 \text{ N/m}$$

(4-16) shows that the second order stiffness of the system with filters is higher than the system without the filters. The increase in stiffness can be attributed to the controller pole since the controller pole has the biggest influence on the stiffness. The difference between the dominant poles of the system without and with filters is the controller pole because the AAF and AIM poles are too far from the system poles to have an influence on the stiffness. The controller pole however is 123 rad/s from the system pole which means that the controller pole will have a big influence on the system response. The effect of the controller pole will be discussed in more detail in section 5.4.5.

### *4.3.3 Dynamic stiffness*

#### Bode diagram

The dynamic stiffness of the MSD with the added poles is shown in Figure 4-17. The dynamic stiffness at 1600 rad/s is $8.085 \times 10^6$ N/m for the system with poles and $1.022 \times 10^7$ N/m for the system without the poles. This proves that the dynamic stiffness of the system with filters is lower than that for the system without it. The lower dynamic stiffness of the system with filters can be attributed to the controller pole as explained in section 4.3.2.

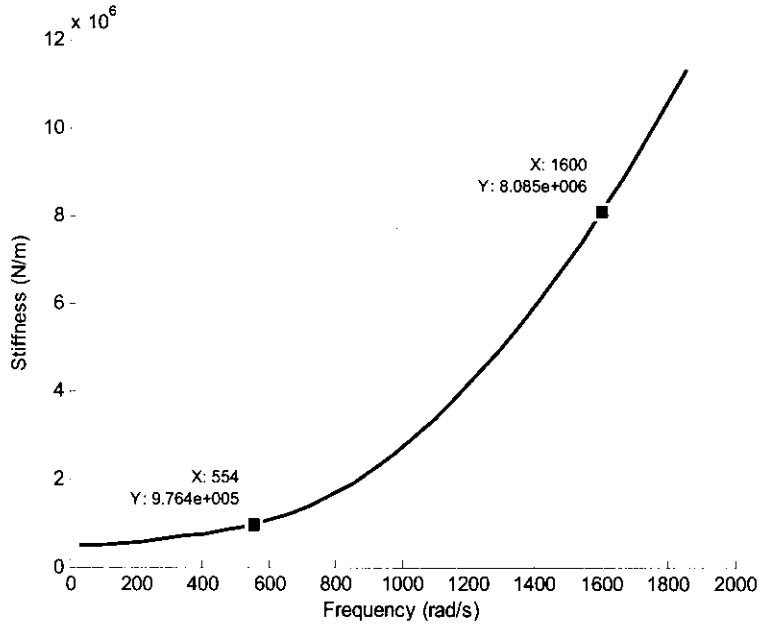


**Figure 4-17: Dynamic stiffness from the bode diagram $K_P$ = 12500 and $K_D$ = 38**

## Disturbance force

The dynamic stiffness of the system obtained from the disturbance force method is shown in Figure 4-18. The results from the two methods are also compared in Figure 4-18 and shows good correlation between the two methods.

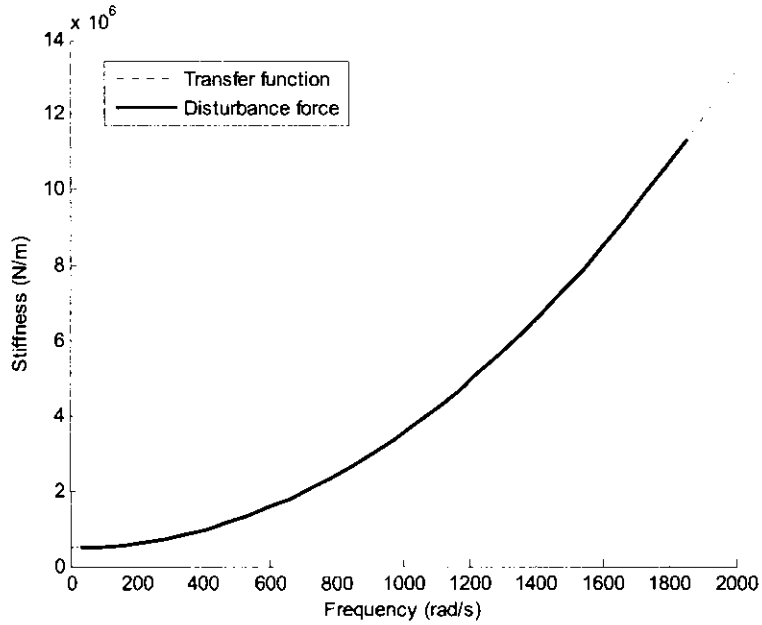


**Figure 4-18: Dynamic stiffness from the disturbance force with $K_P$ = 12500 and $K_D$ = 38**

*In this chapter a MSD model and transfer function is used to determine the static, dynamic and second order stiffness of the MSD. The simulations verified that the static stiffness of the systems with and without poles is the same but that the dynamic stiffness shows a deviation. It is also concluded that the static stiffness and the second order stiffness is not the same and depends on the amount of poles. The dynamic characterisation of the AMB is done in the following chapter to determine the similarities between the AMB and the MSD.*

# 5
# Chapter
# AMB characterisation

*This chapter constitutes the characterisation of an AMB system through accurate simulation as well as actual system measurements. Static and dynamic stiffness are characterised and compared to analytic results from chapter 4. The actual AMB system is also characterised in terms of sensitivity and rotor dynamic effects.*

## 5.1 Characterisation process

The actual AMB system is non-linear in its force-current and force-displacement behaviour as discussed in chapter 2. In this chapter a simulation of the non-linear system is used as analysis platform to investigate the characterisation of an AMB system. The process followed in this chapter is outlined in Figure 5-1.

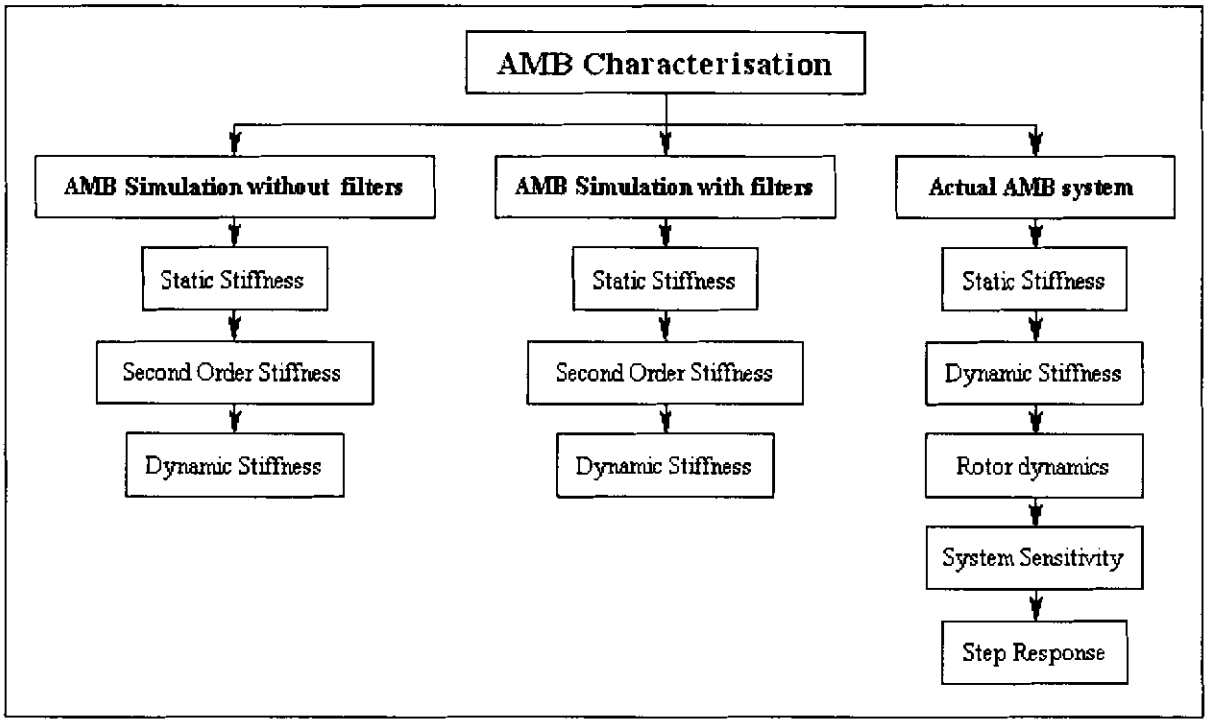


**Figure 5-1: AMB characterisation process**

The AMB system will firstly be characterised through simulation without filters to determine the system response if not filters are used. This is followed by the simulated AMB response with filters to determine the effect of the filters on the system. The simulated response of the system with filters can be compared to the actual AMB system.

Figure 5-2 illustrates the comparison of the AMB and MSD system in chapter 4.

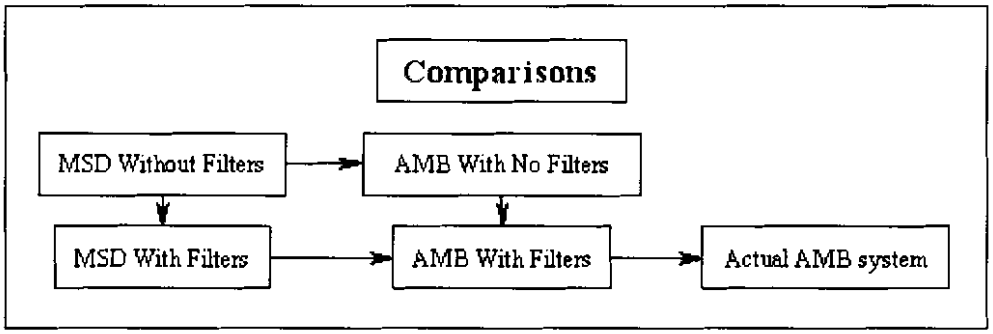


**Figure 5-2: AMB and MSD comparison**

## 5.2 AMB simulation without filters

The nonlinear system as portrayed in Figure 2-19 is simulated in MATLAB® and serves as simulation platform for this chapter. The response of the simulation will be used to determine the effects of the filters on the AMB system and to compare it to the MSD system in section 4.2.

The transfer function of the nonlinear AMB and linear MSD are the same because the MSD simulation uses the nonlinear constants of the AMB system. The transfer function of the AMB system is given in (2-14) and will have the same responses as the MSD in section 4.2.

### *5.2.1 Static stiffness*

Static stiffness of the AMB is measured by applying a disturbance force to the rotor as illustrated in Figure 5-12. The force is applied to the horizontal axis of the rotor position to avoid the gravitational force from having an effect on the measurements. The deviation due to the disturbance force is shown in Figure 5-3. This deviation and the force are used in (5-1) to determine the static stiffness.

$$k_{ss} = \frac{m_d \cdot g}{x_1 - x_2}$$

$$= 5.09 \times 10^5 \text{ N/m} \quad \textbf{(5-1)}$$

The obtained static stiffness has a 0.9 % deviation from the theoretical and MSD static stiffness. In Figure 5-3 it is observable that the system is highly damped since a very small overshoot is observable due to the disturbance step.

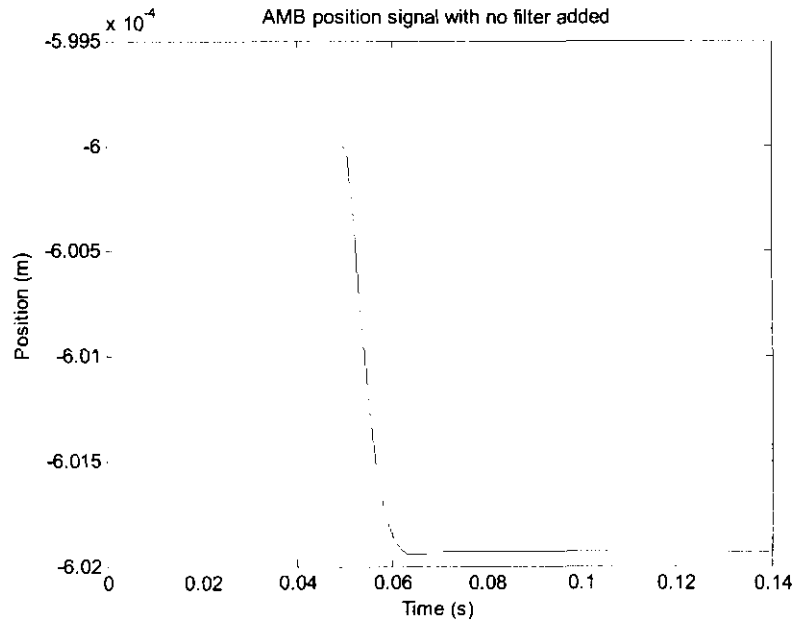


**Figure 5-3: Disturbance response of the AMB simulation without filters or controller pole**

If Figure 5-4 is compared to Figure 4-4 of the MSD the peak around zero is the only difference between the two plots. The peak around zero can be attributed to the simulation. In the simulation the force exerted by the electromagnets are divided by the position of the rotor. If the movement of the rotor is very small the simulation will round the position to a value close to zero which will increase the force and make the stiffness arbitrarily high as illustrated in Figure 5-4.

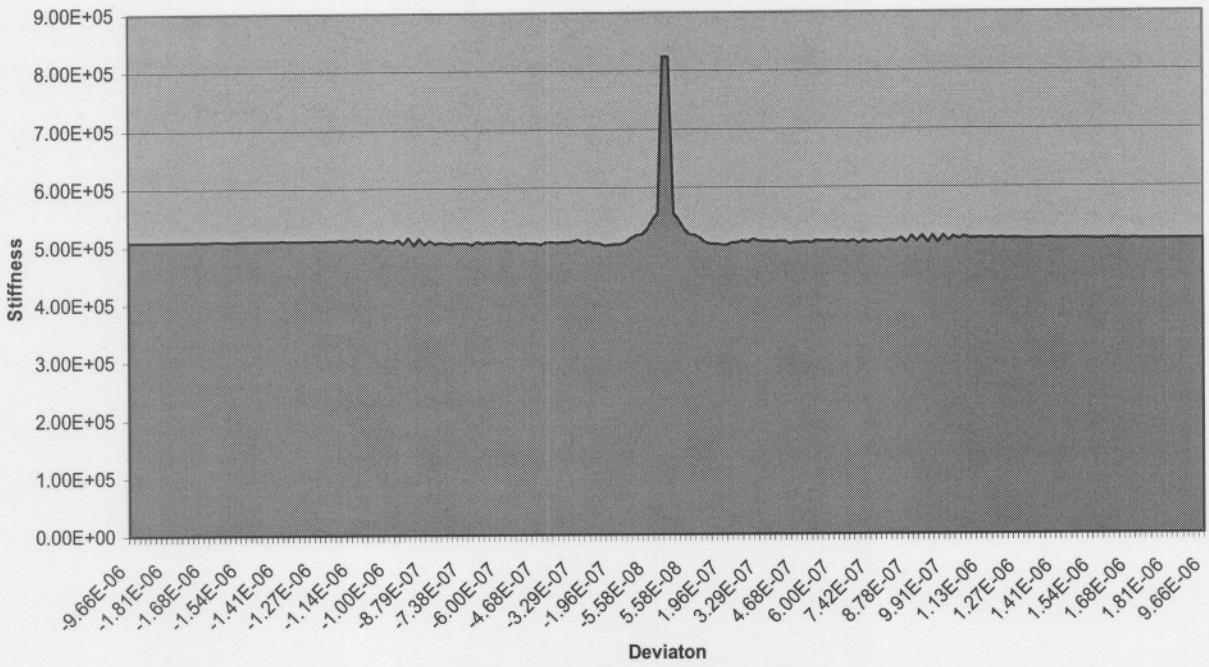


**Figure 5-4: Stiffness to deviation graph of the AMB simulation**

### *5.2.2 Dynamic stiffness*

Figure 5-5 shows the plot of the stiffness vs frequency which is called dynamic stiffness. The dynamic stiffness of the AMB is analysed through simulation with a disturbance force at a specific frequency. This is done by adding a disturbance to the force of the electromagnets and measuring the resulting deviation.

The dynamic stiffness of the AMB in Figure 5-5 can be compared to the MSD in Figure 4-9 since neither systems have filters. The dynamic stiffness of the AMB system is lower at high frequencies due to the sampling time of the simulation.

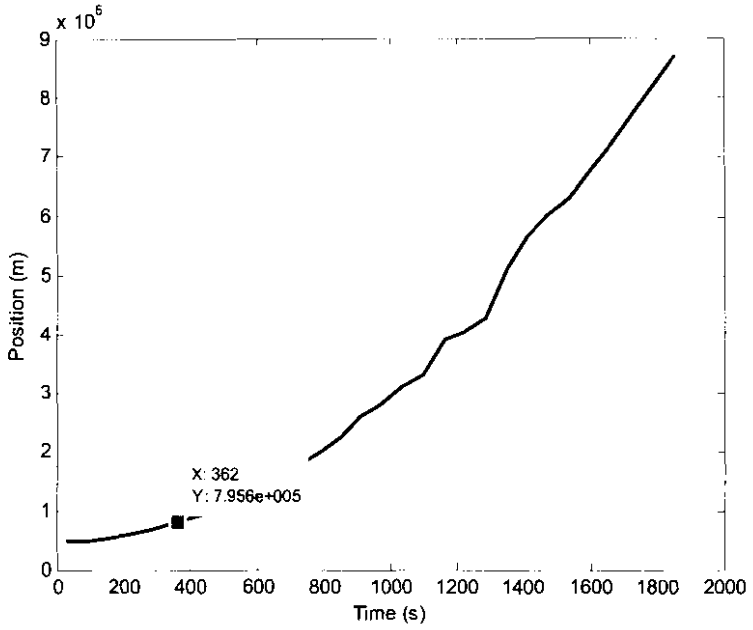


**Figure 5-5: Dynamic stiffness with $K_P$ = 12500 and $K_D$ = 38**

For the simulation without filters it can be said that the MSD and the AMB are almost exactly the same. The only differences between the two simulations are the dynamic stiffness because of the sampling time of the simulation.

## 5.3 AMB simulation with poles

Figure 5-6 demonstrates a reduced block diagram of the nonlinear AMB system as shown in Figure 2-19. The only differences between the system in Figure 5-6 and the one in Figure 2-19 are the AAF, AIM and the differentiator pole that are added to Figure 5-6.

In Figure 5-6 it is shown that the position used by the position stiffness is not filtered. This can be attributed to the fact that the negative position stiffness is a characteristic of the electromagnetic actuator and not a result of the feed back circuit. $F_d$ represents the input of the disturbance force used to determine the static and dynamic stiffness of the AMB.

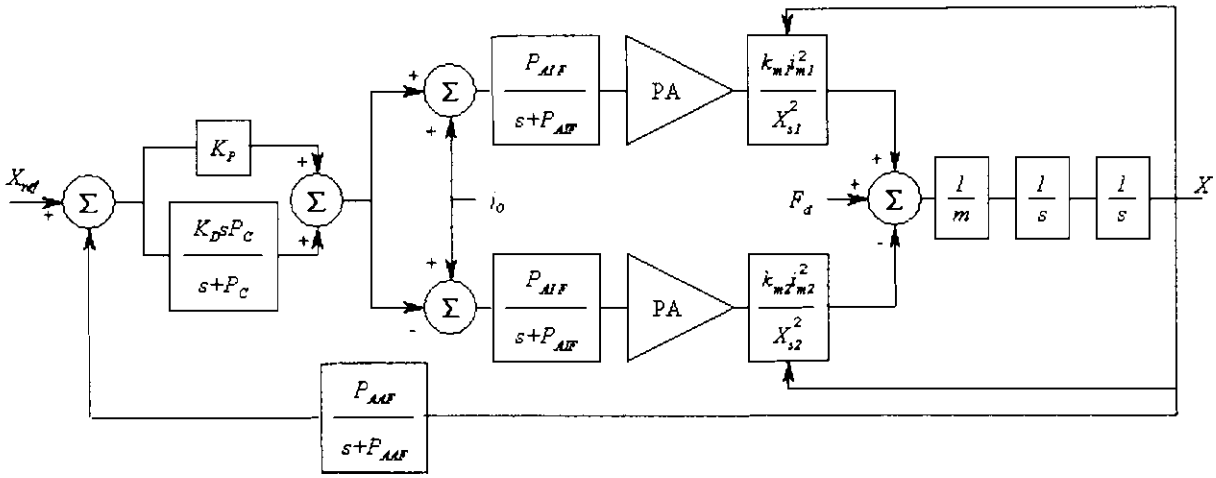


**Figure 5-6 : AMB block diagram with filters and controller pole**

The transfer function of the block diagram in Figure 5-6 will be the same as the one used in section 4.3 in a specific operating point. This means that the static and dynamic stiffness obtained from the transfer functions will be the same for both simulations around the operating point. The static and dynamic stiffness obtained from a disturbance force method will be discussed and determined in the following paragraphs.

### *5.3.1 Static stiffness*

The static stiffness of the AMB simulation with poles is also determined with a disturbance force applied to the system at Fd as shown in Figure 5-6. Figure 5-7 illustrates the deviation of the rotor due to a disturbance force. This deviation and applied force an then used to determine the static stiffness as

$$k_{ss} = \frac{m_d.g}{x_1 - x_2}$$

$$= 4.85 \times 10^5 \text{ N/m} \qquad \textbf{(5-2)}$$

that has a 2.8 % deviation from the theoretical value.

Since the same simulation is used for the AMB with and without filters the envalope of the stiffness to deviation plot in Figure 5-4 is expected to be the same for the system with filters.

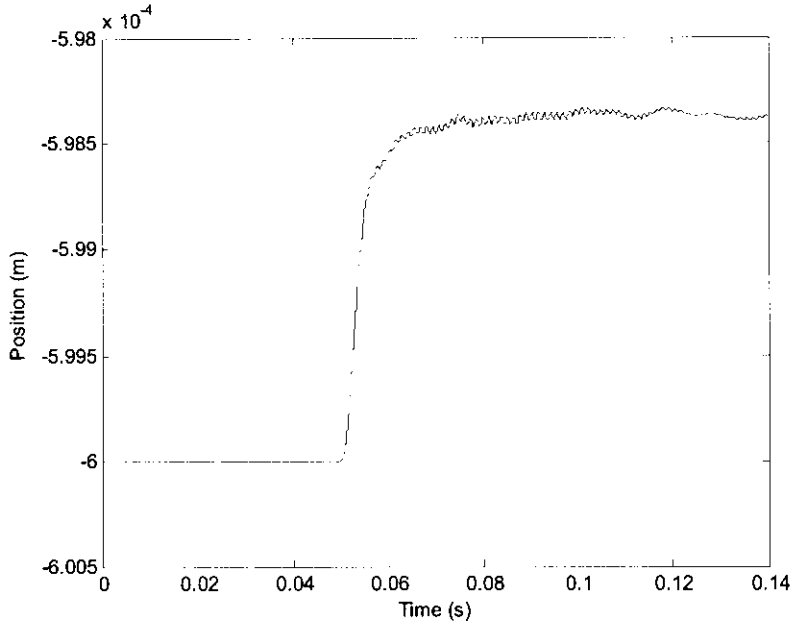


**Figure 5-7: Disturbance response of the AMB with filters and controller pole**

### *5.3.2 Dynamic stiffness*

The dynamic stiffness of the AMB with filters is the most important simulated measurement of the AMB because it gives a realistic stiffness characteristic for the actual AMB system. This measurement can be used to design the filters and the operating stiffness of the system to be within specified safety limits.

Figure 5-8 illustrates the dynamic stiffness of the AMB simulation with the filters and the controller pole. This figure can also be compared to the dynamic stiffness of the MSD Figure 4-18 because the two simulations have the same transfer functions. When comparing the two simulations it was found that the AMB simulation has a lower stiffness at high frequencies because of the sampling time of the simulation.

If the dynamic stiffness of the AMB system without filter and with filters are compared it is found that the dynamic stiffness of the system with filters is lower than that without. This can be attributed to the controller pole that became one of the dominant poles of the AMB system, as will be explained in section 5.4.5.

### 5.4.1 *Static stiffness*

The AMB static stiffness is obtained by applying an external force to the rotor on the horizontal axis as shown in Figure 5-12.

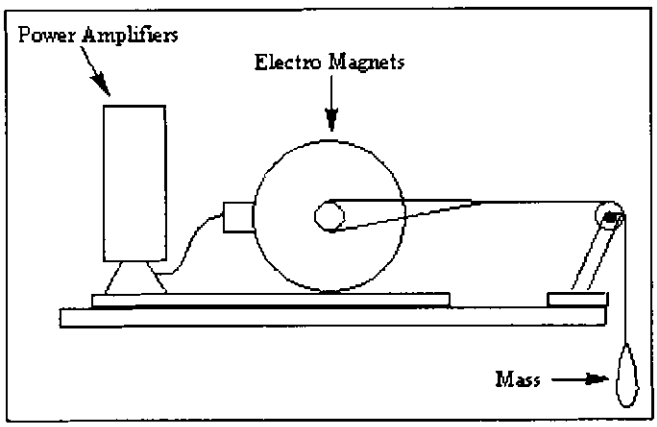


**Figure 5-12: AMB system used to determine static stiffness**

The deviation and disturbance force are substituted into (5-2) to give the static stiffness for different forces as shown in Table 5-1.

**Table 5-1: Static stiffness of the AMB**

| *m* (kg) | *F* (N) | Δx (m) | Static stiffness (N/m) |
|---|---|---|---|
| | | | |
| 1 | 12.27231 | 2.50E-05 | 4.91E+05 |
| 4 | 41.70231 | 9.00E-05 | 4.63E+05 |
| 8 | 80.94231 | 1.85E-04 | 4.38E+05 |

The variation of the static stiffness in Table 5-1 can be attributed to the nonlinearity of the AMB system as the rotor moves away from the centre position between the magnets (section 2.4). As the rotor moves away from the one magnet and closer to the other the current-gain and position-gain of both magnets will change which will change the equivalent stiffness and damping according to (2-15) and (2-16). This is however not evident in the transfer functions of the AMB system as determined in Chapter 4. The systems used to determine the transfer functions of the AMB simulations were linearised around the operating point, assuming the current-gain and position-gain of the both the magnets to be equal.

To explain the decrease in static stiffness for large deviations from the centre position, the current-gain and position-gain of each magnet should be separately determined as shown in Figure 5-13.

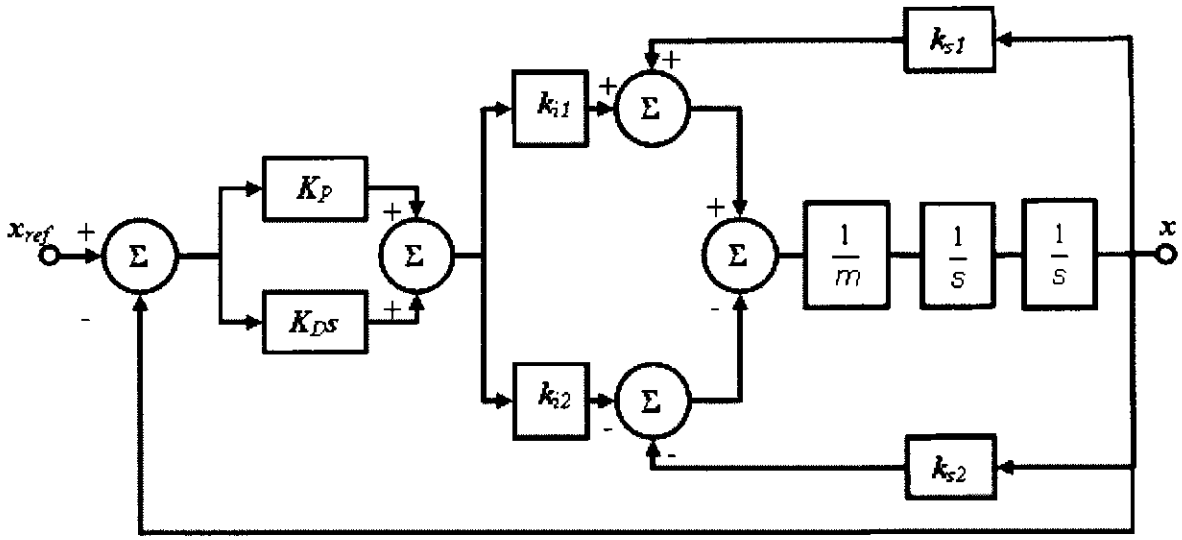


**Figure 5-13: AMB system block diagram**

The transfer function of this block diagram can be obtained by using Mason's rule. The forward paths connecting the input to the output are:

$$P_1 = \frac{K_P k_{i1}}{ms^2}, \qquad P_2 = \frac{K_D s k_{i2}}{ms^2}$$
$$P_3 = \frac{K_P k_{i2}}{ms^2}, \qquad P_4 = \frac{K_D s k_{i1}}{ms^2} \tag{5-3}$$

There are six loops identified:

$$L_1 = \frac{k_{s1}}{ms^2}, \qquad L_2 = \frac{k_{s2}}{ms^2}$$
$$L_3 = -\frac{K_P k_{i1}}{ms^2}, \qquad L_4 = -\frac{K_D s k_{i1}}{ms^2}$$
$$L_5 = -\frac{K_P k_{i2}}{ms^2}, \qquad L_6 = -\frac{K_D s k_{i2}}{ms^2} \tag{5-4}$$

Loops $L_1$ to $L_6$ touch, therefore the determinant is

$$\Delta = 1 - (L_1 + L_2 + L_3 + L_4 + L_5 + L_6)$$
$$= 1 - (\frac{k_{s1}}{ms^2} + \frac{k_{s2}}{ms^2} - \frac{K_P k_{i1}}{ms^2} - \frac{K_D s k_{i2}}{ms^2} - \frac{K_P k_{i2}}{ms^2} - \frac{K_D s k_{i1}}{ms^2}) \tag{5-5}$$

The cofactor of each forward path is evaluated by removing the relevant forward path and determining the cofactor of the remainder. The cofactors are therefore:

$$\Delta_1 = \Delta_2 = \Delta_3 = \Delta_4 = 1 \tag{5-6}$$

By substituting (5-3), (5-4), (5-5) and (5-6) into (5-7) the transfer function is obtained.

$$T(s) = \frac{X}{F} = \frac{P_1 \cdot \Delta_1 + P_2 \cdot \Delta_2 + P_3 \cdot \Delta_3 + P_4 \cdot \Delta_4}{\Delta} \tag{5-7}$$

$$= \frac{K_P(k_{i1} + k_{i2}) + K_D(k_{i1} + k_{i2})s}{ms^2 + K_D(k_{i1} + k_{i2})s + k_P(k_{i1} + k_{i2}) - (k_{s1} + k_{s2})} \tag{5-8}$$

(5-8) is the transfer function of the AMB system if the magnets are separated. The equivalent stiffness and damping obtained from the transfer function are

$$k_{eq} = K_P(k_{i1} + k_{i2}) - (k_{s1} + k_{s2}) \tag{5-9}$$

$$b_{eq} = K_D(k_{i1} + k_{i2}) \tag{5-10}$$

which shows that the equivalent stiffness and damping are dependent on the current and position-gain of each magnet. To verify the effect of the current-gain and position-gain on the equivalent stiffness of the AMB system the current-gain, position-gain and equivalent stiffness is determined for a specific disturbance force.

If a 41 N disturbance force is used, the simulation shows a $7.039 \times 10^{-4}$ m air gap from the left magnets and $4.961 \times 10^{-4}$ m from the right magnet. This deviation changes the coil currents to 4.04 A for the left magnet and 1.44 A for the right magnet. These values are used to determine the current-gains and position-gains of the system in Figure 5-13 as shown in (5-11), (5-12), (5-13) and (5-14).

$$k_{i1}\Big|_{g_0=0.496mm, i_{ref}=1.44A} = 32.47 \text{ N/A} \tag{5-11}$$

$$k_{i2}\Big|_{g_0=0.704mm, i_{ref}=4.04} = 23.45 \text{ N/A} \tag{5-12}$$

$$k_{s1}\Big|_{g_0=0.496mm, i_{ref}=1.44} = 1.87 \times 10^5 \text{ N/m} \tag{5-13}$$

$$k_{s2}\Big|_{g_0=0.704mm, i_{ref}=4.04} = 6.82 \times 10^4 \text{ N/m} \tag{5-14}$$

Using (5-9) equivalent stiffness is equal to

$$k_{eq} = 4.44 \times 10^5 \text{ N/m} \tag{5-15}$$

which shows good correlation with the static stiffness in Table 5-1 and proves that the current-gains and position-gains have an influence on the static stiffness of the system.

The static stiffness of the AMB before filtering was $5.05 \times 10^5$ N/m which has a lower percentage error than the average static stiffness of the system with filters in Table 5-1. Although there is a good correlation between the static stiffness of the system without and with filters the system with filters are not as stiff as the system without.

The effect of the filters is tested by simulating the AMB system without filters and then adding the filters one by one. The static stiffness is measured for each of the systems without and with filters to determine the filters with the biggest effect on the static stiffness. The first filter that was added was the differentiator pole which had no effect on the static stiffness of the system. The other two filters were added separately and they showed a decrease in static stiffness. This decrease in static stiffness can therefore be attributed to the AAF and AIM filter.

### *5.4.2 Dynamic stiffness*

AMB dynamic stiffness is defined as the stiffness as a function of frequency and can be measured in two ways. The first is by using an industrial vibrator and the second by using the transfer function.

#### Dynamic stiffness using an industrial vibrator

A frequency adjustable vibrator can be used to push and pull the rotor at a specific frequency as shown in Figure 5-14. This setup of the vibrator on the rotor has the advantage that the disturbance force is one dimensional and not two dimensional as for the unbalance on the rotor.

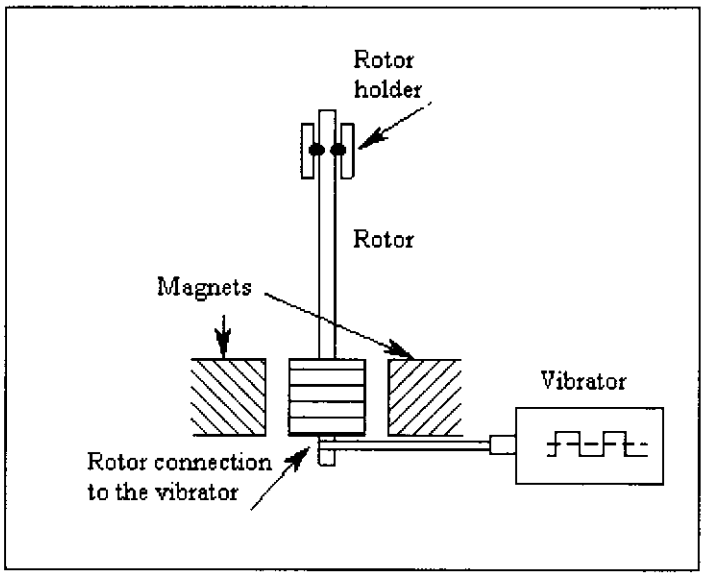


**Figure 5-14: Measuring AMB dynamic stiffness with a vibrator**

The most important objective of this measurement is to secure the vibrator as tight as possible around the rotor to prevent a dead band. The rotor should be pulled from its equilibrium position between the magnets to create a "pull and release" and not a "pull and push" force from the vibrator. This is important since the vibrator may have deadband in the zero position that can influence the measurement of the

dynamic stiffness. If the rotor is pulled from its equilibrium the force exerted by the electromagnets will reduce the effect of the vibrator deadband and result in a much smoother measurement to determine the dynamic stiffness.

A disadvantage of the rotor not being in the equilibrium position is that the magnets will not exert the same force on the rotor. This is due to the quadratic force-position relationship of an AMB. As a result the behaviour of the electromagnets will not be the same and will have an influence on the dynamic stiffness [23].

### Dynamic stiffness using a transfer function

Figure 4-2 shows the MSD block diagram. The transfer function of the block diagram is obtained with Mason's loop rules (section 2.4) to be (5-16) [19]. From (5-16) it is evident that the transfer function of the MSD is equal to the deviation divided by the disturbance force which is the inverse of the dynamic stiffness as explained in section 2.4.2. By inverting the transfer function the dynamic stiffness of the system can be determined.

$$T = \frac{X}{F_d} = \frac{1}{ms^2 + b_{eq}s + k_{eq}} \tag{5-16}$$

This means that if the simulation is used to determine the dynamic stiffness of a system the inverse of the magnitude plot can be used as the dynamic stiffness.

### Actual AMB measurements

Dynamic stiffness on the actual AMB system is not that simple to determine as with the simulations of the AMB and the MSD. The use of an industrial vibrator is an option but has a lot of complications as discussed. If the vibrator is not used the second option is to use the transfer function of the system. The transfer function of an AMB is given by the position of the rotor divided by disturbance force applied to the rotor as explained. The most effortless external disturbance on the actual AMB system is a disturbance on the current reference signal as shown in Figure 5-15 at $Y_{dist}$. The transfer function obtained with Mason's rule and the current reference disturbance as shown in Figure 5-15 is

$$T(s) = \frac{2k_i}{ms^2 + 2K_D k_i s + (2K_p k_i - 2k_s)} \tag{5-17}$$

for the AMB system without filters or the controller pole and

$$T(s) = \frac{2k_i(\frac{P_P}{s+P_P})}{ms^2 - [2k_s - (\frac{P_p}{s+P_p})(\frac{P_C}{s+P_C})(2K_D k_i s)(\frac{P_{AAF}}{s+P_{AAF}}) - (\frac{P_p}{s+P_p})(2K_p k_i)(\frac{P_{AAF}}{s+P_{AAF}})]} \quad \textbf{(5-18)}$$

for the AMB system with the filters and the controller pole.

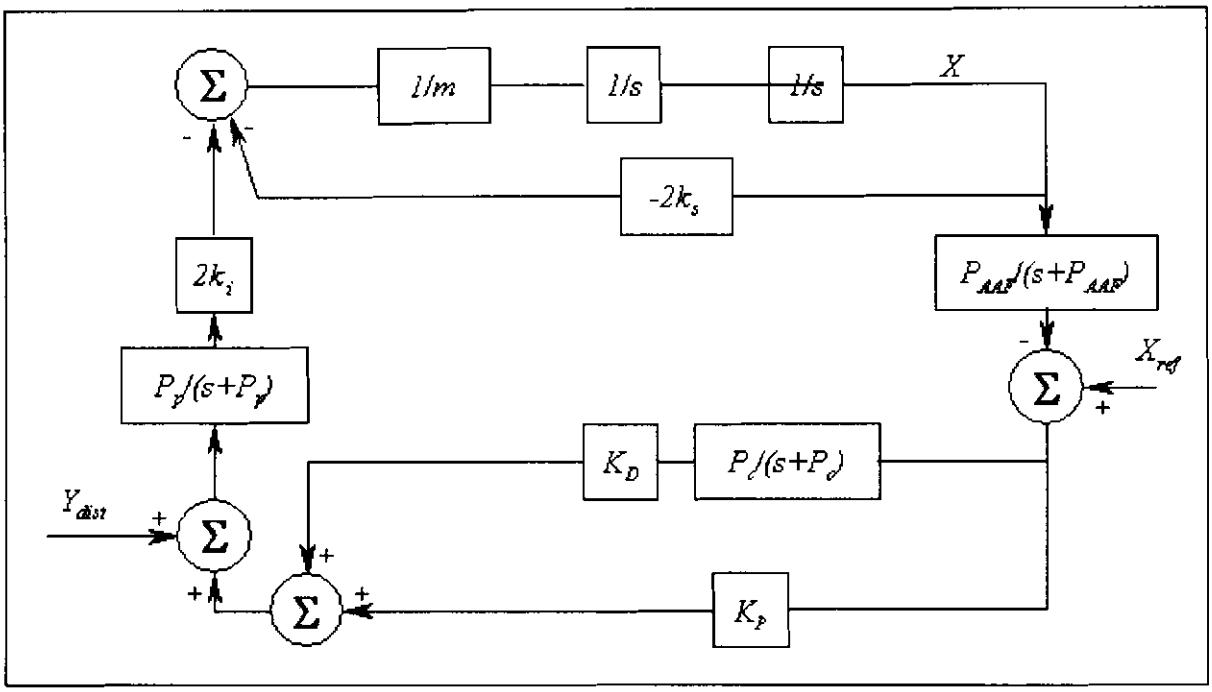


**Figure 5-15 : AMB block diagram for the characterisation**

The difference between these transfer functions and the transfer functions used to determine the dynamic stiffness is the $-2k_i$ in the numerator of the system without filters and $-2k_i$ times the anti-imaging filter pole for the system with filters. This means that the dynamic stiffness of the system with filters can be obtained as shown in
(5-19).

$$k_{ds} = \frac{F_d}{\Delta X} = \frac{2k_i(\frac{P_P}{s+P_P})}{T(s)} \quad \textbf{(5-19)}$$

This method was used to determine the dynamic stiffness of the actual AMB system because of its simplicity. Figure 5-16 shows the dynamic stiffness of the AMB with the flexible rotor. This representation of the dynamic stiffness cannot be compared to the simulation results because the rotor dynamics were not programmed into the simulation.

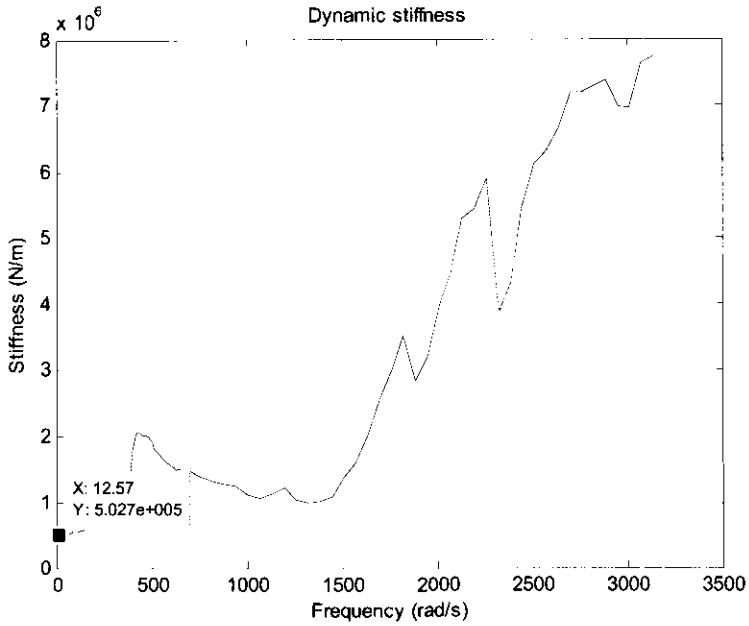


**Figure 5-16: Dynamic stiffness of the flexible rotor**

Figure 5-17 displays the dynamic stiffness of the AMB system with the rigid rotor. This figure is a better representation of the AMB dynamic stiffness with almost no rotor dynamics because of the rigid rotor.

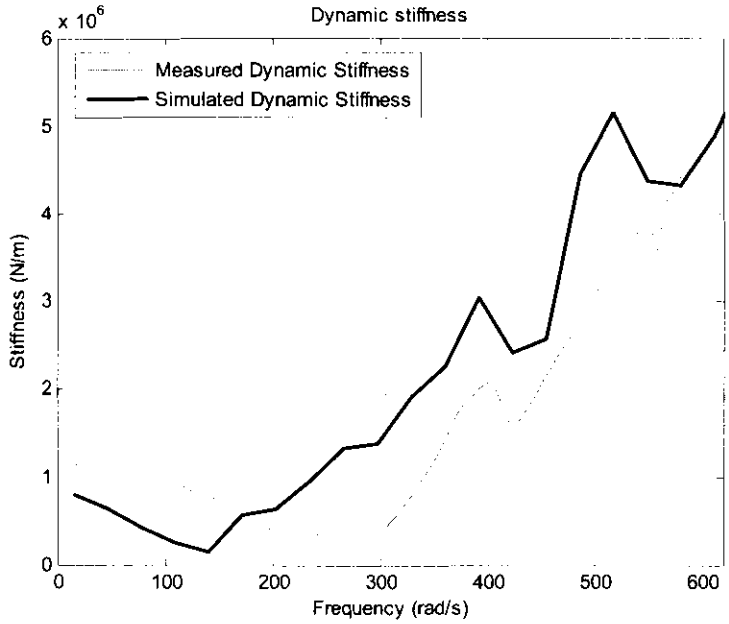


**Figure 5-17: Dynamic stiffness with the rigid rotor**

Although there is still some rotor dynamics present this figure can be compared to the dynamic stiffness of the AMB simulation with the rigid rotor and the same controller constants. A comparison of the two plots is shown in Figure 5-17 where it is evident that the shape of the two plots is almost the same. The

only difference between the two plots is the lower stiffness of the actual system at high frequencies that can be attributed to the bandwidth of the AIFs on the PAs.

This shows that this method is an effective way of measuring the dynamic stiffness of the actual AMB system. This method can also be used to determine the static stiffness as explained above.

### *5.4.3 Rotor dynamics*

A Dyrobes® rotordynamic software was previously done on the flexible rotor used in the AMB system [3]. Figure 5-18 shows the simulated critical speed map of the flexible rotor that can be used to determine the first four critical frequencies of the rotor.

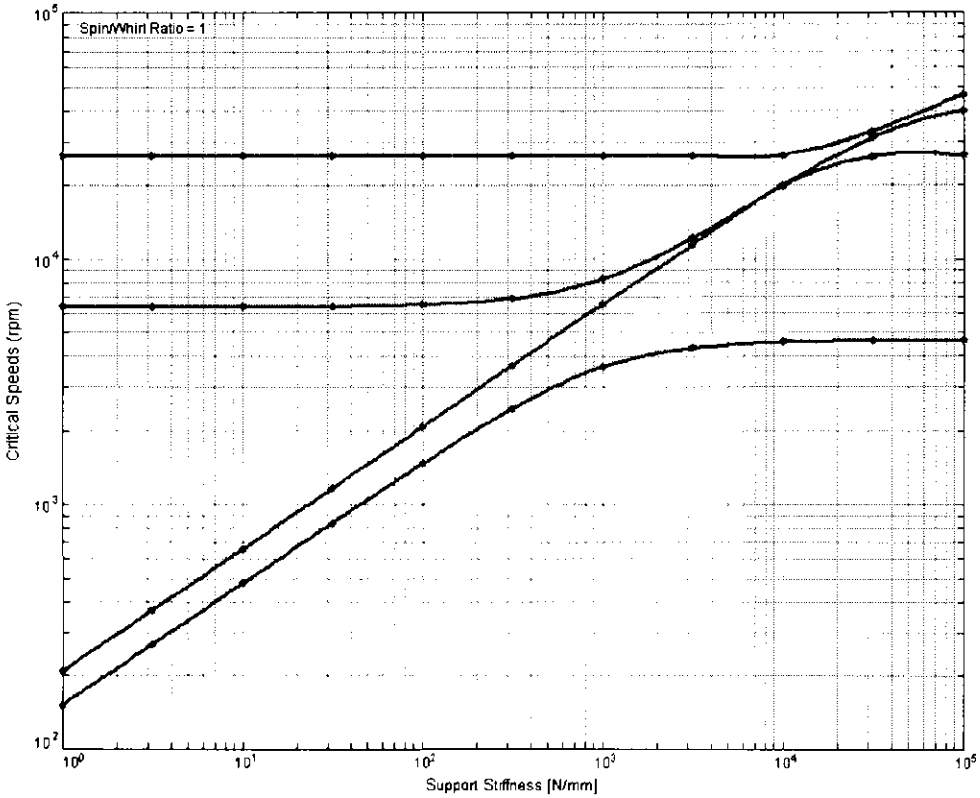


**Figure 5-18: Critical speed map [3]**

The static stiffness of the AMB system before filtering was $5.05\times10^5$ N/m which is used to determine the theoretical critical frequencies of the flexible rotor on Figure 5-18. The dynamic analysis of the flexible rotor before filtering predicted the first critical frequency (cylindrical) at 2,947 rpm, the second (conical) at 4,637 rpm and the third critical frequency (first bending mode) at 7,276 rpm.

The dynamic analysis of the rotor after filtering and a static stiffness of $4.85\times10^5$ N/m predicted the first critical frequency (cylindrical) at 2,600 rpm, the second (conical) at 4,300 rpm and the third critical

frequency (first bending mode) at 7,000 rpm. Critical frequencies in this section of the dissertation are specified as rotational frequencies.

The rotor dynamic response of the actual AMB system without and with filters is compared to each other and to the predicted response of the rotor. The filters that were added to the system are the AAF and AIF as explained in chapter 3.

Figure 5-19 and Figure 5-20 display (a) the vertical and (b) the horizontal peak to peak displacement of the right stator. The critical frequencies attained from Figure 5-19 and Figure 5-20 are given in Table 5-2 and Table 5-3 respectively.

**Table 5-2: Right stator critical frequencies before filtering**

| Horizontal (rpm) | Vertical (rpm) |
|---|---|
| | |
| 3300 | 2900 |
| 4300 | 4000 |
| | 8200 |

**Table 5-3: Right stator critical frequency after filtering**

| Horizontal (rpm) | Vertical (rpm) |
|---|---|
| | |
| 2610 | 2562 |
| 3240 | 3600 |
| | 8369 |

From Table 5-2 and Table 5-3 it is seen that the first two critical frequencies after filtering is lower that that of the system before filtering and that the third critical frequency is almost the same. The biggest difference between the systems before and after filtering is the increase in peak to peak displacements of the filtered system.

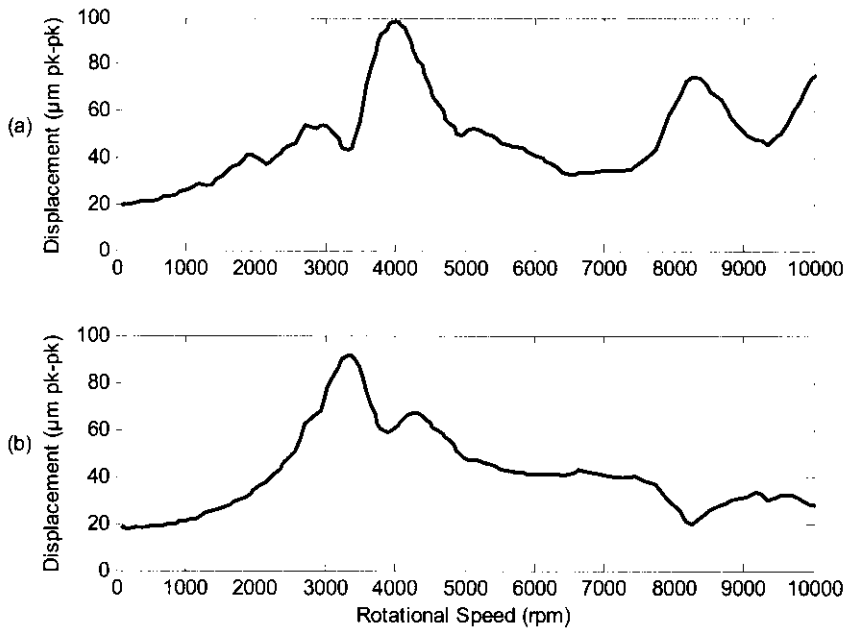


**Figure 5-19: Right stator a) vertical, b) horizontal displacement vs. rotational frequency without the filters [3]**

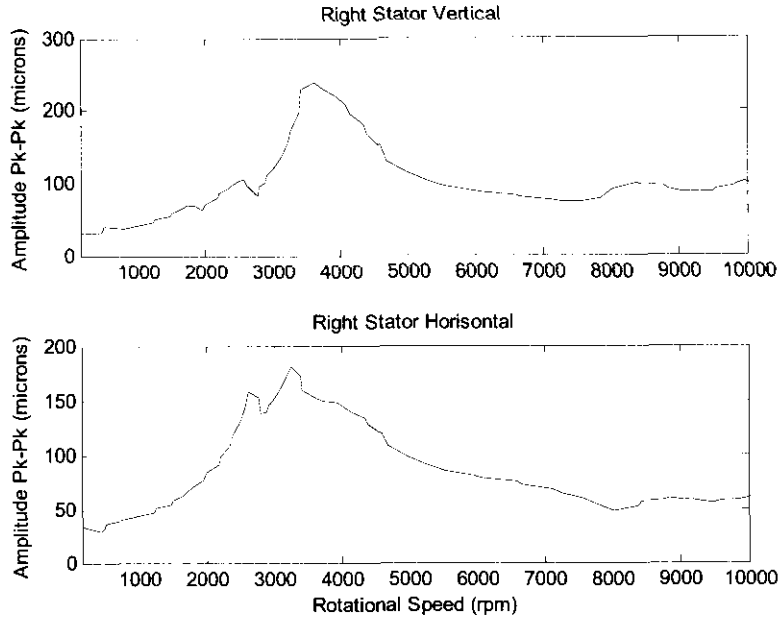


**Figure 5-20: Right stator a) vertical, b) horizontal displacement vs. rotational frequency with the filters**

The left stator response before filtering is shown in Figure 5-21 and after filtering in Figure 5-22. The critical frequencies observed in this two figure are given in Table 5-4 and Table 5-5.

**Table 5-4: Left stator critical frequencies before filtering**

| Horizontal (rpm) | Vertical (rpm) |
|---|---|
| | |
| 3400 | 3000 |
| 4300 | 4100 |
| | 7800 |

**Table 5-5: Left stator critical frequencies after filtering**

| Horizontal (rpm) | Vertical (rpm) |
|---|---|
| | |
| 2763 | |
| 3240 | 3715 |
| | |

The observed frequencies in Table 5-4 and Table 5-5 shows that there is a decrease in critical frequencies in the system with filters and that the observed frequencies are lower than that of the system without filters. Figure 5-22 also shows an increase in the horizontal peak to peak displacement of the left stator.

The left and right stator on the other hand has the same critical frequencies but the amplitudes of the peak to peak displacements are higher for the left stator. This higher amplitude on the left stator shows that the left stator has an unbalance that is not present on the right stator.

only difference between the two plots is the lower stiffness of the actual system at high frequencies that can be attributed to the bandwidth of the AIFs on the PAs.

This shows that this method is an effective way of measuring the dynamic stiffness of the actual AMB system. This method can also be used to determine the static stiffness as explained above.

### *5.4.3 Rotor dynamics*

A Dyrobes® rotordynamic software was previously done on the flexible rotor used in the AMB system [3]. Figure 5-18 shows the simulated critical speed map of the flexible rotor that can be used to determine the first four critical frequencies of the rotor.

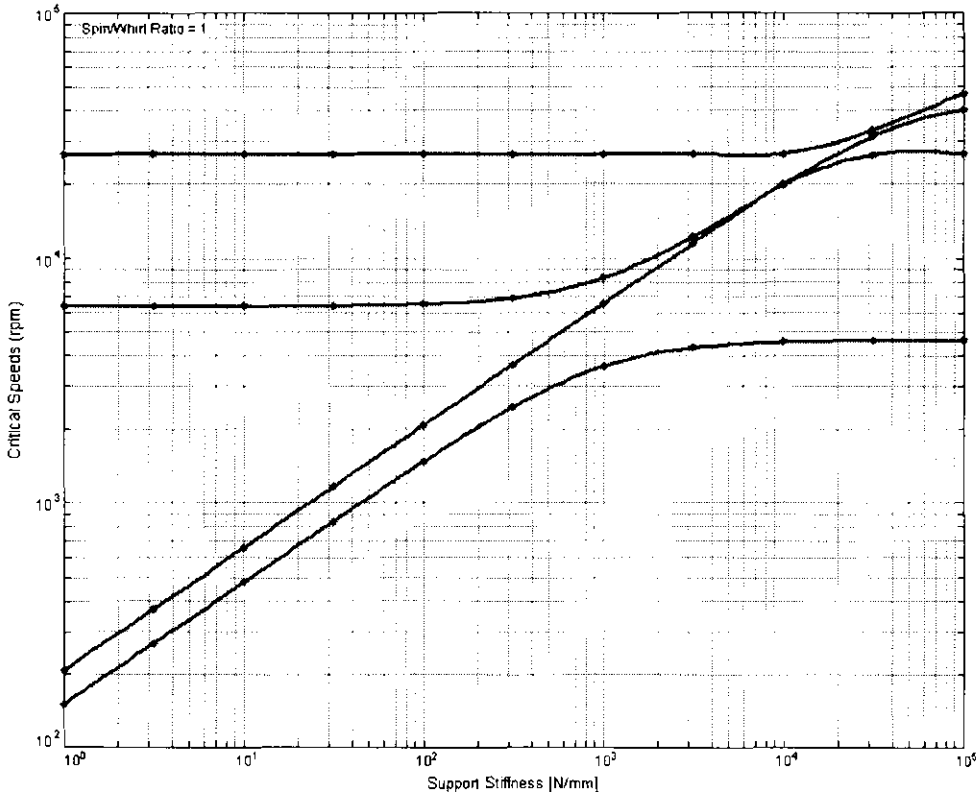


**Figure 5-18: Critical speed map [3]**

The static stiffness of the AMB system before filtering was $5.05\times10^5$ N/m which is used to determine the theoretical critical frequencies of the flexible rotor on Figure 5-18. The dynamic analysis of the flexible rotor before filtering predicted the first critical frequency (cylindrical) at 2,947 rpm, the second (conical) at 4,637 rpm and the third critical frequency (first bending mode) at 7,276 rpm.

The dynamic analysis of the rotor after filtering and a static stiffness of $4.85\times10^5$ N/m predicted the first critical frequency (cylindrical) at 2,600 rpm, the second (conical) at 4,300 rpm and the third critical

frequency (first bending mode) at 7,000 rpm. Critical frequencies in this section of the dissertation are specified as rotational frequencies.

The rotor dynamic response of the actual AMB system without and with filters is compared to each other and to the predicted response of the rotor. The filters that were added to the system are the AAF and AIF as explained in chapter 3.

Figure 5-19 and Figure 5-20 display (a) the vertical and (b) the horizontal peak to peak displacement of the right stator. The critical frequencies attained from Figure 5-19 and Figure 5-20 are given in Table 5-2 and Table 5-3 respectively.

**Table 5-2: Right stator critical frequencies before filtering**

| Horizontal (rpm) | Vertical (rpm) |
|---|---|
| | |
| 3300 | 2900 |
| 4300 | 4000 |
| | 8200 |

**Table 5-3: Right stator critical frequency after filtering**

| Horizontal (rpm) | Vertical (rpm) |
|---|---|
| | |
| 2610 | 2562 |
| 3240 | 3600 |
| | 8369 |

From Table 5-2 and Table 5-3 it is seen that the first two critical frequencies after filtering is lower that that of the system before filtering and that the third critical frequency is almost the same. The biggest difference between the systems before and after filtering is the increase in peak to peak displacements of the filtered system.

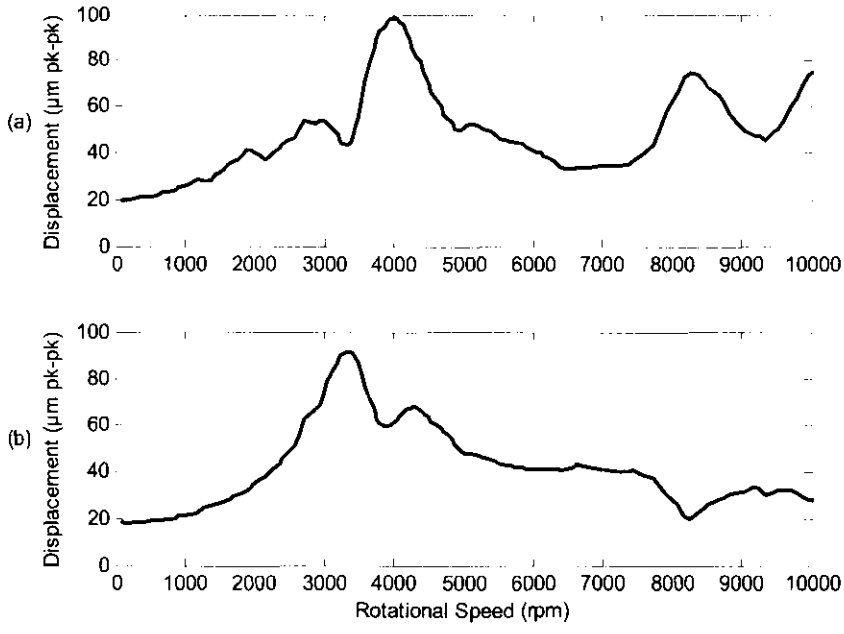


**Figure 5-19: Right stator a) vertical, b) horizontal displacement vs. rotational frequency without the filters [3]**

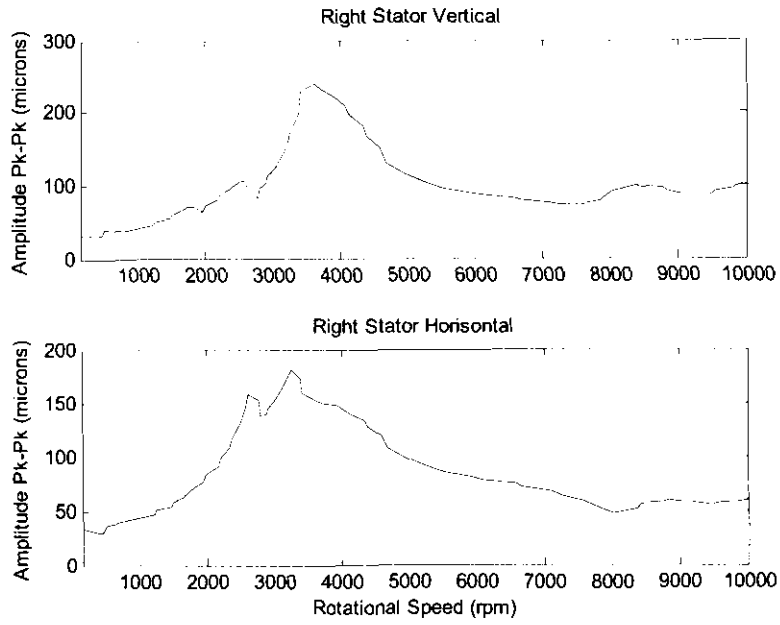


**Figure 5-20: Right stator a) vertical, b) horizontal displacement vs. rotational frequency with the filters**

The left stator response before filtering is shown in Figure 5-21 and after filtering in Figure 5-22. The critical frequencies observed in this two figure are given in Table 5-4 and Table 5-5.

**Table 5-4: Left stator critical frequencies before filtering**

| Horizontal (rpm) | Vertical (rpm) |
|---|---|
| | |
| 3400 | 3000 |
| 4300 | 4100 |
| | 7800 |

**Table 5-5: Left stator critical frequencies after filtering**

| Horizontal (rpm) | Vertical (rpm) |
|---|---|
| | |
| 2763 | |
| 3240 | 3715 |
| | |

The observed frequencies in Table 5-4 and Table 5-5 shows that there is a decrease in critical frequencies in the system with filters and that the observed frequencies are lower than that of the system without filters. Figure 5-22 also shows an increase in the horizontal peak to peak displacement of the left stator.

The left and right stator on the other hand has the same critical frequencies but the amplitudes of the peak to peak displacements are higher for the left stator. This higher amplitude on the left stator shows that the left stator has an unbalance that is not present on the right stator.

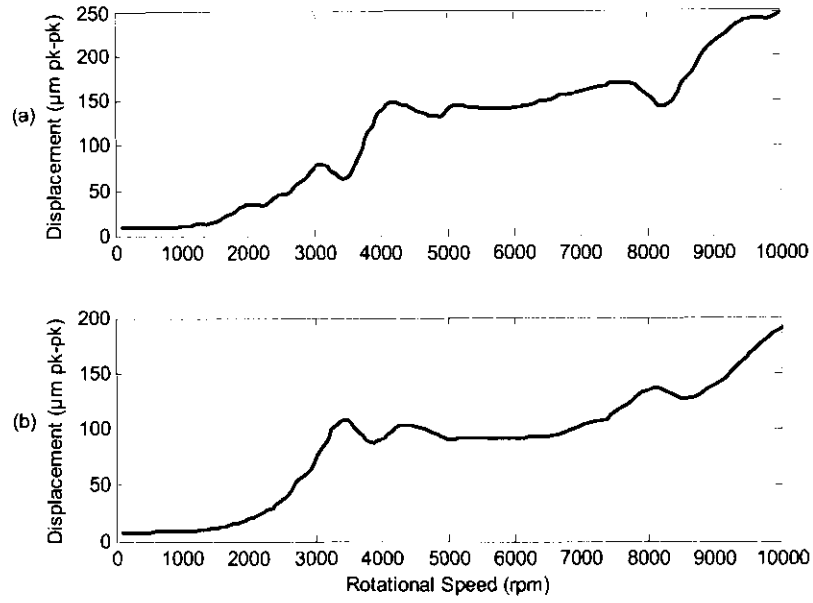


**Figure 5-21: Left stator a) vertical, b) horizontal displacement vs. rotational frequency without the filters [3]**

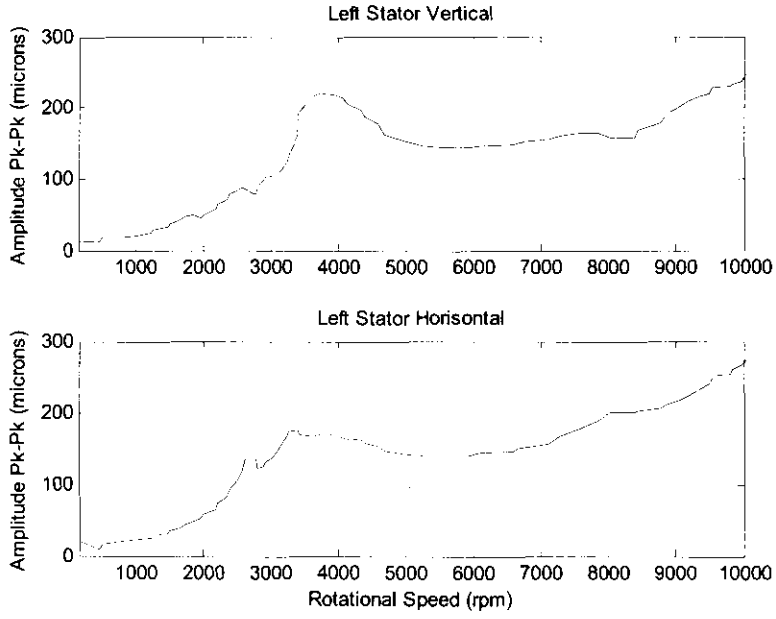


**Figure 5-22: Left stator a) vertical, b) horizontal displacement vs. rotational frequency with the filters**

The centre mass peak to peak displacement as a function of rotational frequency is shown in Figure 5-23 for the system without the filters and Figure 5-24 for the system with filters. The critical frequencies observed on the peak to peak displacement figures are shown in Table 5-6 and Table 5-7.

**Table 5-6: Centre mass critical frequencies before filtering**

| |
|---|
| 3000 rpm |
| 4000 rpm |
| 5050 rpm |

**Table 5-7: Centre mass critical frequencies after filtering**

| |
|---|
| 2490 rpm |
| 3600 rpm |
| |

A comparison showed that the critical frequencies occurred at lower frequencies for the system with the filters and that the peak to peak displacements of the system with filters are higher than that without the filters.

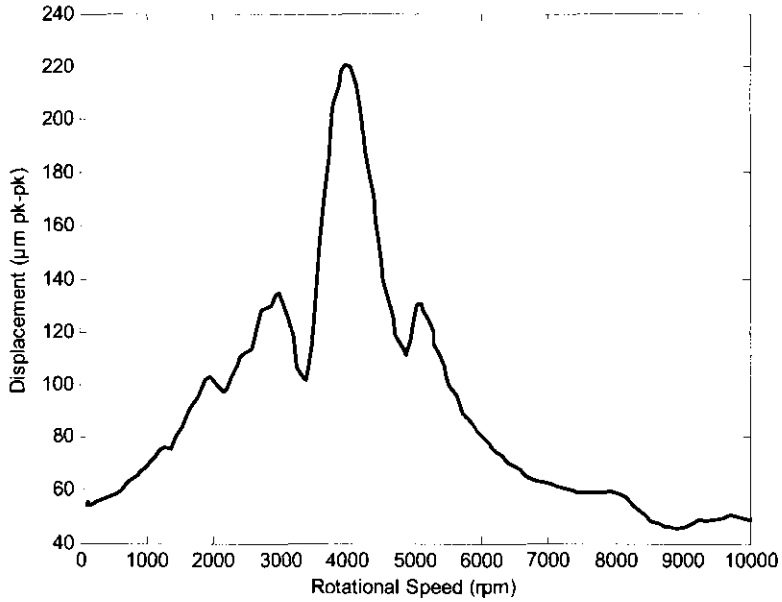


**Figure 5-23: Centre mass displacement vs. rotational frequency without the filters [3]**

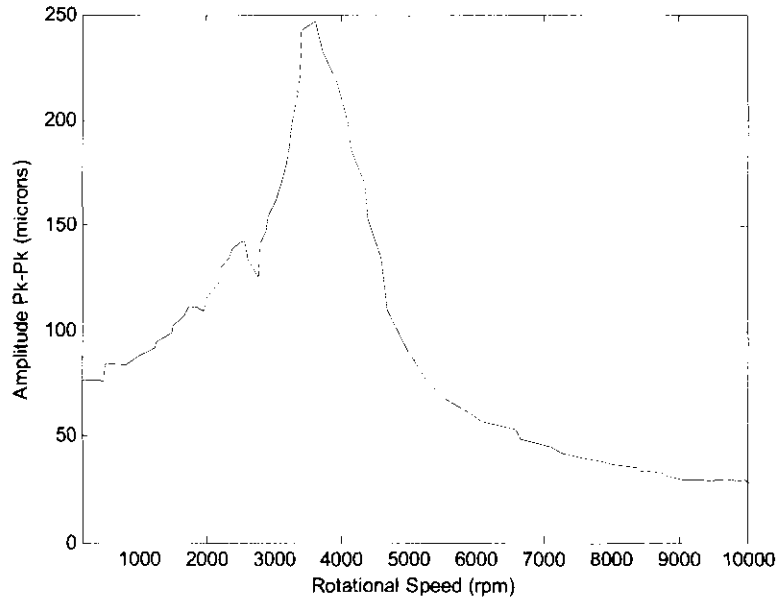


**Figure 5-24: Centre mass displacement vs. rotational frequency with the filters**

To conclude, the lower critical frequencies and higher peak to peak values of the AMB system with filters can be attributed to the lower stiffness because of the filters as explained in section 5.4.1. A lower stiffness will move the stiffness line through the critical speed map (Figure 5-18) to a smaller value on the x-axis and thereby move the critical frequencies to lower values.

### *5.4.4 AMB sensitivity*

System sensitivity is the error of the system due to a position disturbance as explained in section 2.6. The sensitivity of a system is obtained by measuring the sensitivity of the horizontal and vertical axis in each stator. The element with the highest sensitivity determines the sensitivity of the system. Table 2-1 can then be used to characterise the response of the system to other machines [24].

Figure 5-25 shows the sensitivity of the right horizontal stator of the AMB system before filtering. This measurement is however not according to standard since sensitivity should be measured to the maximum of three times the operating speed or 2 kHz [24]. The measurement can be used to compare it to the sensitivity of the system after filtering.

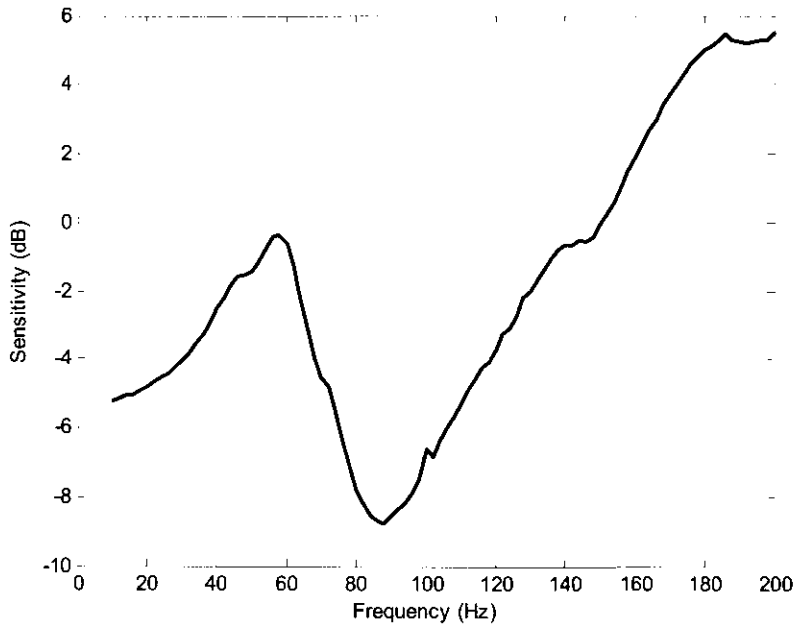


**Figure 5-25: System sensitivity without the filters [3]**

Figure 5-26 and Figure 5-27 shows the sensitivity of the AMB left stator. The comparison of Figure 5-26 and Figure 5-27 showed that the horizontal and vertical sensitivity of the left stator are almost identical. By comparing the sensitivity of the left stator after filtering to the right stator before filtering it is found

that the system with the filters has a higher sensitivity. A higher sensitivity in Table 2-1 shows a decrease in system reliability.

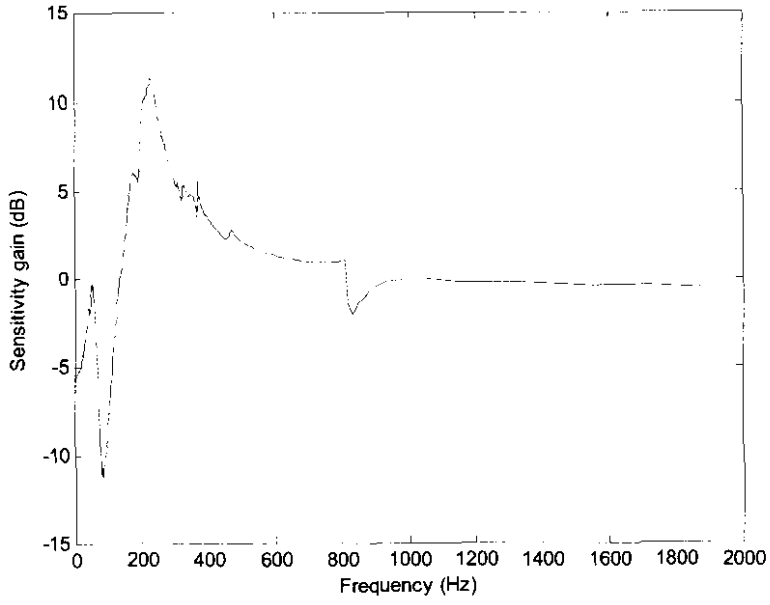


**Figure 5-26: Left horizontal AMB sensitivity**

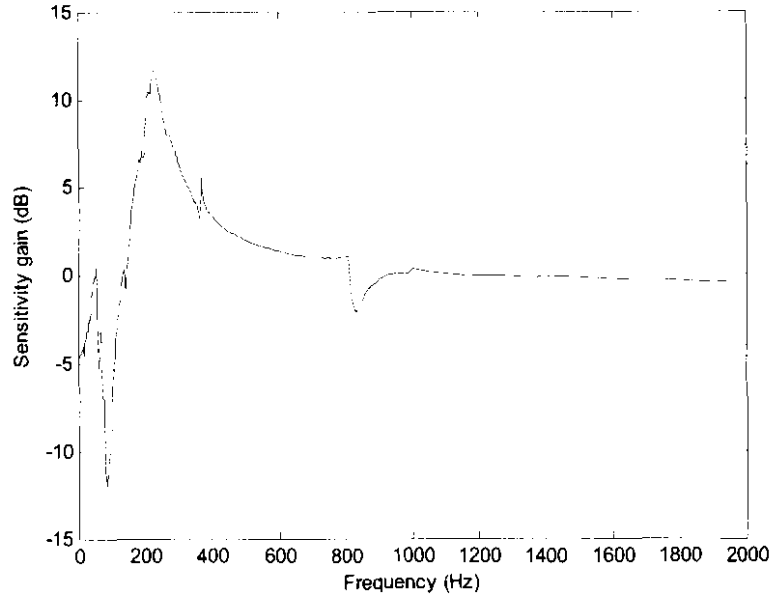


**Figure 5-27: Left vertical AMB sensitivity**

Figure 5-28 and Figure 5-29 shows the sensitivity of the AMB right stator. The highest sensitivity of the two figures are 10.2 dB for the horizontal axis and 11.3 dB for the vertical axis.

Figure 5-28 can also be compared to the right axis before filtering as shown in Figure 5-25. A comparison of the two figures showed that the system after filtering is more sensitive than the system before filtering. This can be attributed to the bandwidth of the AMB system that is impaired due to the filters resulting in large errors at high frequencies and therefore a high sensitivity from (2-23).

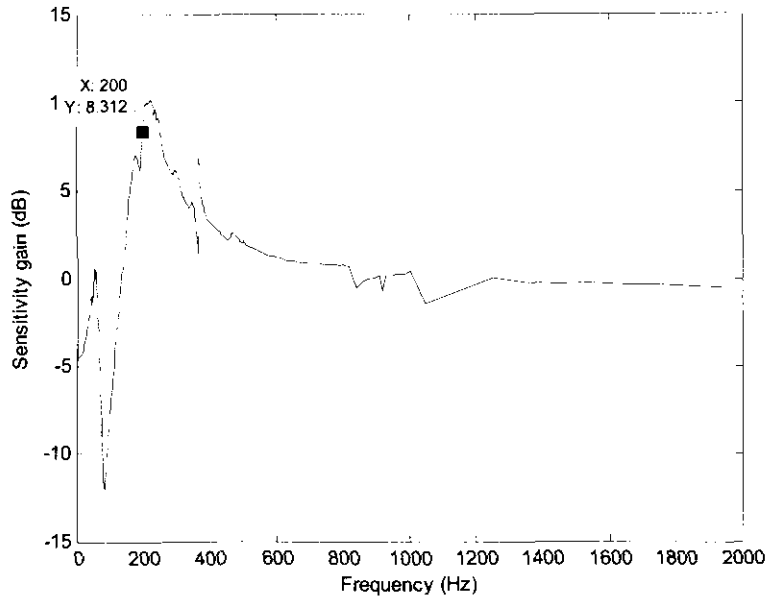


**Figure 5-28: Right horizontal AMB sensitivity**

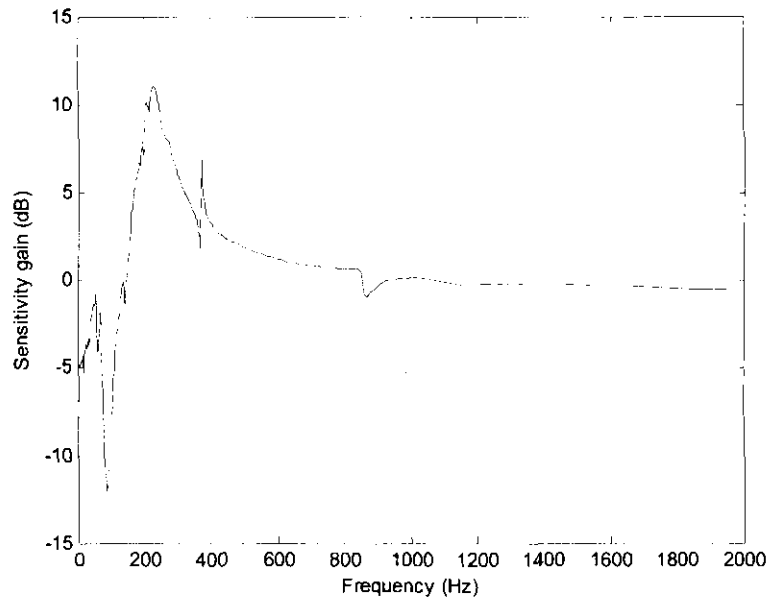


**Figure 5-29: Right vertical AMB sensitivity**

To determine the effect of the differentiator pole at 159 Hz the pole was moved to 3.14 kHz. The sensitivity of the left horizontal axis with a differentiator pole at 3.14 kHz is shown in Figure 5-30. By comparing Figure 5-30, Figure 5-28 and Figure 5-25 it is seen that the differentiator pole has a big influence on the sensitivity of the system and that the sensitivity of the system in Figure 5-30 has the lowest sensitivity of the three figures at 200 Hz. This verifies that the AAF and AIF do not have a big influence on the sensitivity of the AMB system. If the AMB should be operated at a controller pole position of the 3.14 kHz the machine can be seen as a newly commissioned machine (Table 2-1).

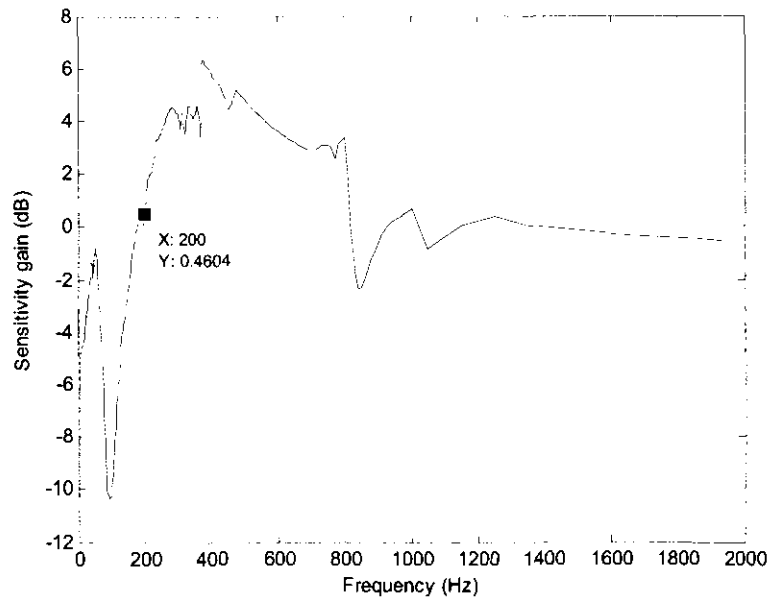


**Figure 5-30: Left horizontal AMB sensitivity with the controller pole at 3.14 kHz**

### *5.4.5 Step response*

The step response of the AMB system was tested on the right stator horizontal axis of the flexible rotor. A 100 μm step is introduced onto the reference signal to step the rotor to a new position. Figure 5-31 illustrates the step response of the AMB system before filtering. This figure shows that the rise time of the simulation is slower than the rise time of the actual AMB system and that the percentage overshoot of the actual AMB is higher.

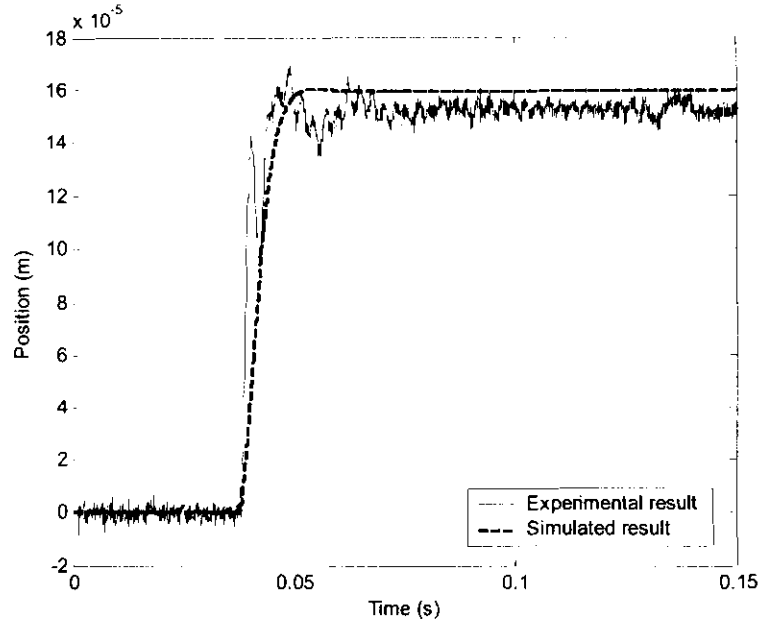


**Figure 5-31: Horizontal step response before filtering (100 µm step) [3]**

The slow rise time and low overshoot of the AMB simulation can be attributed to the differentiator pole of the controller that were not added in Figure 5-31. Figure 5-32 illustrates the AMB simulation with the controller pole but without the AAF and AIF. This step response of the simulation is much closer to the actual AMB step response.

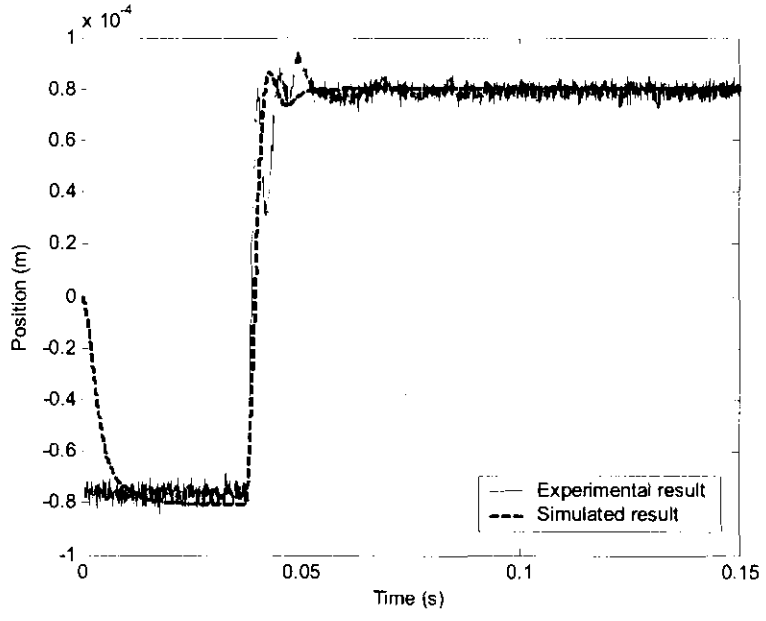


**Figure 5-32: Horizontal step response with the controller pole (100 µm step) [3]**

Figure 5-33 illustrates the AMB and simulation response of the system with filters and controller pole. The actual AMB sensor signals are cleaner than before filtering which shows that the filters have an effect on the signal to noise ratio. The oscillation in the rise time of step response in Figure 5-31, Figure 5-32

and Figure 5-33 are the only responses that could not be explained from the information obtained in the step response.

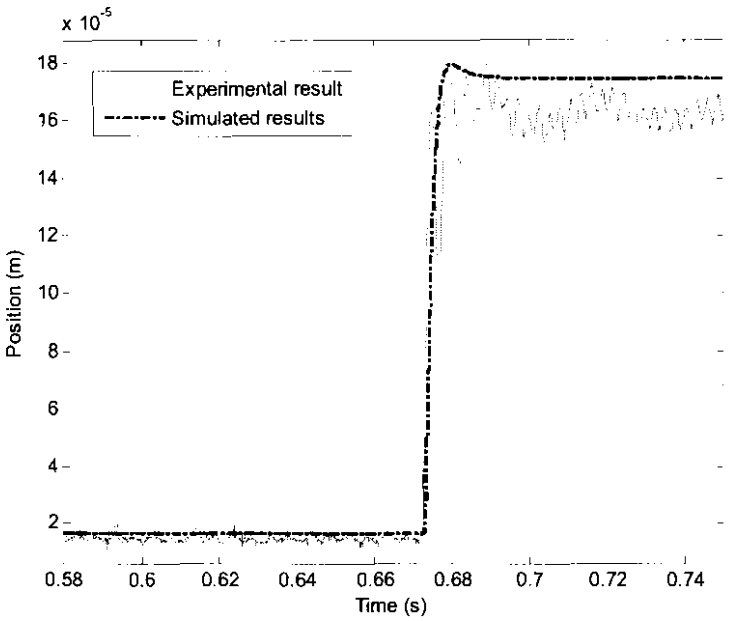


**Figure 5-33: Horizontal step response with the filters (100 μm step)**

To explain this oscillation the root locus of the AMB was used. An enlarged root locus of the AMB system is shown in Figure 5-36. The root locus shows that the three dominant poles in the system are the controller pole and the second order system poles. These poles are so close to one another that the system will not show pure second order behaviour.

The controller pole will have a slow rise time and no overshoot as illustrated in Figure 5-34(a) and the second order system poles will have a fast rise time and 22.6 % overshoot as illustrated in Figure 5-34(b). Since the three poles are so close to one another the resulting response of the system is shown in Figure 5-35 that explains the AMB response.

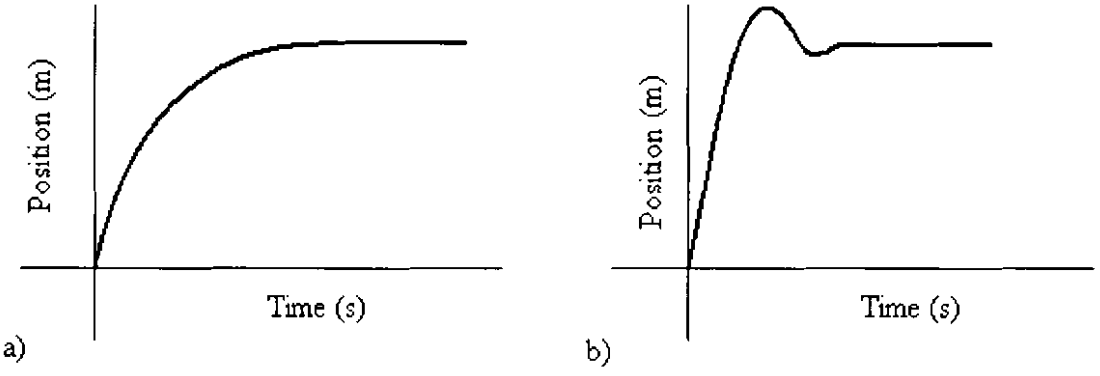


**Figure 5-34: A step response for a) the controller pole and for the b) second order system poles**

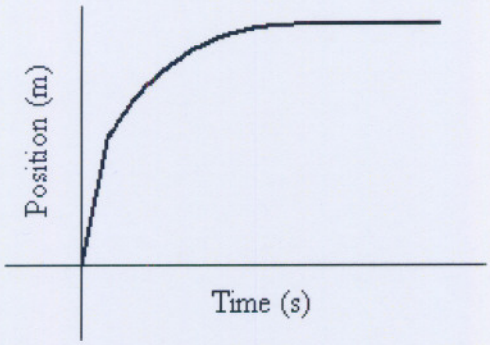


**Figure 5-35: Added step response of Figure 5-34 (a) and (b)**

To prove the statement above the controller pole of the AMB system was moved from 1 kHz to 3.14 kHz. Figure 5-37 shows the response of the AMB system for a 100 μm step. The reduced oscillation on the rise time and two different rise times as explained above can be seen on the figure. This proves that the controller pole has an important role in the response and design of the AMB system.

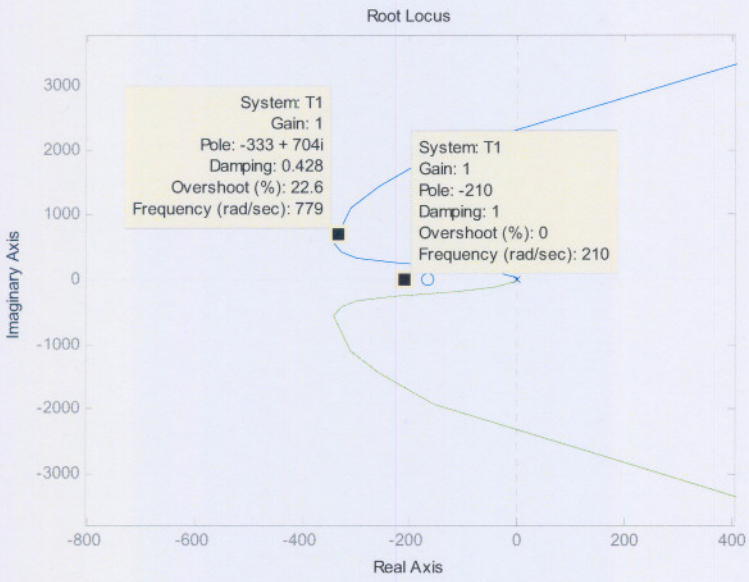


**Figure 5-36: A zoomed in root locus of the AMB system with filters**

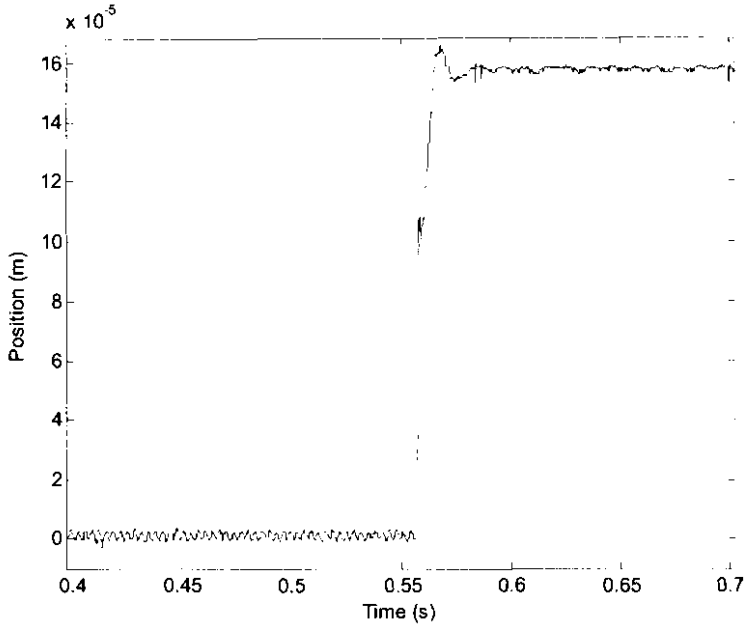


**Figure 5-37: Step response with the controller pole at 3.14 kHz**

*Chapter 5 discusses the characteristics of the AMB system. The characteristics that were discussed are the static stiffness, dynamic stiffness, rotor dynamics, system sensitivity and step response. The deviations between the predicted, simulated and experimental results are discussed in chapter 6.*

# 6 Chapter

# Conclusions and Recommendations

*Chapter 6 contains conclusions and recommendations both in terms of the noise analysis and the AMB characterisation. The dissertation is then concluded with some final remarks.*

## 6.1 Dynamic stiffness from natural frequency

The minimum of the AMB dynamic stiffness must be higher than the specified stiffness on the design specifications [20]. To design for this specification the minimum of the dynamic stiffness plot should be determined from the simulations and from the actual AMB system. This initiated the need to find a way of measuring the minimum of the dynamic stiffness plot without measuring the entire dynamic stiffness. This can be done if the frequency of the minimum is known and the dynamic stiffness in that specific point.

As explained in section 4.2.3, the frequency of the minimum is dependent on the stiffness and is equal to the natural frequency of the system. The dynamic stiffness at this frequency is derived by reducing the transfer function of the dynamic stiffness in the natural frequency as shown in (6-1).

$$k_{dyn}(s) = ms^2 + b_{eq}s + k_{eq}\,.$$

$$\begin{aligned} k_{dyn}(s)\big|_{s=j\omega_n} &= -m\omega_n^2 + j\omega_n b_{eq} + k_{eq} \\ &= \left(k_{eq} - m\omega_n{}^2\right) + j\omega_n b_{eq} \\ &= \left(k_{eq} - k_{eq}\right) + j\sqrt{\frac{k_{eq}}{m}} \cdot b_{eq} \end{aligned}$$

$$\begin{aligned} \therefore \quad \left|k_{dyn}(s)\big|_{s=j\omega_n}\right| &= b_{eq}\sqrt{\frac{k_{eq}}{m}} \\ &= b_{eq}\omega_n \end{aligned} \tag{6-1}$$

To validate the derived statement it is implemented on the MSD and a fitted second order system on the AMB system.

### 6.1.1 *MSD without filters*

To determine the minimum dynamic stiffness of the MSD system the damping and natural frequency of the system is needed as shown in (6-1). The natural frequency of the MSD system as measured from Figure 4-5 is 360 rad/s. The MSD damping is determined from the step response of the system and is equal $2.5\text{x}10^3$ N.s/m. By substituting these values into (6-1) the dynamic stiffness at the natural frequency is

$$k_{dyn} = 8.99\times10^5 \text{ N/m} \tag{6-2}$$

which is higher than the static stiffness. This can be attributed to the inertia of the rotor that started to increase the stiffness of the system before the minimum could occur.

The value obtained in (6-2) also agrees with the dynamic stiffness from the plot in Figure 4-9 at the natural frequency.

### 6.1.2 *Actual AMB system*

To test this statement on the actual AMB system the system had to be reduced to a second order system because the equations only apply to second order systems. The reduction of the actual system to a second order system was done by fitting a second order response through the actual AMB step response as shown in Figure 6-1.

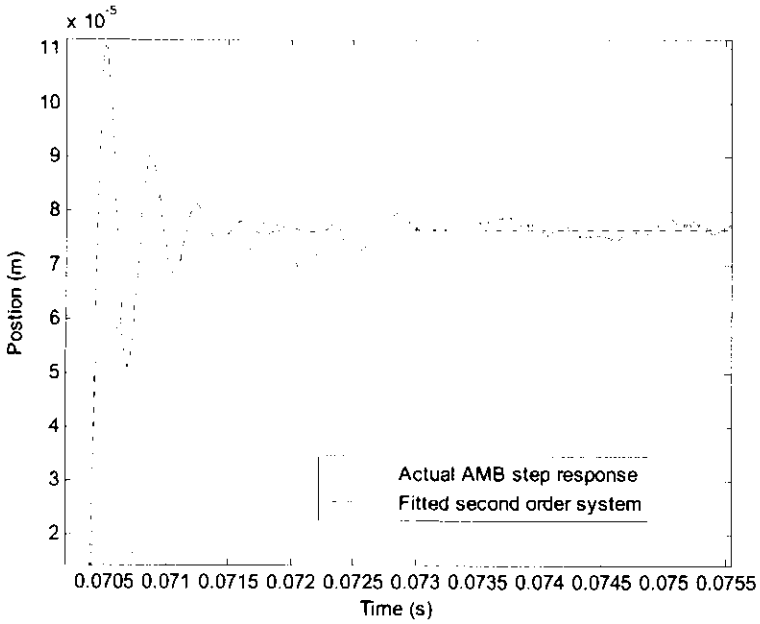


**Figure 6-1: Fitted second order response on the actual AMB system**

This gave a transfer function of

$$T(s) = \frac{-148.2s + 1.56\times10^{6}}{s^{2} + 599.6s + 1.01\times10^{6}} \tag{6-3}$$

which has one zero, two poles and a natural frequency of 979 rad/s as measured on the phase diagram in Figure 6-2.

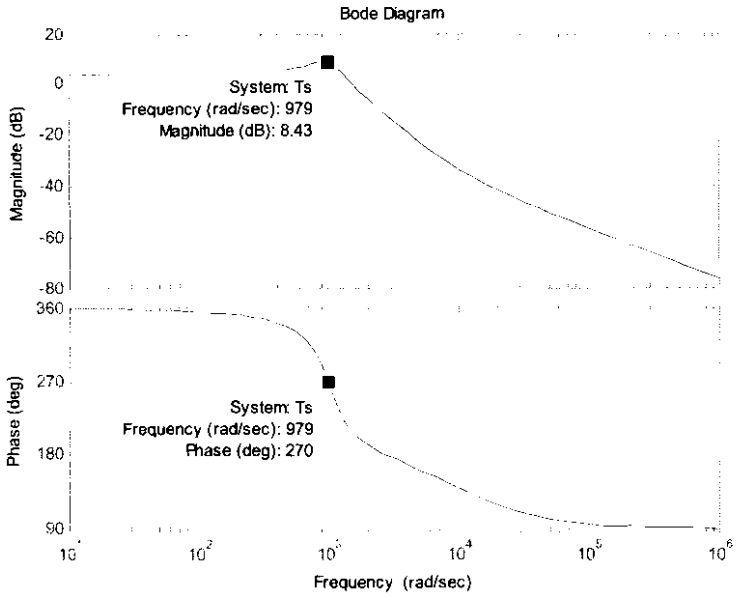


**Figure 6-2: Bode diagram of the fitted second order system**

The damping of the fitted system is $2.315\text{x}10^{3}$ N.s/m which give a dynamic stiffness of $2.31\text{x}10^{6}$ N/m as shown in (6-4).

$$k_{dyn} = b_{eq}\omega_{n} = 2.315 \text{ N/m} \tag{6-4}$$

(6-4) shows good correlation with the dynamic stiffness of the MSD (Figure 4-9) in the natural frequency of the fitted system. This is a first trial for this type of calculation, but it still needs some refinement to determine the minimum stiffness of the actual AMB system.

## 6.2 Conclusions

### *6.2.1 Noise analysis*

The noise analysis of the AMB system showed some radiated and conducted noise. The first step in reducing conducted noise was to implement AAFs and AIFs on the signals before the ADC and after the DAC. This addition of filters showed some improvement on the signal to noise ratio of the signals to and from the controller. To improve the signal to noise ratio of the signals even more the ADC was

synchronised with the PAs to measure when the PAs are not switching. The switching of the PA is one of the main sources of noise on the position signals.

The positives of implementing the filters are the reduced signal to noise ratio and the higher stability. The negatives of the filters are the increase in system sensitivity and the reduction in static stiffness of the system.

### *6.2.2 AMB characterization*

The characterization of the nonlinear AMB system started with a simulation of the linear MSD system. This was done to understand the principles of a second order system and implement them on a complex system like the AMB. The characterization of the linear MSD system showed some remarkable correlations to the theoretical values and to the nonlinear AMB system.

The linear simulation of a MSD system was followed by a nonlinear AMB simulation and the actual AMB system measurements. The characteristics from this AMB simulation were compared to the actual measurements of the AMB and to the MSD system. The AMB simulation was used as a link between the linear MSD system and actual AMB system that is highly nonlinear.

The actual AMB characteristics showed some deviations from the simulated values. One of these deviations was the lower static stiffness on the actual AMB that were attributed to the nonlinearities of the AMB system.

A second deviation in the AMB system was the dip in the position signals of a step response, which was explained as the controller pole added by the differentiator path. An increase in the cut-off frequency of the pole showed that the sensitivity and step response of the system were affected by the pole.

To conclude, the filters and synchronisation increased the signal to noise ratios of the system dramatically and made the system more stable. The characterisation of the AMB system showed that it is possible to design an AMB system to a stiffness specification and that the elements critical to the system's dynamic stiffness are the controller pole, filters, PA bandwidth and controller bandwidth.

## 6.3 Recommendations

### *6.3.1 Noise*

The first improvements on the AMB noise problem should be the shielding of the sensor and cables from the controller to the PAs.

If the shielding is improved a Faraday cage can be implemented to shield the electronics from the radiated noise.

If the signals are shielded and AAF and AIF are still needed these filters should not be of a higher order than second order filters for analogue filters but can be of higher order for digital filters. An analogue filter has a bigger phase shift and time delay for higher order filters than digital filters. It is therefore recommended that digital filters should be used to filters the signals to and from the controller and that the controller's ADC and DAC should be fast enough to do this.

### *6.3.2 AMB*

The in-house developed AMB showed some good characteristics but can still be improved. One of these improvements is to digitise the signals to and from the PAs to the controller and to control the system with a microcontroller and not with dSpace®. The digitizing of the analogue signals will reduce noise on the AMB system.

The system should also be characterized by using dynamic damping and bandwidth to be able to design the system from that perspective as well. The data obtained from this characterization can however be used to design an AMB system from the specified operating stiffness.

The MATLAB® simulation of the AMB system shows relatively good correlation to the analytical predictions as well as the experimental results. Further refinement of the simulation model is however needed to better explain the deviations in the results.

## 6.4 Closure

The objective of this project was to improve and characterise an in-house developed AMB system. A noise analysis had to be done and the noise in the system had to be reduced to an acceptable level. From

the results in chapter 3 it is shown that the signals have a higher signal to noise ratio and that the system is more stable.

The characterisation of the AMB system started of with a MSD simulation which is a linear representation of the AMB system. This simulation was used to understand the responses of a second order system and to compare it to the nonlinear AMB simulation. The nonlinear AMB simulation represented the actual AMB system and was used to simulate the effects of the filters on the AMB system. The results obtained from the simulation were also compared to the actual system results to understand the results of the actual system.

The characteristics of the actual AMB system showed good correlation with the linear and nonlinear simulation. These results showed that the AMB system can be designed from the stiffness specifications and that the characterisation facilitated the understanding of AMB design.

# *APPENDIX*

## *Appendix A: Data CD*

1. **Dissertation in MS Word format**

2. **Matlab® simulation**

| | |
|---|---|
| *MSD simulations without and with filters*: | Static stiffness |
| | Root locus |
| | Bode diagram |
| | Dynamic stiffness |
| *AMB simulations without and with filters*: | Static stiffness |
| | Dynamic stiffness |

3. **dSpace® model of the AMB controller**

# *REFERENCES*


[1] Revolve Magnetic Bearings Inc. Magnetic bearings. [Online]. Available: http://www.revolve.com/ Technology/magbearings.html, [Date of access: February. 2003].

[2] D.J. Peel, C.M Bingham, *et al*. "Simplified characteristics of active magnetic bearings," *Journal of Mechanical Engineering Science*, Vol. 216, Issue C5, pp 623-628.

[3] E.O. Ranft, "The Development of a Flexible Rotor Active Magnetic Bearing System", North West University, School of Electrical and Electronic Engineering, 2005

[4] All Business, Chapions of small business, [Date of access: 4 April 2006] http://www.allbusiness.com/periodicals/article/314067-1.html

[5] M.E.F. Kaskarda and P.E. Allaire. (1997, Jan). The measurement and characterization of power losses in high speed magnetic bearings. ROMAC Report No. 407.

[6] G. Schweitzer, H. Bleuler, A. Traxler, "Active Magnetic Bearings: Basics, Properties and Applications of Active Magnetic Bearings", Authors Reprint, Zürich, 2003.

[7] D.C. Meeker and E.H. Maslen. (1997, May). Prediction of rotating losses in heteropolar radial magnetic bearings. ROMAC Report No. 414.

[8] M.E.F. Kasarda, P.E. Allaire, P.M. Norris, E.H. Maslen, and C. Mastrangelo. (1997, Aug). Comparison of Measured Rotor Power Losses in Homopolar and Hetropolar Magnetic Bearings. *Proceedings of MAG '97*. pp 323-333.

[9] Prof. J.E.W. Holm, Personal conversation with C.H. Marais and E.O. Ranft

[10] E.C. Ifeachor, B.W. Jervis, "Digital Signal Processing", Second Edition

[11] Introduction to Digital Audio http://www.cems.uwe.ac.uk/~lrlang/multimedia/audio2.pdf [Date of access: August 2005]

[12] MATLAB® 7.0.1 release 13, Help File, May 05, 2006

[13] http://www.murata.com/emc/knowhow/pdf/re04ed-1/21to28.pdf , [Date of access:1 May 2006]

[14] P. Colborne, Personal e-mail to C.H. Marais

[15] "What is a Butterworth Filter", [Date of access: August 2005] http://www-k.ext.ti.com/SRVS/Data/ti/KnowledgeBases/analog/document/faqs/bu.htm

[16] "What is a Chebyshev Filter", [Date of access: August 2005] http://www-k.ext.ti.com/SRVS/Data/ti/KnowledgeBases/analog/document/faqs/ch.htm

[17] "What is a Bessel Filter", [Date of access: August 2005], http://www-k.ext.ti.com/SRVS/Data/ti/KnowledgeBases/analog/document/faqs/bes.htm

[18] G. Daryanani, "Principles of active network synthesis and design", 1976

[19] R.C. Dorf, R.H. Bishof, "Modern control systems", Ninth Edition, Prentice, Hall, New Jersey, 2001, pp36-47, pp 227-233

[20] F. Worlitz, H. Stegemann, T. Rottenbach, A Dörrer, R. Hampel, "Simulation-based design method of active magnetic bearings according to the criterion of dynamic stiffness (DDS)", Institute of Process Technique, Automation and Measurement Technique, University of Applied Science Zittau/Görlitz

[21] G Schweitzer, "Active magnetic bearings – chances and limitations", International Centre for Magnetic Bearings, ETH Zurich, CH-8092 Zurich

[22] ISO TC108/SC2/WG7, "Active magnetic bearing – Evaluation of stability margin", ISO CD148393-3, Oct 7, 2003

[23] J.G. Roberts, Personal conversation with C.H. Marais

[24] ISO 2002IS002, "ISO Standardization for Active Magnetic Bearing Technology", Apr., 2002